AUTOMATIC ALIGNMENT METHODS FOR VSM USING MAGNETIC LOW-ANISOTROPIC SAMPLES WITH REDUCED TIME AND HIGHER PRECISION

by

Kolton J. Dieckow, B.S.

A thesis submitted to the Graduate Council of
Texas State University in partial fulfillment
of the requirements for the degree of
Master of Science
with a Major in Physics
May 2021

Committee Members:

Wilhelmus Geerts, Chair

Erik Samwel

Casey E Smith

Yoichi Miyahara

FAIR USE AND AUTHOR'S PERMISSION STATEMENT

Fair Use

Duplication Permission

DEDICATION

This thesis is dedicated to my family who was there supporting me every step of my education.

Also to Pam Wilson, thank you for teaching me to read it is a gift that has helped define my life.

ACKNOWLEDGEMENTS

This work was supported in part by NSF through an DMR-MRI Grant under Award 1726970 and in part by DOD through a HBCU/MI grant (W911NF2010298).

We would like to thank Dean Koehne of ARSC and the ARSC of Texas State for help with experimental tasks and modifications to the VSM.

We would like to thank Erik Samwel for his support with this thesis and his help with understandoing the MicroSense software.

Also a large thanks is due to the members of the committee who provided feedback when writing and on the work itself.

And finally, we would like to thank MicroSense for its support on the project by giving us access to their drivers for the VSM and financial support to purchase the ThorLabs motor setup.

Pieces of this work have been presented in the following conferences:

1. Kolton Dieckow, Sarah Beth Ragan, Chandan Howlader, Binod D.C., Wilhelmus Geerts, Biaxial VSM Sensitivity and Crosstalk Measurement Dependence for $S_{xx}(x,y,z)$, $S_{xy}(x,y,z)$, and $S_{xz}(x,y,z)$, **poster presentation Fall-2019 meeting of the TSAPS**, Lubbock, October 25-26, 2019.
2. Kolton Dieckow, Chandan Howlader, Tanjina Ahmed, Maria Camila Belduque, Jitendra Tate, Wilhelmus Geerts, “Effect of Field Orientation and Infill Percentage on the VSM calibration factor of FFM 3D printed samples”, **MMM**

2020 conference, oral presentation, Palm Beach Florida, November 2

3. Sarah Beth Ragan, Kolton Dieckow, Binod D.C., Wilhelmus J. Geerts, “Biaxial VSM Angular Measurements with Alignment”, **Wise conference** March 6, 2020, Texas State University.

TABLE OF CONTENTS

Page

LIST OF TABLES

Table **Page**

LIST OF FIGURES

Figure **Page**

ABSTRACT

Vibrating Sample Magnetometers (VSM) are used to measure the magnetic properties of ferro or ferrimagnetic materials. They have a wide range of users in both industry and in universities. Currently VSMs require a manual alignment for each sample loaded in the instrument. If the sample is not centered within the pickup coils, systematic errors are introduced into the data. Centering the sample requires significant time to complete and needs to be repeated after each field angle, field or temperature change. For this thesis project an automatic alignment system was designed, implemented and tested. The system measures the position of the sample after each field angle change and corrects for sample shifts after a field angle change avoiding large systematic errors in the M_y signal.

I. INTRODUCTION

Vibrating Sample Magnetometers (VSMs) have been in use to characterize magnetic materials for several decades now. They are used over a variety of applications from research to product testing in different industries. A few examples of uses for VSMs are in the development of electric cars motors, magnetic tape storage, and even power generation. Each of these previously mentioned industries are experiencing prolific growth. Auto manufacturers are currently shifting more and more to electric vehicles. This requires the production of electromotors with magnetic rotors or stators and novel sensors that include magnetic materials. The data storage sector has seen explosive growth as companies shift more to a digital environment. Long term reliable storage of information is necessary in many places like universities, hospitals, and companies like Amazon for back up of systems and other needs. The energy sector has also seen large changes as countries shift to more sustainable methods of power generation. Texas now has the largest number of windmills in the US and all incorporate permanent magnets to generate electricity. All of these industries use magnetic material in their products so need or use VSMs for development and testing.

Many modifications and changes have been made to improve a typical VSM's sensitivity and functionality and as of 2021, a commercial VSM allows for measurements of the magnetic moment in the 10^{-7} emu range where Johnson noise in the pickup coils starts to obscure the sample's magnetic signal. However, one thing has remained necessary for valuable, and error free magnetic measurement readings and that is the physical alignment of samples prior to the actual measurement. The sensitivity of modern biaxial VSMs depend on the sample's location between the pickup coils. The

measurements of the instrument are only valid when the sample is magnetically centered similarly to the sample that was used to calibrate the instrument. If a measurement is taken with a non-centered sample, a systematic error is observed in the magnetic signal. The current commercial VSMs use a manual alignment method that was first introduced by Foner (Foner, Versatile and Sensitive Vibrating-Sample Magnetometer, 1959). The sample is aligned by hand based on continuous magnetic readings. For a scalar VSM this is done by first minimizing the M_x signal by moving the sample in the x direction (or parallel to the field) and then maximizing M_x by moving the sample in the y direction (perpendicular to the field). For a typical alignment, this process is repeated several times. The alignment of the sample needs to be repeated every time the field, field angle or temperature is changed since these measurement conditions can influence the position of the sample. So, for a manual sample adjustment approach, the user needs to stay near the equipment. This is not desirable as certain magnetic measurements can take up to several hours to complete.

This work presents a new method for alignment that no longer relies on users' physical skills and no longer requires the user to be present near the instrument during the full measurement period. Sample positioning corrections are done by an automated algorithmic approach that can operate independently, under computer control, and uses servo motors to move the sample in between the pickup coils. Rather than doing separate scans in the x and y-directions like the traditional approach mentioned above, the sample is moved in a circle in between the pickup coils. While this happens the X and or Y-coil set signal is measured and recorded. The samples center position relative to the coil sets can be determined from the measured signals. After a scan completes the sample is then

moved straight to said central position without the need for more adjusting. In this thesis, this method, is referred to as the Phi-scan method. The mathematics behind it, and the programing that was used to implement it are discussed. Also, the challenges presented by this thesis project, assumptions made about the samples, and issues with the software integration are discussed.

Project Goals

The goal of this thesis project is to establish a new automated sample alignment technique for VSMs. Using this new method will require little additional time and will be at least comparable to a precise manual alignment. It also will reduce systematic errors in the VSM measurements. Examples of such measurements are: torque measurements (measurements as a function of the field angle), hysteresis curve measurements (measurements as a function of the field magnitude), and moment versus temperature measurements. In each of these cases there can be large errors introduced by the movement of the mounting rod on the measured magnetic moment as the field angle, the field, and or the sample temperature is changed. For torque measurements misalignment of the sample on the mounting rod causes the sample's position to depend on the field angle. This leads to errors in the torque curve and part of the signal dependence is not caused by the sample but the change of the position with the field angle. This change of sample position with field angle is called wobble [Binod]. A completely autonomous VSM system will allow industry and educational researcher groups the benefit of running measurements with automatic sample position correction without user intervention.

Project Layout

This Thesis project builds upon previous work done by others [Richter, Benito, Binod D.C., Inv. Disc]. In particularly the work of Binod D.C. who derived equations describing the dependence of the sensitivity of a modified Mallinson coil set and the subsequent Invention disclosure [Inv Disc] were important steppingstones for the automatic sample positioning system. A review of the physics was done by modeling in Mathematica the expected interactions of the coils with the magnetic sample. From there software was developed in LabVIEW that would automate the data acquisition process and alignment process of the sample. Proof of concept was done using Oriel Encoder Mikes available in the Optical Characterization lab. These were later on replaced with a more modern servo-motor set up acquired from Thorlabs and paid for by MicroSense-KLA. The MicroSense EZ-9-HF VSM at Texas State was then modified to accommodate the servo motors to control the position. Also plans were made to allow further integration with the MicroSense software suite where necessary. An extensive LabVIEW program was written to accommodate new data acquisition and test procedures. The main testing focused on the system's accuracy and repeatability over the iterative design process. Issues with higher-than-expected anisotropy in the test-samples lead to the need for lower anisotropic test samples. Final tests were done by using the system to automatically correct the sample position while measuring the torque curve with the MicroSense software. An angular correction table that includes the sample's position as a function of the field angle was measured after loading the sample but before starting the MicroSense software. The content of this table was then used by a small program running in the background of the MicroSense software to make corrections to the sample position

upon changes of the field angle. The measured torque curve of a mu-metal test sample no longer showed a significant 1θ component.

II. VSM AND ITS USES

VSMs are in use over a wide variety of industries and research labs. Examples of use can be found at Texas State University where magnetic thin film samples including epitaxial MBE-grown Fe-doped Ga_2O_3 are routinely characterized in the VSM (Mia, 2020). Other materials being investigated are magnetic composites to be used as raw material for Magnetic Field Assisted Additive Manufacturing (3D printing) samples (MFAAM). For MFAAM, the magnetic composites are 3D printed in a magnetic field allowing one to create materials with a position dependent anisotropy distribution. MFAAM samples have application in novel devices including Halbach cylinders for portable MRI equipment, flux guides for wireless charging applications, and small magnetic robots for drug delivery. In industry we typically see VSMs used for research and development and quality control and testing of magnetic products. Including for example Magnetic Tape/disk Storage, Magnetic RAM (MRAM), Sensors, and permanent magnets (for electromotors etc.). Though VSMs have been in use for several decades now the overall knowledge of them outside of those using them is relatively small so in this section we will discuss the physics and design of VSMs.

VSM Concept

The original development of VSMs comes from a desire for a magnetometer that could make rapid and accurate measurements for different material properties of small magnetic samples. Several different Magnetometers were considered for this with one being the Vibrating Coil Magnetometer (VCMs) which as the name suggest vibrates the coils around or near a magnetic sample [Smith, D. O.] (see Fig. 1a below). VCMs

function by first inserting a sample into an external magnetic field. This external field induces a dipole moment in the magnetic sample. A set of coils are vibrated around the sample inducing a current proportional to the dipole moment of the sample because of Faraday's induction law. Another design considered was the Vibrating Sample Magnetometer (VSM). This is a Magnetometer that instead of vibrating the pickup coils like the mentioned VCM, vibrates the sample near stationary pickup coils [Foner, S.] (see Fig 1b below). Unlike the VCM a magnetic sample is vibrated in the external magnetic field. This field again induces a magnetic dipole moment on the sample. The (vibrating) motion of the sample causes the field created by the magnetic dipole moment of the sample in the detection coils to change. This induces a voltage in the set of coils surrounding the sample because of Faraday's induction law.

$$V = -N\frac{\delta\Phi}{\delta t}$$

With N being the number of turns in the coil, and Φ the flux through the coil.

This voltage is measured by one or more lock-in amplifiers. These lock-in amplifiers and other equipment feed the VSM information to a compute. Figure 2 below shows a diagram of electromagnet, pickup coils, and vibrating sample.

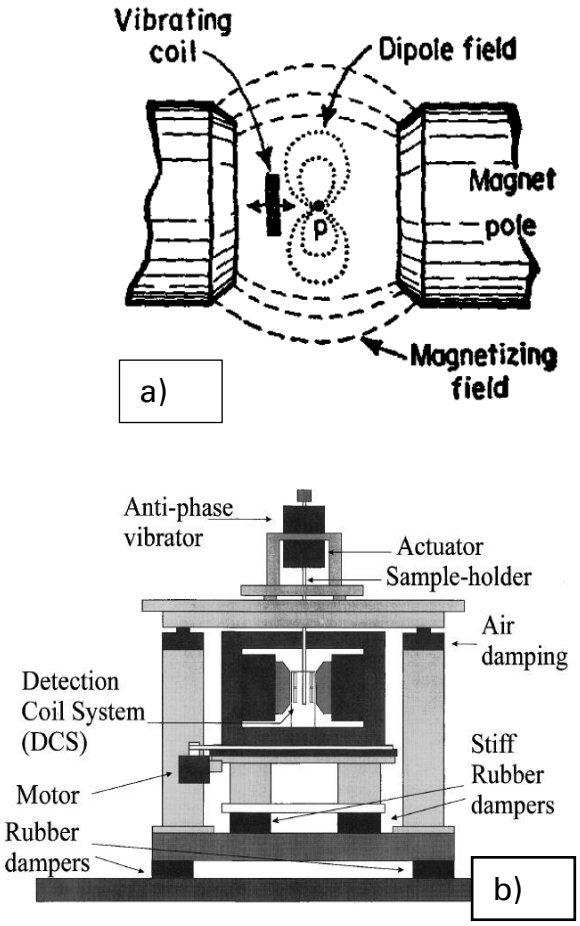

Figure 1: Here an example of the VCM [Smith, D. O.] a) and VSM [Samwel] b) are shown.

VSM Layout

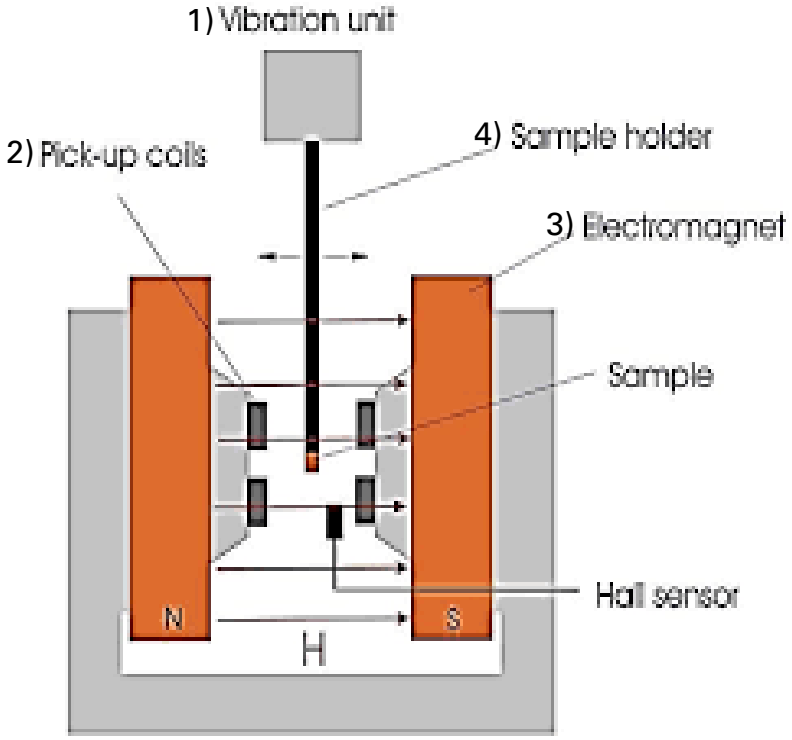

Figure 2: A basic diagram of a VSMs different components. Note that the field is primarily between the 2 pole faces. The diagram suggests a homogeneous field between the 2 magnet coils.

Typically, VSMs consist of four specific components:

1. The vibrational head, where the mounting rod is inserted to vibrate the sample.
2. The coil set, between which the sample is oscillated, and which senses the magnetic moment of the sample.
3. The large electromagnet, which is placed around the sample and coils to apply an even magnetic field to the sample.
4. The mounting rod, where the sample is attached to the vibrational head.

An example of how these components look can be seen in figure 2.

The coil set is designed for maximum sensitivity; to simplify the use of the equipment, to reduce electromagnetic interference of other equipment in the lab, and or to minimize the sample position dependence of the sensitivity function. Typically, VSM coil sets consists of several coils symmetrically placed around the sample. A variety of different coil configurations have been proposed in the literature (see Fig. 3). From here on we will discuss a few of these designs and their different uses.

Mallinson:

The Mallinson coil set consist of only four coils arranged in sets of two on both sides of the sample with one coil above another. The sets are placed near the poles of the electromagnet and directed parallel to the applied field. The Mallinson coil set has higher inherent sensitivity to magnetic samples than many other coil set designs. This is because it has a very low signal to noise ratio. The signals from the coils however have a large dependence on the sample's position compared to other coil designs. This is due to the placements of the coils directly parallel to the field. As the sample moves towards or away from one of the coils the signals will increase or decrease. The design while beneficial only allows for the detection of the M_x component from the sample's magnetic dipole moment. Mallinson calculated the sensitivity of the coil set using the reciprocity theorem. The Reciprocity theorem states that the flux between two coils, in this case a coil and the sample, are the same. His work allowed for an early set of equations to be used for coil designs. These equations were independent of the sample's properties; however, they were only valid for point magnetic dipoles and did not account for the samples shape. [Mallinson]. The Mallinson coil set is now the most used pickup coil

configuration for commercial scalar-VSMs as it provides a strong sensitivity that though is slightly dependent on the position of the sample.

Modified Mallinson:

A modified Mallinson coil set uses an additional coil set now perpendicular to the applied field. This second set is used exclusively to detect the transverse component of the sample's magnetic dipole moment allowing more detailed measurements to be conducted. So, with a modified Mallinson coil set it is possible to determine two components of the magnetic dipole moment: one component (M_x) parallel to the applied field and another component perpendicular to the applied field (M_y). The modified Mallinson coil set is nowadays often used in vector-VSMs.

Bowden:

A Bowden coil set consist of eight coils arranged in a cubic configuration with the coils parallel to the applied field. The Bowden coil configuration is far less sensitive to sample position than the Mallinson coil sets. The Bowden coil sets design allows for the measuring of both the M_x and M_y components thanks to the coil's matrix. The calculation to determine these components comes from the equations below which use the coils voltages to find M_x and M_y:

$$M_x \sim (V_1 - V_2 - V_5 - V_6) + (V_3 + V_4 + V_7 + V_8)$$

$$M_y \sim (V_1 - V_4 - V_6 - V_7) + (V_2 + V_3 + V_5 + V_8)$$

$$* V_1, V_2 \; etc \; refers \; to \; the \; coils \; and \; their \; positions$$

For VSM access the Bowden coil set is the easiest. The coils can be mounted

directly to the magnets pole pieces. There is still draw backs as the sensitivity of the Bowden coil set is typically two to three times less than the sensitivity of the modified Mallinson coil set. [Richter]

Benito:

A more recently developed design for coils is the Benito coil set. This Design consist of 2 coil sets. The xy-coil set of 4 pickup coils used to measure the magnetic dipole moment in the x and y directions and another coil set of 2 pickup coils to measure the magnetic dipole moment in the z-direction. The first coil set consist of coils placed at the four corners of a square perpendicular (facing in the direction of vibration specifically) to the field. The coils in these sets are actually a multi stack of three separate coils. The upper and lower coils are wound in the same orientation while the middle coil is wound opposite. These coils can be used to determine the M_x and M_y signals by subtracting and adding induction voltages based on the equations below:

$$M_x \sim (V_1 - V_3) + (V_4 - V_2)$$

$$M_y \sim (V_1 - V_3) - (V_4 - V_2)$$

$$* V_1, V_2 \; etc \; refers \; to \; the \; coils \; and \; their \; positions$$

This coil set configuration was shown to have a high sensitivity allowing for a much larger area in between the pickup coils. Having a larger area between the coils allows for larger sample sizes to be used. This also allows for a more robust furnace to be used for temperature based measurements.

The coils of the z-coil set are larger and are placed at equal distance from the sample perpendicular to the applied field. These coils are also faced in the direction of

vibration but unlike the others are a set of two stacked coils both wounded in the same direction. These coils are used then to find the M_z component of samples.

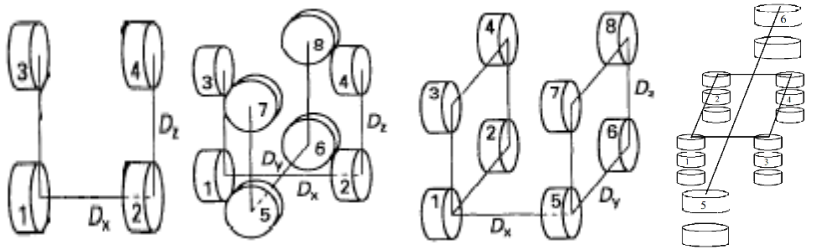

Figure 3: Various pickup coil set, i.e. (a) Mallinson; (b) Modified Mallinson; (c) Bowden; (d) Benito.

Significant research and development has been performed on the vibration mechanism of a VSM. There were initially several different designs used. One design was a coil based system that forced the rod back and forth on a mounted track at a set frequency which provided rigidity and assured the vibration was always along one axis [Smith]. Another design was based on a singular loudspeaker driven system that oscillates the rod at a set frequency the user could manipulate. Using such an approach meant the system was not as rigid and vibration could happen along multiple axis. However, as time went on MicroSense included a membrane of a 2nd loudspeaker (spider) as a support for the sample rod resulting in a robust vibrator [Samwel]. With this set up the sample can be vibrated at varying frequencies thus allowing optimization of other system aspects (for examples to avoid resonance frequencies) in the direction of the main axis.

VSM Measurement Techniques

The measured voltage across the pickup coils is proportional to the sample's magnetic dipole moment. This information can be used to determine various magnetic properties including the magnetization (the materials dipole moment per unit of volume

or per unit of mass), the coercive field (field dependent measurements), the magnetic Anisotropy of the sample (angle dependent measurements), and even the Curie temperature (temperature dependent measurements) [manual of MicroSense VSM]. Listing all of the measurement techniques that a modern VSM is capable of would require a much larger discussion, so here we will focus primarily on hysteresis curve measurements and torque measurements. These measurement techniques are pertinent to this work's goals as they will see potential a large benefit from correction of sample position.

One of the most important measurements performed with a VSM is the Hysteresis curve measurements used to determine many of the important magnetic properties of the sample under study. This method scans across a range of field values while recording the magnetic dipole moment in the x (parallel to the field) and y (perpendicular to the field) directions. It then plots the magnetic dipole moment or the calculated Magnetization in the X and Y direction as a function of the field [Binod D.C.]. From the hysteresis loop, one can determine the remanence (y-intersect) and the coercivity (x-intersect), and even the saturation magnetization (values at large field values). The shape of the hysteresis curve largely depends on the magnetic reversal mechanism in the sample. An example of a hysteresis loop scan is shown in Figure 3 below.

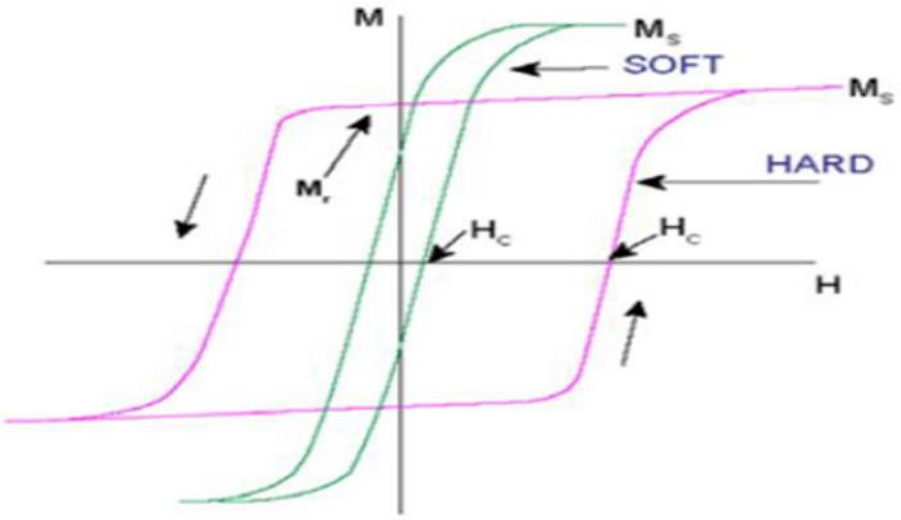

Figure 4: Here is an example of a Hysteresis curve for a soft or hard magnetic material.

Soft magnetic materials are materials which are easily magnetized and demagnetized. Hard magnetic materials are those that are hard to magnetize or demagnetize.

Another important magnetic measurement method is the Torque measurement. This refers to a measurement of the torque acting on the sample as a function of the applied field angle q. A torque curve provides information on how the magnetic properties depend on the direction of the field. The MicroSense setup at Texas State University actually includes a Torque Magnetometer that measures the true torque acting on a sample. The torque sensor can measure torques from 5E-9 through 4E-5 Nm. The true torque head can only be used at room temperature as the gas flow of the cryostat will cause noise in the torque measurements. The standard vibrational head and biaxial coil set up however is just as capable of measurements of the torque on the sample although in a more indirect way. The torque on the sample is equal to the cross product of **m** and **H** so:

$$\vec{\tau} = \vec{m} \times \vec{H} = \left(m_x \hat{\imath} + m_y \hat{\jmath}\right) \times (H\hat{\imath}) = H m_y \hat{k}$$

So, the torque is proportional to the y-component of the magnetic dipole moment. These measurements are performed by rotating the sample (change the field angle q) and recording the M_y component. This torque curve is then used to determine the easy and or hard axis of the sample. The angle-dependence of the M_y signal is used to determine the magnetic anisotropy of the sample under study below in Figure 5 an example of torque measurements done on a circular sample of sheet metal. The torque curve shows a 4θ and a 2θ component.

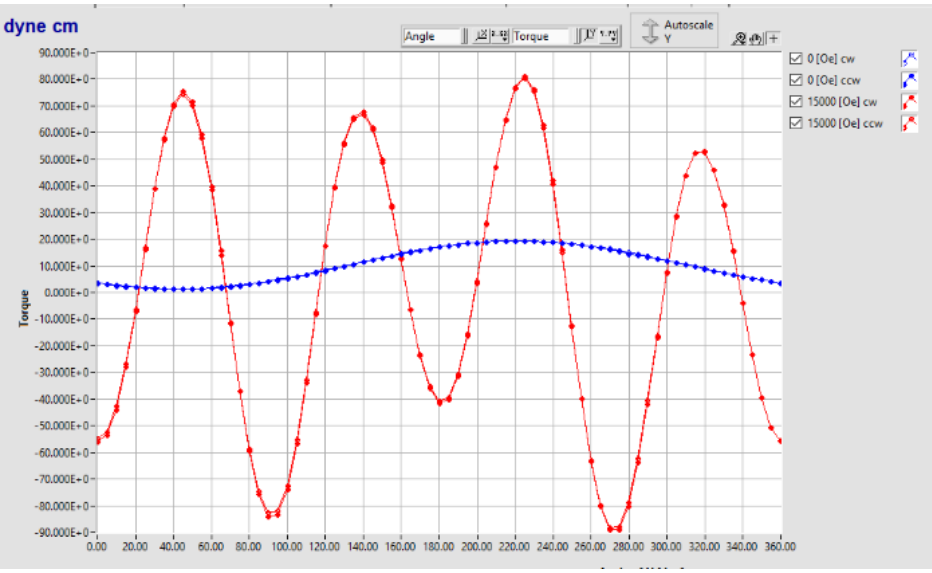

Figure 5: Torque curve measured by torque head on a Nickle calibration sample.

Effect of Wobble on the torque curve

The main focus of this section will be on the systematic measurement errors inherent to the shift of the sample position during a VSM measurement. This shift can be due to a field change, a temperature change, or a field angle change. Here we will mainly consider sample position shifts due to a field angle change. This error that is to be discussed will be referred to as wobble which was previously addressed by others (D.C.,

2019) (Richter) (Benito). Wobble is a change of the sample's position when changing the field angle. The reason for wobble can be attributed to misalignment of the sample's magnetic center with the center of rotation of the sample-rod or rotational head. For such misalignment, the sample will have a different position for every field angle. If the sample is rotated to change the field angle q, the sample moves in a circle in between the pickup coils as shown in the figure below.

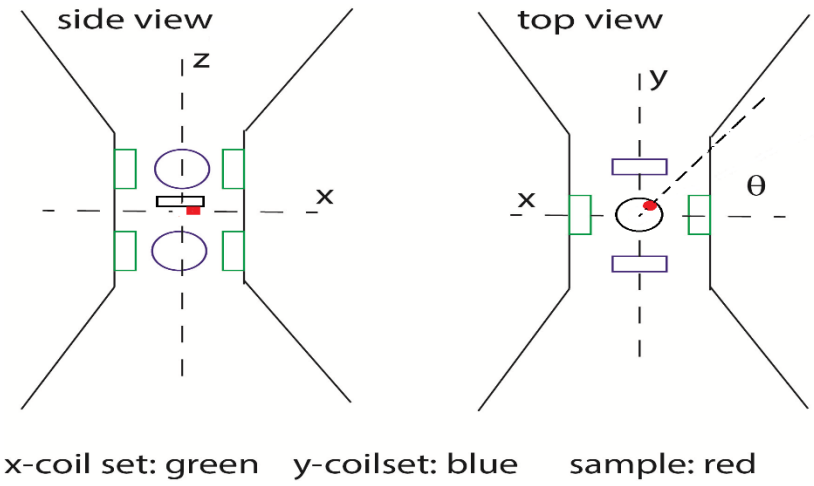

Figure 6: An example of a poorly mounted sample on a Mounting rod.

Since the position of the sample determines the sensitivity of the setup, the measured magnetic moment of the sample will contain an angle dependent term unrelated to the magnetic properties of the sample. Figure 6. below shows a surface plot of the calculated M_x for a Mallinson coil set as a function of the sample location. The M_x signal looks like a saddle and increases when the sample is moved towards one of the x-coils and decreases when the sample is moved towards one of the Y-coils. The circle plotted in the surface plot shows the trajectory of the sample as the field angle is changed. So, the signal is not constant but will vary sinusoidally with the field angle q as the sample's position and the sensitivity are changing with field angle. Even for an isotropic sample a

two theta dependence of the X-coil signal is observed. You can see an obvious variation of the sensitivity as the sample is rotated. For a uniaxial anisotropic sample, the angle dependence of this signal cannot be distinguished from the angle dependence caused by the magnetic anisotropy; the sensitivity of the Y-coils varies similarly.

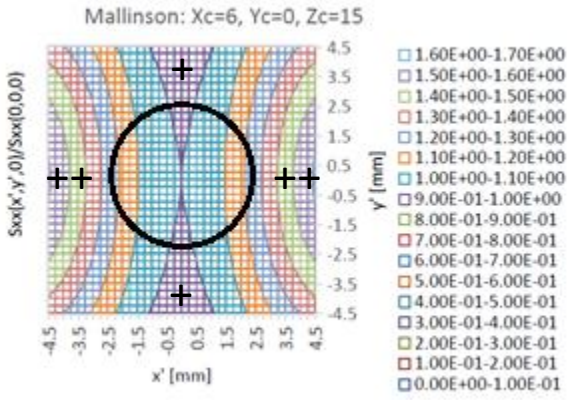

Figure 7: A Surface plot of the Mx signal generated in Mathematica based on the position of a sample in a VSM with a Modified Mallinson coil set.

In addition to the sensitivity of the VSM, the cross-talk of the coil set is also affected by the wobble. For a perfectly centered sample the magnetic dipole moment in the x-direction will not result in a signal in the Y-coils (see Figure 7. below). However, if the sample is no longer centered within the pickup coils, the M_x magnetic dipole moment will cause a signal in the Y-coil set. This is illustrated in the figure on the right below. Similarly, the X-coil signal can be affected by the sample's M_y magnetic dipole moment in the case the sample is not centered.

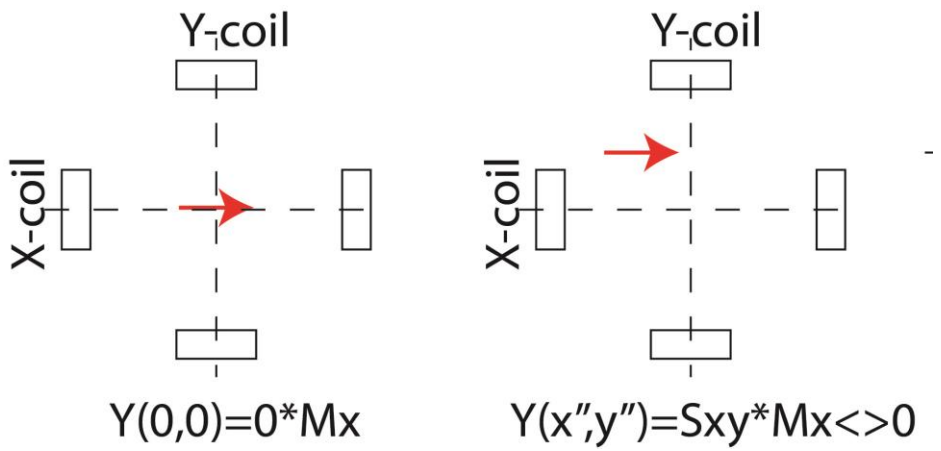

Figure 8: A depiction of the samples positions effects when properly centered and when sifted in the y direction.

So, the X-coil and Y-coil signal depend on both the M_x and M_y signal, i.e.

$$X = S_{xx}M_x + S_{yx}M_y \qquad [1]$$

$$Y = S_{xy}M_x + S_{yy}M_y \qquad [2]$$

As pointed out, the cross-talk also depends on the position of the sample. Figure 9 below shows the cross-talk for a Mallinson coil set as a function of the position. The function again looks like a saddle, similar to the Sensitivity, but is now rotated by 45 degrees. The circle indicates the sample position as a function of the field angle caused by the wobble. One can conclude that the cross-talk is not constant but depends on the field angle. The field angle dependence of the cross talk is sinusoidal as well and has a two-theta component. It differs from the effect of the sensitivity in that it is a sine function.

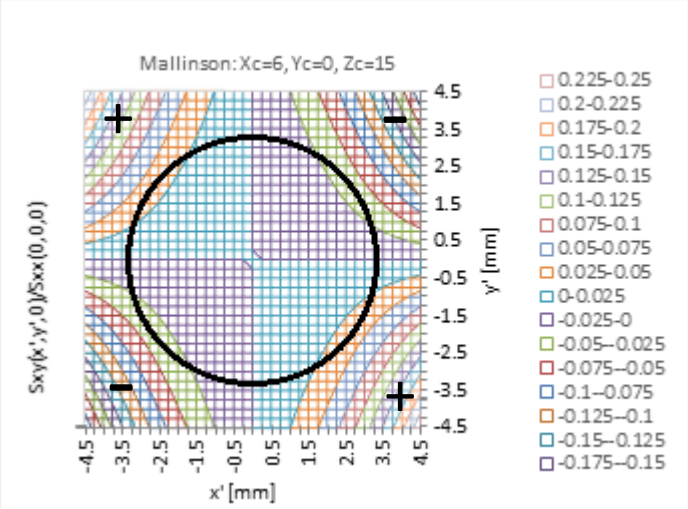

Figure 9: A Surface plot of the My signal generated in Mathematica based on the position of a sample in a VSM with a Modified Mallinson coil set.

Now if we assume that the sample is saturated in the x-direction, the earlier equations above are simplified because M_y is now negligible:

$$X \approx S_{xx} M_x \qquad [3]$$

$$Y = S_{xy} M_x \qquad [4]$$

So, if a wobble is present, S_{xx} and S_{xy} depend sinusoidally on the field angle with two-theta. The two-theta component in the y-signal will not be distinguishable from the two-theta component of the magnetic anisotropy, which causes large errors as illustrated in the figure below. Figure 10a shows a sample's torque measurement done with a vibrational head. Compared to figure 10b, the same mounted sample, measured on a torque head. We can see that the results are largely different with an added two theta component between the two.

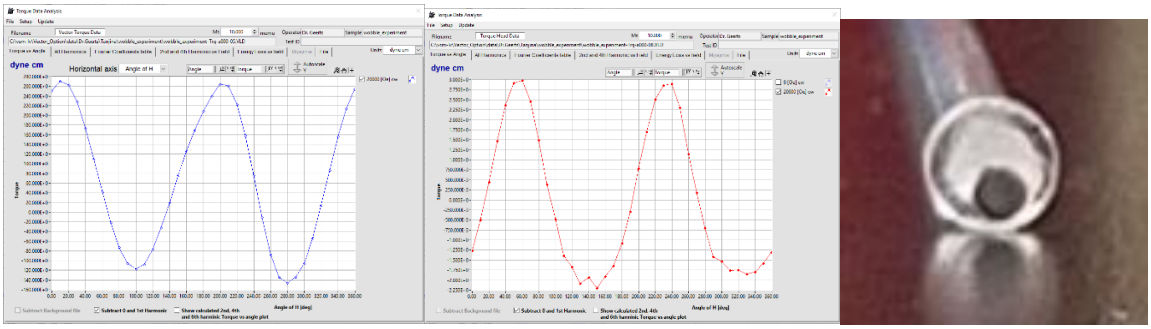

Figure 10: Biaxial torque (a) and true torque (b) curves of 2 mm mu-metal sample misaligned on 5 mm transverse rod (c).

Besides wobble, there are potential other causes for changes in the sample position, and these should be discussed as well for completeness. The first commonly encountered is the bending of the rod from uneven heating and cooling during measurements at low or high temperatures. In addition, thermal contraction of the sample rod might cause sample movement up or downwards. Note that sample shifts caused by thermal effects can have an additive effect on the wobble.

Another source for sample movement is the bending of the rods when measuring samples with a large magnetic moment (greater than 1emu, see Ch 5.4 for more details) under high magnetic field values. To prevent sample shifts from these magnetic forces, thicker sample rods could be used. However, doing so would introduce more material into the system and cause more background signal from the sample rod possibly obscuring the sample's magnetic moment in some cases. Note that this issue though unlike the deforming of the rod does not necessarily have an additive effect on the wobble as the bend in this case will follow the direction of the applied field.

Finally, there are also errors that are present from noise. These only become prevalent with samples that have a very low magnetic moment. This is the background noise that has many different causes. Some of the larger contributions to this can be

attributed to the VSM's functions. Coil vibration caused by the vibrations of the sample, Electrical noise from the electromagnets power supply unit, and imperfect vibration of the sample. These are not all the causes of noise on the system, but they are some that will have larger effects on the signals [Samwel]. One other cause of noise is the Johnson noise. This is directly related to the resistance the coils and is seen as the limit of VSM measurements.

Conventional VSM Alignment Procedure

The conventional method to align samples dates back to Foner's original paper on the subject (Foner, Versatile and Sensitive Vibrating-Sample Magnetometer, 1959). The method is used for all modified Mallinson systems and relies on the dependence of the detection coil sensitivity on the sample position. It looks for the saddle point of the sensitivity function shown in the section VSM Measurement Techniques. After inserting a sample into the VSM and engaging the vibrational head at a frequency of 75Hz, a field high enough to saturate the sample is applied to the sample so the M_x is maximal and constant. An added benefit is that the M_y component is negligible. The simplified equations of the section VSM Measurement Techniques now apply. The user will adjust the x position to minimize the X- signal. Subsequently the y position is adjusted to maximize the X-signal. This process is repeated for the x and y position until there is no longer any visible change. It is important though to mention that, as seen in the contour plots of Figure 7 of the Sensitivity, the region where the sensitivity is highest and lowest for the sample will be spread over a relatively large area. So, when positioning, carefully movement with micrometers is required for optimal centering of the sample. Besides the

x and y position it is also necessary at times to adjust the z position. This is done in the same manner as the y position. Adjusting the z position though does not affect signal greatly. After all of this the sample should be centered and ready to be measured using the VSM. The variation of the signal as a function of the x and y-positions of the sample are shown in Figure 11 below and summarize the conventional alignment procedure.

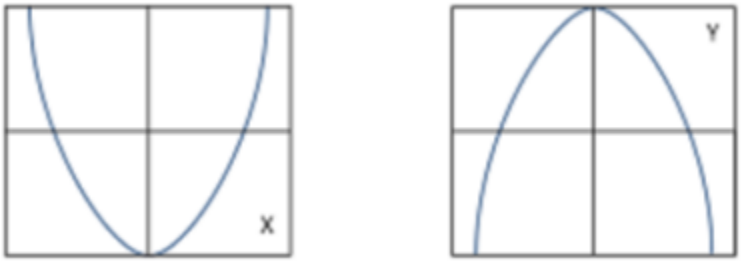

Figure 11: A depiction of the Signal from the x coil set based on the x position and then the y position.

Autonomous Alignment Method

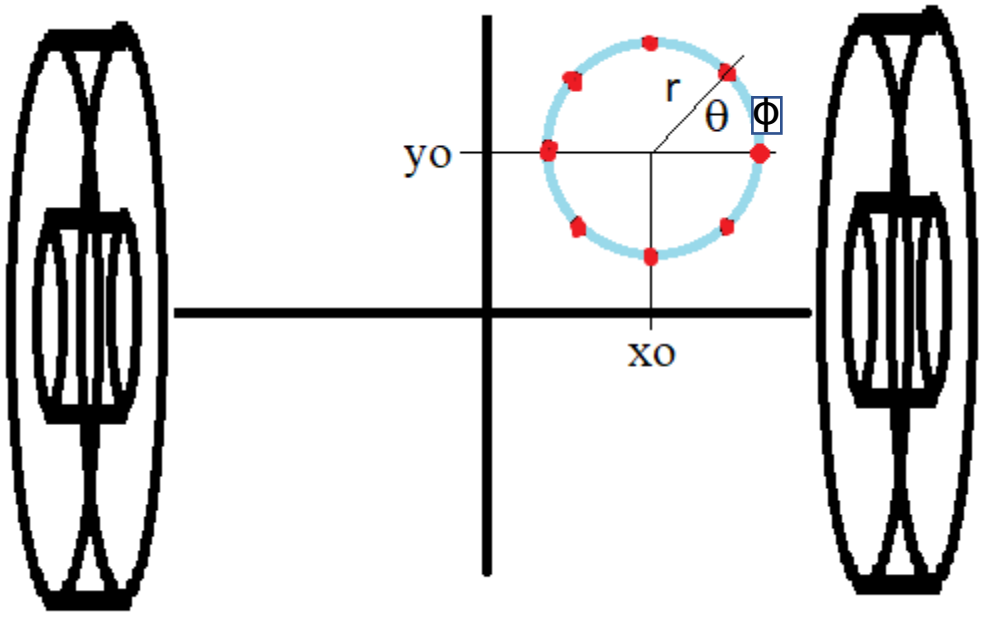

Figure 12: A top view of a Phi-scan showing its different components.

The new alignment method will use the signals form the coil sets on a Modified Mallinson VSM. As seen in the section VSM Measurement Techniques the samples change in position has a large effect on the signal of the coil sets. Here we do not move the sample linearly but move it in a circular trajectory. This effect on the signals will be similar to the effect of wobble however it will not be related to the field angle θ but depend on the polar angle φ of the circular trajectory. So, the signals will depend on the polar angle φ, the radius r of the trajectory, and on the position of the sample from its initial center position. Figure 12. Above shows an example of this relation which we will discuss further below.

Earlier (Fig 6, 8) we showed an example of the Modified Mallinson coil sets signals in relation to the sample's position. Using the traditional method of alignment

requires several scans across the signals to properly align the sample. If instead the sample were moved in a circle around a point at a radius r we would measure sinusoidal coil signals (see Fig 12.). Depending on where that sample's initial location was the shape of the sinusoidal wave changes. In particularly the 1ϕ components increase when the center of the circle is farther from the coil set center. Using this information we can determine the sample's position (x_o,y_o) with respect to the actual coil center. This means that instead of preforming multiple single direction scans by the traditional method a singular circular scan can be used to determine the exact position of the sample and to correct the sample's position to the center of the coil set.

The process for these scans as expressed above will require a circular scan around a central point (x_o,y_o). The circle will have a radius of r that can be changed as needed. Along this circular scan the sample will need to regularly stop and record data (see Fig 12.). These points will be decided by the angular increment φ. The signals collected along this circular scan can then be used to find the values for (x_o,y_o). This then tells us the sample's proper centered position as well. To accomplish this scan, process the movement of the sample will need to be automated.

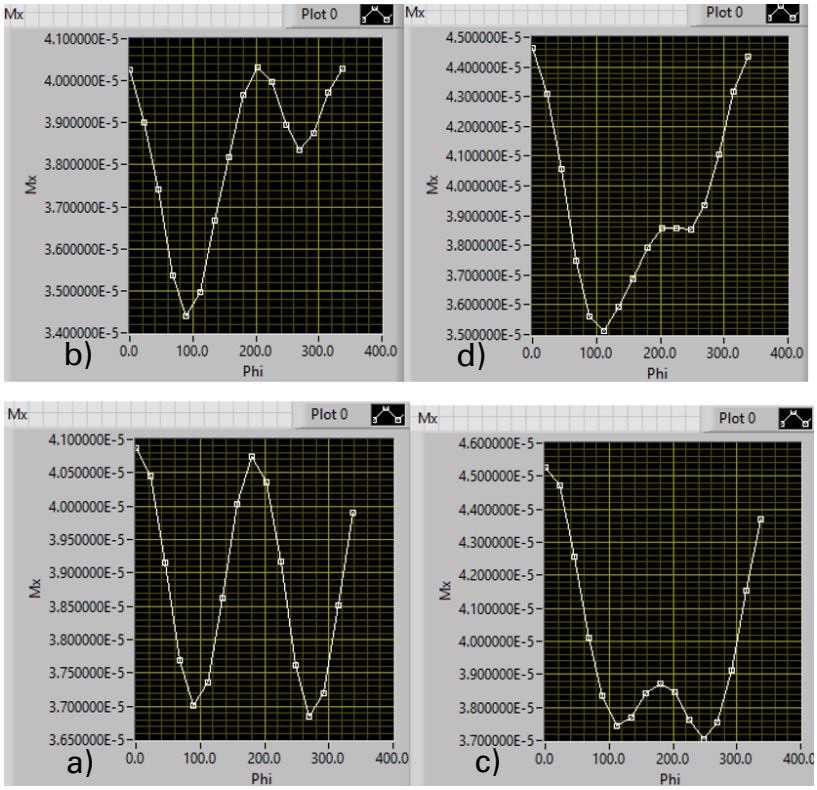

Figure 13: An example of four different Phi-scans around positions a) (0,0) b) (1,0) c) (0,1) and d) (1,1).

III. MATH REVIEW AND MODELING DISCUSSION

The physics behind the work done in this thesis is based solely on some of the most fundamental theories of electromagnetism. A VSM function relies on Faradays law of induction. This is how the magnetic moment of the samples is measured. The coil placement determines how a VSM makes these measurements. This chapter will discuss the general math and calculations used in the VSM and the calculations that went into finding the relations between the sample's position and the sensitivity. We will also, discus the model that was created for the modified Mallinson's coil set and the theories behind it.

Phi-scan Method discussion

The Phi-scan builds upon the thesis work of Binod D.C. who calculated the effect of wobble on the sensitivity and cross-talk for a Mallinson coil-set. A Phi-scan will move the sample in a circular trajectory in between the coil-sets. We assume that the sample is moved along the trajectory described by:

$$x' = r*\cos(\phi) + x'_o$$

$$y' = r*\sin(\phi) + y'_o$$

where (x',y') are the coordinates of the trajectory with respect to the center of the X-coil set, r is the radius of the Phi-scan, (x'_o,y'_o) is the center of the Phi-scan with respect to center of the X-coil set, and (r,f) identifies a particular point of the Phi-scan trajectory in polar coordinates with respect to the center of the Phi-scan (x'_o,y'_o). See also Fig. 11 of chapter 2. The Phi-scan trajectory can also be defined with respect to the center of the Y-coil set:

$$x'' = r*\cos(\phi) + x''_o$$

$$y''= r*\sin(\phi) + y''_o$$

where (x'',y'') are the coordinates of the trajectory with respect to the center of the Y-coil set, r is the radius of the Phi-scan, (x''_o,y''_o) is the center of the Phi-scan with respect to center of the Y-coil set, and (r,f) identifies a particular point of the Phi-scan trajectory in polar coordinates with respect to the center of the Phi-scan (x''_o,y''_o). As the sample is moved symmetrically around the center of the pickup coil set, both the X-coil and Y-coil signals will only show even sinusoidal terms, i.e., 2ϕ, 4ϕ etc. If the center of that circular scan is not centered within the pickup coil set, additional components are observed 1ϕ, 3ϕ, etc. So it is possible to determine the center of the Phi-scan (x'_o,y'_o) from the 1ϕ components. So the position of the Phi-scan center can be determined from a Fourier analysis of the X(ϕ) or Y(ϕ) signals. This allows us to find where the Phi-scan's center is relative to the center of the coil set. So, substituting f for q in the expressions Binod derived for the wobble we find the following expressions for the f dependence of the Phi-scan signals (Geerts & D. C., 2019) (D.C., 2019):

$$Sxx(x', y') \approx \frac{NA3\mu_0\alpha\omega Z_c}{4\pi\left[X_c^2+Z_c^2\right]^{\frac{7}{2}}} \cdot \left\{4\left(X_c - x'_o\right)^2 + 4\left(X_c + x'_o\right)^2 - 2\left(y'^2_o + Z_c^2\right) + 3r^2 + 4r^2\cos(2\phi) + 16x'_o r \cdot \cos(\phi) - 4y'_o r \cdot \sin(\phi)\right\} = A'_o + A'_\phi\cos(\phi) + A'_{2\phi}\cos(2\phi) + B'_\phi\sin(\phi) \quad [1]$$

&

$$S_{xy(x'', y'')} \approx \frac{60NA\mu_0\alpha\omega Z_c}{4\pi\left[Y_c^2+Z_c^2\right]^{\frac{7}{2}}}\{12r^2\sin(2\phi) + r(x''_o\cos(\phi) + y''_o\sin(\phi)) + x''_o y''_o\} = C''_o + C''_\phi\cos(\phi) + D''_{2\phi}\sin(2\phi) + D''_\phi\sin(\phi) \quad [2]$$

$$Syy(x'', y'') \approx \frac{NA3\mu_0\alpha\omega Z_c}{4\pi\left[Y_c^2+Z_c^2\right]^{\frac{7}{2}}} \cdot \left\{4(Y_c - x''_o)^2 + 4(Y_c + x''_o)^2 - 2\left(y''^2_o + Z_c^2\right) + 3r^2 + 4r^2\cos(2\phi) + 16x''_o r \cdot \cos(\phi) - 4y''_o r \cdot \sin(\phi)\right\} = A''_o + A''_\phi\cos(\phi) + A''_{2\phi}\cos(2\phi) + B''_\phi\sin(\phi) \quad [3]$$

&

$$S_{yx(x',y')} \approx \frac{60NA\mu_0\alpha\omega Z_c}{4\pi\left[X_c^2+Z_c^2\right]^{\frac{7}{2}}}\{12r^2\sin(2\phi) + r(x'_o\cos(\phi) + y'_o\sin(\phi)) + x'_o y'_o\} = C'_o +$$

$$C'_\phi\cos(\phi) + D'_{2\phi}\sin(2\phi) + D'_\phi\sin(\phi) \quad [4]$$

Where N is the number of windings of the individual coils, A is the cross sectional area of the coils, a is the amplitude of the vibration, w is the angular frequency of the vibration, (X_c, Z_c), (X_c, -Z_c), (-X_c, Z_c), and (-X_c, -Z_c) ((Y_c, Z_c), (Y_c, -Z_c), (-Y_c, Z_c), and (-Y_c, -Z_c)) are the position of the individual X-coils (Y-coils) whose Sensitivity is being measured, (x'$_o$,y'$_o$) ((x"$_o$,y"$_o$)) is the center of the circle of the Phi-scan trajectory the sample is moved around with respect to the center of the X-coil (Y-coil) set, and finally (r, ϕ) are the polar coordinates of the sample along said circles. It is clear from above expressions that the 1ϕ components are linear in x'$_o$, y'$_o$, x"$_o$, or y"$_o$. So determination of the 1ϕ components of X(ϕ) and Y(ϕ) should provide information on the position of the sample with respect to the center of either coil set.

This are the earlier mentioned circular scans introduced in chapter 2, which we refer to as the Phi scan. Its center distance from the true center can be determined from the f components. These scans are done symmetrically with a constant sampling rate at different polar angles f with a count of 2^N sample's for the complete scan. A further discussion of this process will be postponed until the section Phi Scan Program. For now the Phi-scan trajectory can be thought of as a circular trajectory around (x'$_o$,y'$_o$) or (x"$_o$,y"$_o$). The Phi-scans X(ϕ) and Y(ϕ) can be thought of as the angular dependence of the coil signals along that trajectory. Both are sampled symmetrically at every $2p/2^N$ polar angle. Using this sample rate allows the use of the Fast Fourier transform to

determine the harmonic components of the Phi-scan. To remove the effect of the constant factor in the 1ϕ components we take the ratio of the the phi component over the two phi component. This will allow us to determine the Phi-scan's center without needing a calibration.

For x' and y' the position relative to the X-coil set:

$$\frac{A\prime_{\phi}}{A\prime_{2\phi}} = \frac{16x\prime_o r}{4r^2} = \frac{4x\prime_o}{r}, \qquad \frac{B\prime_{\phi}}{A\prime_{2\phi}} = \frac{4y\prime_o r}{4r^2} = \frac{y\prime_o}{r}$$

So

$$\frac{r}{4} * \frac{A\prime_{\phi}}{A\prime_{2\phi}} = x'_o \qquad [5]$$

$$r * \frac{B\prime_{\phi}}{A\prime_{2\phi}} = y'_o \qquad [6]$$

And then again for x" and y" the position relative to the Y-coil set:

$$\frac{C"_{\phi}}{D"_{2\phi}} = \frac{x"_o r}{12r^2} => \frac{x"_o}{12r}, \qquad \frac{D"_{\phi}}{D"_{2\phi}} = \frac{y"_o r}{12r^2} => \frac{y"_o}{12r}$$

So

$$12r * \frac{C"_{\phi}}{D"_{2\phi}} = x"_o \qquad [7]$$

$$12r * \frac{D"_{\phi}}{D"_{2\phi}} = y"_o \qquad [8]$$

With these equations and the results from the Fast Fourier transform we can find the center of the Phi-scan and thus the distance the samples are from the center position of either the X or Y-coil sets.

General Math Used

Generally, the physics behind the VSM is surprisingly simple, a basic understanding of EMT is more than enough to understand what is happening. A VSM vibrates a magnetic sample in a magnetic field. The change in the position due to the vibration of the sample, causes the flux enclosed by the detection coils to change and this induces a voltage in the coils according to Faradays laws of induction:

$V = -N\frac{d\Phi}{dt}$, with N the number of turns in the coil and dΦ the change in flux.

Because the sample motion is periodic (sinusoidal), the change in flux is also periodic and this results in an AC signal in the coils. This voltage is measured with a lock-in amplifier which is basically a very sensitive narrow bandwidth AC voltmeter.

When a magnetic structure has an external magnetic field applied to it, a magnetic dipole is induced in it. This happens as the applied magnetic field acts on the spinning and orbiting electrons of the material, the force causing this is the Lorentz force, pulls the electrons changing their orbit. The magnetic dipole moment of the electrons then orientates itself parallel to the field, similar to a compass needle lining up along the magnetic field of the earth. This orientation of the magnetic moments creates a bound current across the surface of the magnetic material, however, these currents are not released from the atom, so they cannot be directly measured by an ammeter. They do though create a magnetic field around the sample that can be measured. To do this though

we need to develop and understanding of the equations behind the magnetic field. We will start by looking to the bound currents of a magnetized sample which can be calculated from the magnetic moment volume density M via (Griffiths):

$$\vec{J}_b = \nabla \times \vec{M} \quad [9]$$

$$\vec{K}_b = \vec{M} \times \hat{n} \quad [10]$$

The bound currents can be used to calculate the magnetic vector potential **A**. The curl of **A** is the magnetic induction and using the reciprocity theorem should also relate to the induced voltage on the VSM's coil sets.

For a homogeneously magnetized sample the bound volume current density is zero and only a surface current density remains as shown in Figure 14 below. Another way to think about the magnetic stray field of a magnetic sample is that it originates from the north and south poles (Jackson equation 5.100):

$$\rho_m = -\nabla \cdot \vec{M} \quad [11]$$

$$\sigma_m = \vec{M} \cdot \hat{n} \quad [12]$$

The magnetic poles can then be used to calculate the scalar magnetic potential and the gradient of the scalar potential is the **H**-field. These processes are well understood and can be found in many textbooks like Jackson and Griffiths. Depending on the structure of the material and in cases like thin film materials what the layers are made of varying dipole strengths can be seen.

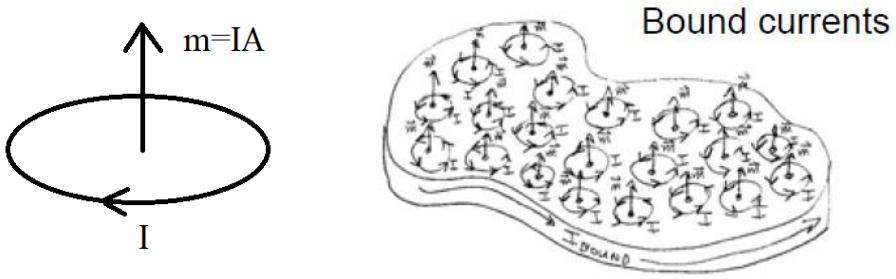

Figure 14: Magnetic Dipole (left) and bound current density of a magnetized sample (right)

The sample's dipole moment produces a magnetic field around the sample and in the detection coils. When the sample vibrates this will induces a current in the detection coils due to the changing field. For a VSM, samples are small, typically a few millimeters wide and tall for two reasons: (1) it is difficult to vibrate a larger sample at a frequency of 40-80 Hz; (2) For larger samples not all parts of the sample equally contribute to the measured signal.

Mathematica Modeling

Bernards' paper (Bernards, Design of a detection coil system for a biaxial vibrating sample magnetometer and some applications, 1993) (Zijlstra, 1967) describes the field generated by a coil given the inner and outer diameter and length. Using the reciprocity theorem from Mallinson's paper [Mallinson] it provides us with an interesting opportunity to create a working model of a modified Mallinson VSMs coil set based on the sensitivity of the individual coils. The expressions derived by Binod D.C. for the sensitivity and cross-talk assume that the coils are infinitely small. Bernards however assumes coils with finite dimensions, so his approach is a more realistic way to model the VSM coil set. Creating such a model is important as it will allow us to test the

mathematical procedure that we will use for our scans to determine the sample's center position with less assumptions. For this modeling we used Wolframs Mathematica. This software provides an easy way to implement the equations using its math-based language. The model allowed for the calculation of the Sensitivity and Crosstalk as a function of the position, as well as the determination of the position of the sample from the Phi-scans. Since this model is based on the equations in Bernards' work, we first define the main constants based on the VSM that we will be using at Texas State: the coil positions (which are uniform for each set) and the coils inner and outer diameter and length.

With these defined we can begin setting up the equations to be used for the model. Bernards' calculates the sensitivity of a single coil from the reciprocity theorem. The mutual inductance between the coil and the sample is the same for both directions, i.e., $M_{coil\ sample} = M_{sample\ coil}$, where $F_{coil} = M_{sample\ coil} * I_{sample}$ and $F_{sample} = M_{coil\ sample} I_{coil}$. Assuming that the sample is a point dipole one can determine the mutual inductance between the sample and the coil from the mutual inductance between coil and sample. This can be calculated from the magnetic scalar potential of the extended coil, $V_c(x,r)$. This defines the coil's potential along its x axis. The radius in the equation though defines the radial distance from the sample to the coils center. The magnetic scalar potential has to have azimuthal symmetry. The sensitivity and cross talk of a singular coil is equal to the z-derivative of the gradient of the potential.

$$\text{Sensitivity: } S_x = \frac{d^2}{dx\,dz} V_c(x,r)$$

$$\text{Crosstalk: } S_y = \frac{d^2}{dy\,dz} V_c(x,r)$$

One of the derivatives originate from the fact that the field is the gradient of the electric potential, and the other originates from the vibration in the z-direction.

The potential described here is written as $V_c(x,r) = \sum_{l=1,3,5,..} B_l \frac{1}{r^{l+1}} P_l\left(\frac{x}{r}\right)$ where the B_l values for the first three coefficients are calculated by hand. To the Right of the B_l values is a Legendre polynomial of the x position of the sample and the radial distance to the sample. To again simplify things, the calculation of the polynomials is saved for later in the worksheet. The position and the coefficients for this are also listed in Jan Bernards' paper. Below are the three smallest values for B_l.

$$B_1 = \left(\frac{C_b}{2}\right)^2 \frac{\beta}{6}(\alpha^3 - 1)$$

$$B_3 = -\left(\frac{C_b}{2}\right)^6 \frac{\beta}{120}[9(\alpha^5 - 1) - 20\beta^2(\alpha^3 - 1)]$$

$$B_5 = \left(\frac{C_b}{2}\right)^4 \frac{\beta}{336}[15(\alpha^7 - 1) - 84\beta^2(\alpha^5 - 1)]$$

Where α and β are just

$$\alpha = \frac{C_d}{C_b}, \qquad \beta = \frac{C_l}{C_b}$$

Here C_d is defined as the coil diameter, the C_b is the coil bore (inner diameter), and the C_l is the coil length [Bernards, 1992].

This gives us the general equations we will need to model the coils used in the VSM. For simplicity we will only be using the two x-coil sets as the Crosstalk can be found by rotating the x coil sets 90 degrees. We start by first defining the three B constants listing α and β constants in their alternate forms. From here we list the individual magnetic potentials for each of the four coils doing this by alternating their coil positions in the x and z planes. The equation for sensitivity of the sample is then determined by taking the derivative first with respect to x and then z also here is when the earlier mentioned Legendre polynomials are calculated. To make this work with the Phi

scan technique we replace the x and y components with the forms $x = x_o + \rho cos(\phi)$ and $y = y_o + \rho sin(\phi)$. From here it is just a matter of inserting the sample's parameters, using the position the sample will be located at, and plugging in the radius of the Phi-scan (p).

Later, the model was adapted for other uses for both this project and for other work by fellow students. The modifications made to this were varied but two stood out: one was to give a contour plot of the area between the coils for the Sensitivity and the other to imitate 3D printed samples with finite dimensions and find their Sensitivity. It will also be possible to adapt the model and investigate how imperfections of the coil set affect the ability to determine the exact position of the sample. The coils could be slightly misoriented with respect to each other or have a small difference in the number of windings. And with this type of model those defects can be accounted for and be correlated to experimental values.

Correction Methods

One of the issues found later in the research (which led to a new alignment method being considered) was that the equations originally used were incomplete. After initial testing of the Phi-scan method, it was noticed that for samples that were largely misaligned, the accuracy was much lower. It appeared that the two phi components are not constant but depend on the center position of the Phi-scan trajectory i.e., x'_o and y'_o (x''_o and y''_o). This was a fundamentally large issue for samples that were misaligned by larger distances. Attempts were made at first to correct for this issue by assuming that the two phi components of the sensitivity and crosstalk contained a quadratic term Ax^2 - By^2

$$Sxx(x',y') \approx \frac{NA3\mu_0\alpha\omega Z_c}{4\pi\left[X_c^2+Z_c^2\right]^{\frac{7}{2}}} \cdot \{4\left(X_c - x'_o\right)^2 + 4\left(X_c + x'_o\right)^2 - 2\left(y'^2_o + Z_c^2\right) + 3r^2 + r^2(4 + A'x'^2 - B'y'^2)\cos(2\phi) + 16x'_o r \cdot \cos(\phi) - 4y'_o r \cdot \sin(\phi)\}$$ [13]

&

$$S_{xy} \approx \frac{60NA\mu_0\alpha\omega Z_c}{4\pi\left[Y_c^2+Z_c^2\right]^{\frac{7}{2}}}\{r^2(12 + A''x''^2 - B''y''^2)\sin(2\phi) + r(x''_o\cos(\phi) + y''_o\sin(\phi)) + x''_o y''_o\}$$

[14]

This drastically affects the resultant equations for the x and y positions.

For x' and y'

$$\frac{A\prime\phi}{A\prime_{2\phi}} = \frac{16x\prime_o r}{r^2(4+A'x'^2 - B'y'^2)} = \frac{4x\prime_o}{r_{(4+Ax'^2 - B'y'^2)}}, \qquad \frac{B\prime\phi}{A_{2\phi}} = \frac{4y\prime_o r}{r^2(4+A'x'^2 - B'y'^2)} = \frac{y\prime_o}{r_{(4+A'x'^2 - B'y'^2)}}$$

So

$$\frac{r_{(4+Ax'^2 - By'^2)}}{4} * \frac{A\prime\phi}{A\prime_{2\phi}} = x'_o, \qquad r_{(4 + A'x'^2 - B'y'^2)} * \frac{B\prime\phi}{A\prime_{2\phi}} = y'_o$$

For x'' and y''

$$\frac{C''\phi}{D''_{2\phi}} = \frac{x''_o r}{12r^2_{(4+A''x''^2 - B''y''^2)}} => \frac{x''_o}{12r}, \qquad \frac{D''\phi}{D''_{2\phi}} = \frac{y''_o r}{12r^2_{(4+A''x''^2 - B''y''^2)}} =>$$

$$\frac{y''_o}{12r}$$

So

$$12r_{(4 + A''x''^2 - B''y''^2)} * \frac{C''\phi}{D''_{2\phi}} = x''_o, \qquad 12r_{(4 + A''x''^2 - B''y''^2)} *$$

$$\frac{D"_{\phi}}{D"_{2\phi}} = y"_{o}$$

To use this method though, we would first need to find the A and B values for the X-signal and the Y-signal. The difficulty then becomes finding the position using the quadratic formula. After several attempts to use this method, the accuracy was found to be no better than the original and at times worse, so we moved on to a different approach. Rather than calculate the position from both the 1ϕ and 2ϕ components we introduced calibration constants called D and E that relate the f components to the motor position coordinates. The program uses these calibration constants to calculate the position from the phi-components, i.e.

$$x'_{o} = A'_{\phi}/D' \qquad y'_{o} = B'_{\phi}/E' \quad x"_{o} = D"_{\phi}/D" \qquad y"_{o} = E"_{\phi}/E"$$

In this thesis we will refer to this approach as the calibrated Phi-scan method.

The 2ϕ component is not in actuality a constant as shown above but rather has a small non-linear term that grows or shrinks with position. To deal with this we instead chose to use a correction value for the sample's one phi component. These values are linear vs the position and can easily be found with just a normalizing constant. To validate this, we worked with MSEC student Chandan Howlader to create an analytical solution to these issues and were able to generate several sets of data presented below in figures 15 and 16. The issues can be seen in figure 15(a) and 15(b) where there is clearly a linear relation to the one phi component vs the position. Shown in figure 16(a) and 16(b) are the two phi components which are not constant and depends on the sample position. So, the equations above that use the 1ϕ and 2ϕ components to determine the center of the Phi-scan only work for points near the center. For larger distances away

from the center of the coil set, these equations are not correct.

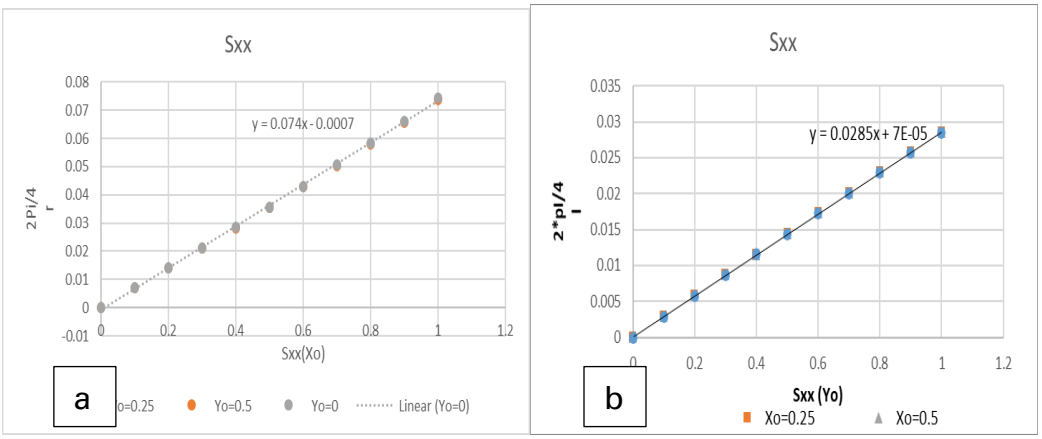

Figure 15: These graphs were found analytically with the help of Chandan Howlader showing a Linear one phi component for a) the real and b) the imaginary X-coil set signal.

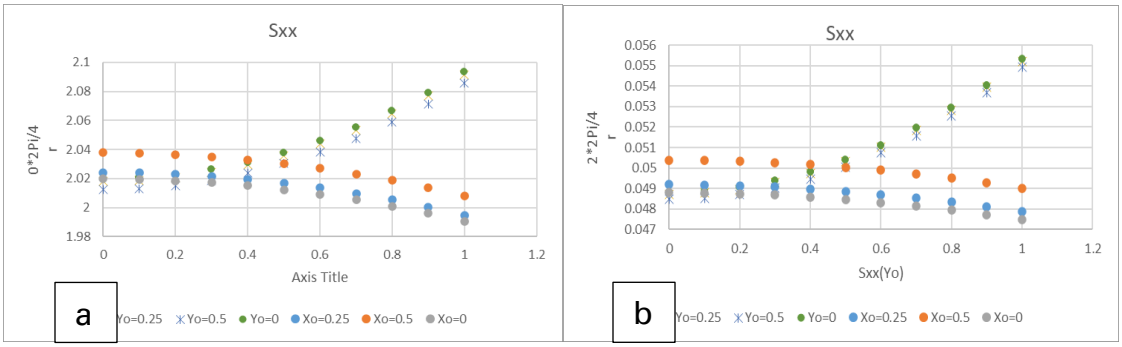

Figure 16: These graphs show a) the DC component vs the position and b) the Non-Linear two phi component X-coil set signal.

To solve this issue a new method referred to now as the Calibrated Phi-scan method, was used. This method first measures the relation between the sample position and 1ϕ components of the different coil sets. This relation is approximated using the slope formula of a straight line to find the position based on the 1ϕ components. These corrections will need the addition of an initial scan sequence. For this sequence, the sample is first centered with the original method and then three Phi-scans are done. One at 1mm in the x and y direction, the next at the center position, and the final at negative 1mm in the x and y directions. After this the different 1ϕ components are then used to generate the D and E callibration values. The values are referred to for the X-coil set as

D’ for the real component and E’ for the imaginary component, and for the Y-coil set D” and E”. From then on whenever a scan is preformed it can call these values and determine its new center position from the 1ϕ components.

IV. LABVIEW PROGRAMING AND METHOD

LabVIEW was chosen mainly as mentioned for compatibility with the MicroSense VSM software suite. There are other benefits though one of them being simplicity. The Physics department at Texas State has many pieces of equipment that use LabVIEW. Because of this there are many people versed in the language and able to provide guidance on the work. For this project, several different scans and programs were developed. These programs focused on communication between the different pieces of equipment used for scans. These components included the Gauss meter and power supply used to control the field strength on the VSM. The system's Lockin amplifiers for reading the signal on the coils. Finally, the Motor controllers with LabVIEW functionality or with the capability to build in said functionality.

Motor Controller set up

During the initial program testing it was decided to first use an older Oriel Encoder motor setup for testing with the VSM. However, as testing moved forward the limits of the older systems functionality and their precision became apparent. A modern set of Thorlabs Motor controllers was then purchased to replace the Oriel Encoder setup. This lead to several issues as the way the two controllers communicated through LabVIEW was fundamentally different. Thanks to the setup of the programing though the issues were contained in one singular program. For now, we will go over the two separate controllers and their general abilities.

Oriel Controller

Preliminary experiments were done with two Oriel encoder Mikes and a controller. These were bought second hand to reduce testing cost. The Oriel Encoder Mikes and the model 18011 Oriel Encoder Mike controller has been in use in lab spaces since the 1990s. It provides a fully contained package with three servo motors drivers per controller, a serial port for read and write commands, and several different motor functions and controls. The motor controller contains two nonvolatile memories for an Absolute and Relative positioning, which are kept for each of the three separate motors. Its functions allow for control over step sizes and of the velocity of the steps. The Oriel Encoder Mikes that are used with the controller have a minimum step size of 0.1um with a unidirectional repeatability of +/-2um. Although an older system, the Oriel motor controller does have serial I/O via a 25 pin D-connector that allows for remote control through software. LabVIEW specifically has a built-in functionality to communicate with serial devices which helped immensely.

It should also be noted that due to the age of the controller an adapter serial connecter had to be made to allow the controller to be connected to a 9 pin D-connector of a USB to RS232 convertor. The commands for control had to be researched then hard coded to work correctly and a write up of this can be found in the appendix. The Computer control allows for easy access to the two current motor positions and furthermore allows for control of most of the controller's functionality. It does not however have very fast access and the position cannot be accessed while the motors are in motion. Another limitation for this device is that only one motor can be controlled at a time meaning motors must be moved one at a time so synchronous motion is impossible

increasing scan times significantly. The motors though were very useful as they retained their position after each power cycle and unless moved while unpowered retained high accuracy. The maximum speed of the motors depends on the axial load and is 260 um/sec for zero load and drops below 100 um/sec at 15kgf. The minimum linear speed of the motors was 0.5 um/sec.

Thorlabs Motor Controller

Figure 17: Pictured above is the Thorlabs Motor Control units for the X and Y stages.

The Oriel Encoder Mikes and controller were replaced by a Kinesis K-Cube Brushed DC servomotor system from Thorlabs seen in figures 17, 19, and 21. We chose two Thorlabs KDC101 Brushless motor controllers paired with two Thorlabs Z812 DC Servo Motor Actuators. The Controllers were mounted to the KCH301 control Hub (Figure 17.) to reduce system complexity. The Thorlabs Motor controller set provided several benefits over the Oriel system. First being it is a modern and available system with updated connection standards. Other improvements included that the system's communication now allows for simultaneous control of the motors, resulting in

significantly reduced scan times. Also, the motors allowed for overall more control of system parameters like individual motor acceleration to velocity (see spec sheet below for ranges) [Thor_Z812]. The maximum velocity that can be achieved with these motors is noticeably higher than the Oriel motors. This speed increase reduced required scan times by 90%. We can also now determine the position while in motion and unlike the Oriel, the system also has built in LabVIEW support.

This change to the Thorlabs servomotor controller also resulted in many issues, because the provided drivers and communication was much more complex than the Oriel drivers. The .net LabVIEW drivers provided by Thorlabs were used. This software was much more complex compared to the serial commands of the Oriel controller and required more programing to prevent issues with scans. This sometimes led to errors in data acquisition when testing and significant time delays to rework the programs were encountered. The other issue present is that the Thorlabs Controller only has one position saved in memory per motor. This can be worked around but the programming was initially built to work with two separate position values, so changes were required. Also, it must be mentioned that though the Thorlabs motors have more precision than the Oriel Encoder Mikes, with a minimum incremental movement of 0.05μm and a minimum repeatable movement of 2μm. Other specifications for the Z812 Encoder motors can be found in the included specification sheet below. However, on startup it must home to the minimum limit switches to determine its exact position meaning when power is cycled all position information is reset to zero and registration is lost.

Specifications	Value
Travel Range	12.0 mm
Backlash	<8 µm
Bidirectional Repeatability	<1.5 µm
Home Location Accuracy	<2 µm
Homing Repeatability	±1.0 µm
Vertical Load Capacity	4.5 kg (Max)
Horizontal Load Capacity	9 kg (Max)
Vertical Load Capacity[a]	<4.0 kg
Horizontal Load Capacity[a]	<7.5 kg
Velocity[b]	2.6 mm/s (Max)
Acceleration	4 mm/s^2 (Max)
Absolute On-Axis Accuracy	95 µm
Maximum Percentage Accuracy	0.82%
Motor Type[c]	6 VDC Servo
Motor Coil Temperature	85 °C (Max)
Phase to Phase Resistance	33.0 Ω (Max)
Phase to Phase Inductance	0.6 mH (Max)
Limit Switch Life Time	<100,000 Cycles
Minimum Achievable Incremental Movement	0.05 µm
Minimum Repeatable Incremental Movement	0.2 µm
Operating Temperature Range	41° to 104° F (5° to 40° C)
Weight	0.134 kg

a. Recommended
b. At 2.6 mm/s, velocity ripple and distortion of the acceleration/deceleration profile may occur. For improved control, the maximum velocity should be limited to 2.3 mm/s.
c. The nominal motor drive voltage is 6 V. Voltages up to 12 V can be used with pulse width modulation (PWM) controlled outputs. [Thor_Z812]

Figure 18: The specification sheet for the ThorLabs servo motors.

VSM Modifications

When installing the servo motors to the system, several changes were needed to make the set-up work. The MicroSense VSM at Texas state university was designed to allow the vibrating head to be tilted up and be slid to the side allowing a torque head to be used. This means the x position of the sample is controlled directly by this x stage, which for the system is a sliding stage and the y position of the sample is controlled by the tilt of the vibration head which is a rotational stage. So, changes in the y position also imply changes in the z height of the sample. These stages are physically aligned with a

screw and a micrometer. The screw is located on the far left edge of the sliding stage controlling the x stage. The micrometer is located right below the vibrating head controlling the y position of the sample through a rotation with respect to the electromagnet's core. The sample is located roughly a half a meter from the rotation point of the vibration head and the servomotor is approximately 15cm from this point.

This set up while fine for most alignments does not lend itself to high precision. The connection of the sliding stage to the screw was a large magnet. This approach was not compatible with the motors, so two springs were added that pulled the stage against a micrometer and servo motor. This allowed for reproducible x-control in both the positive and negative direction. The rollers on the x-stage add a slight mechanical hysteresis to the system which was solved for in the software. The y stage rotation reduces the resolution for the y-position as the motor is mounted far from the sample so there a 1 to 3 reduction in the precision due to this, as well as a small change in z height when y is moved. The change in z height should have negligible effects as the maximum change in height that can be experienced is 0.05mm which is too small to make any noticeable changes in signal occur. We also planned to allow for manual movement without the motors so on each stage we added a micrometer parallel to the servomotor so the machine can still be manually aligned with the micrometers.

X-stage Modifications

Figure 19: Pictured above is the redesigned X stage mount for the Motor and Micrometer.

Figure 20: Pictured above are the brackets set up for the springs on the x stage.

The first change that was made to the x stage was a redesign of the x stage manual control. Originally this control was through a fine thread screw in a straight aluminum block secured to an aluminum platform holding the vibration head and torque-head structures. This block contained a fine-thread screw connected to the lower rolling stage by a permanent magnetic coupling. Turning the screw would adjust the x-position of the linear x-translation stage holding the vibration head. To replace the screw with two micrometers the straight aluminum block was removed and replaced by an L-bracket from plexiglass. To account for the shorter distance of the servo motor and manual micrometers, the straight aluminum block was replaced with a L bracket placing the edge closer to the upper rolling stage and giving us a larger movement range. This L bracket had two holes drilled side by side on the upper bracket allowing the manual micrometer to be mounted parallel with the servomotor driven micrometer. Two smaller holes were

added on the lower bracket matching the mounts for the old bracket, it was fastened down with a pair of bronze bolts after this.

In addition to this bracket, we added in two Hillman extension springs (11/32x2-3/8x0.035", 0.47 kg safe working load, working extension 1') to pull the upper rolling stage towards the micrometers. The springs applied roughly 2N of force on the stage. To secure the springs two brackets were added: one to the X-translation stage and one to upper platform of the translation stage. The upper bracket was 7"x3"x2" and the lower bracket 6"x1.5"x1.5" made of stainless steel sheet metal that had 90 degree bends on each side. They were then mounted with the bent sections facing inwards with one under the L bracket and the other at the edge of the X-translation stage. The springs were then added insuring they were equal distance from the edges of both brackets so that during travel they would not slip off the mount (seen in Fig 20).

Y-stage Modifications

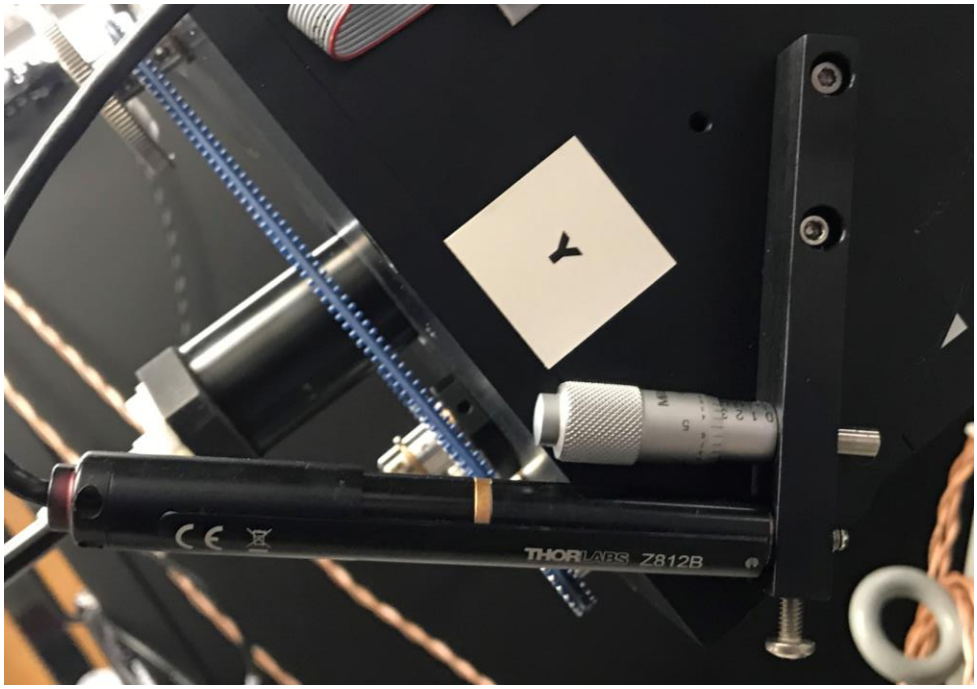

Figure 21: Pictured is the modified Y stage Bracket Motor and Micrometer.

For the y stage adding the servo motor merely required drilling a second hole into the system's current aluminum bracket that holds the y-micrometer (seen Fig. 21). To secure the motor a small side hole was drilled and tapped to allow a screw to secure the motor. The issue with the 1 to 3 ratio though first required a physical adjustment to the software to ensure that the given step sizes were corrected for the angular ratio. We also later conducted a more stringent verification of the ratio by inserting a 5mm transverse rod and then recording the movement distance of the rod vs the extension of the motor head. Also, another issue encountered later was slight changes in sample position from the flexing of the Thorlabs servomotors ridged wiring. This was fixed by creating a more secure mounting layout for the wiring and to ensure that the wiring was free to move where necessary when the x stage was in motion but did not pull on the rotational head as the x or y stage moved.

Generalized Programs

Before going into a more detailed discussion on the main programs, the base programs that allow for communication between the motor controllers, the VSM hardware, and other pieces of hardware is discussed. The main base program is termed the SubVI. This is the only VI with any direct commands to the Motor controllers as in all commands to the controller are located here. This was done for safety as well as simplicity when a position is given to the motors they first go through a check to confirm they are within the preset limits of the machine. These limits are also dependent on the type of rod in use which provides even more assurance for scans. This set up also helps with controlling the motors as for motor control first an instance needs to be created, which is then carried on through the main programs till their end, where it is then terminated. It was easy to accomplish this with a singular VI as it was only located there, and any calls were easy to order into the proper sequence to ensure that the motors operated correctly. Also, the VI was set up such that multiple instances of it could be opened at once.

From here we have several other VIs that called specific functions in the SubVI like a move function, a current position function, and finally a function to control the initialization process. There are also programs that we call to gather data form the VSM or control the VSMs settings. These programs rely specifically on the MicroSense LabVIEW package, so we have access to most basic commands for the system this means field control, angle control, and the Lockin amplifiers sensitivity readings.

Finally, for ease of use we created a unified program containing all the different VIs to accelerate testing procedures. This software is designed to allow quick calling of

all the different available scan methods as well as moving the sample manually it also will display current motor position, X and Y Lockin amplifier signals, and field strength values. It also allows the use of a more simplified but slower alignment process referred to as linear scans. Linear scans are an automated version of the traditional alignment process. It measures the coil signal as a function of the sample's x or y position and then determines the minimum or maximum of the curve. You can find the main GUI of the unified program in the figure below with its readouts cleared.

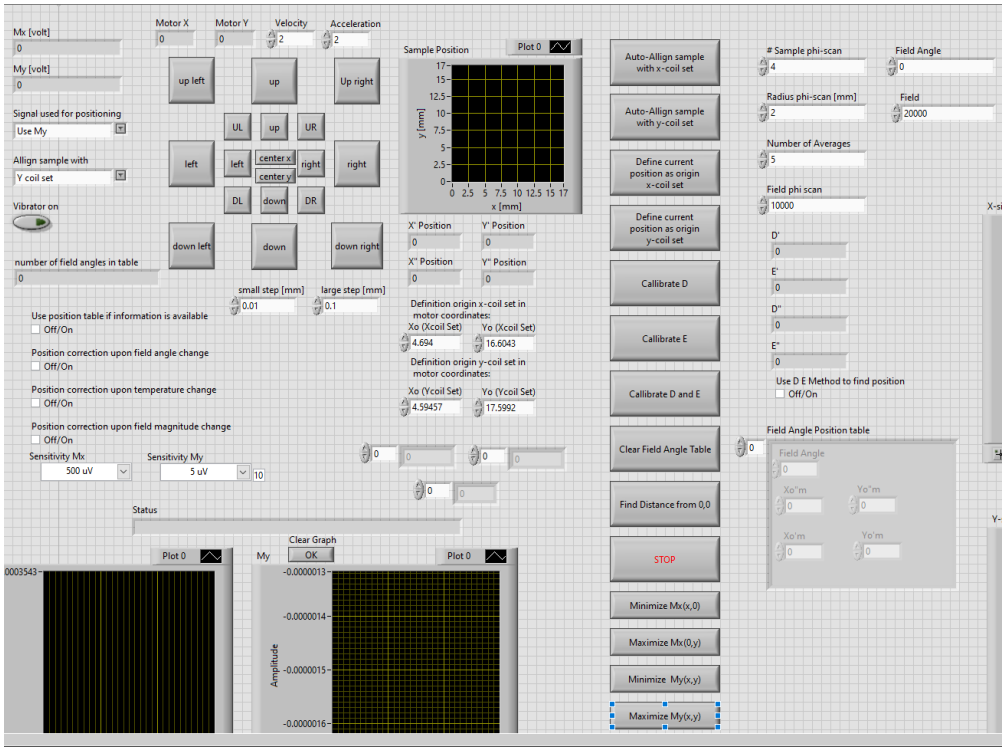

Figure 22: Pictured here is the general programs main screen and the options available to users.

Phi Scan Program

The main scan program is the Phi-scan which begins by checking the motors status and homing them if necessary. It will then if applicable initialize the VSM hardware to the preset values stored in another VI. After these two processes

are complete, we move to the actual scan. The scan begins by first checking the resolution. This refers to the number of sample positions during the scan which should be a power of two (2^N). This is done to ensure that it is possible to use the Fast Fourier Transform algorithm when determining the position from the phi-scan data. Note that N is the resolution of the scan and will determine the number of points sampled for a full circle phi-scan.

Inside this loop is where motor movement and data collection will occur. First, we choose the current location of the sample as the center of a circle with a radius R. The polar angle of the sample position is then determined by dividing 360 by the resolution number then multiplying by the current loop's iteration. This gives us the polar angles we will use with a radius R to find the X & Y change in position of each scan point. Once these two values have been determined, it is then sent to the move program so the motion of the X & Y Motors can begin. This all occurs in a sequence to ensure proper call order. The X & Y Motors are called simultaneously this is to speed up movement.

The next sequence begins a wait timer to allow reduction in the rod vibrations from the earlier x and y movements. Once the wait timer ends the current X coil and Y coil signals are collected into an array and displayed to the user. After all points have been scanned the array values for the X coil signal, Y coil signal, and the angles are saved to a text file to be accessed by the interpreter VI which will determine the center position of the phi-scan with respect to the X-coil set and Y-coil sets. Note that the general information about the sample is saved as well. After this, the VSM if necessary is reset to initial values and similarly the motor controllers are also returned to the center position and, if necessary, the motors are disabled.

Data Interpreters

The data obtained by the Phi-scan VI is interpreted by two other VIs. The interpreters will open the text file containing the Phi-scan data and depending on the coil set we are aligning to, will read the X-coil signal or Y-coil signal, the angular values, and the radius. The data is then fed into a Fast Fourier transform VI which returns the real and imaginary 1ϕ and 2ϕ components. These will then be separated into two arrays containing the coordinates of the center position of the phi-scan with respect to either the X-coil set, or the Y-coil set. From here we begin the analysis. Two methods were used for determining the position those being the Phi-scan method and the Calibrated Phi-scan method. These two methods were used at various intervals either for testing or for actual sample alignments. The Phi-scan method is completely independent only reliant on a singular scan and uses the 1ϕ and 2ϕ components. While the Calibrated Phi-scan method will require a calibration scan process for the current sample and only uses the 1ϕ component. The reason this is necessary is that at larger distances from the center the samples 2ϕ components is no longer constant and changes with the distance which has a large effect on the center position determined with the Phi-scan method. An example of the issues this can cause can be seen in Figures 23 and 24 which show a scan process using the Phi-scan method to align at various points.

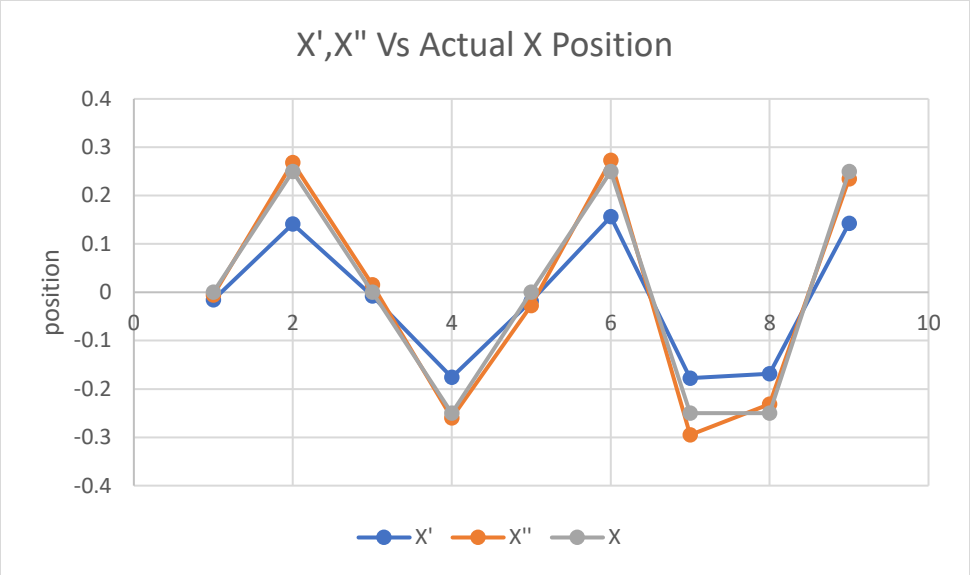

Figure 23: An Example of the deviation of the x position from the actual movement of the motors for the Phi-scan method of alignment for motor positions (0,0), (0.25,0), (0,0.25), (-0.25,0), (0,-0.25), (0.25,0.25), (-0.25,-0.25), (-0.25,0.25), (0.25,-0.25).

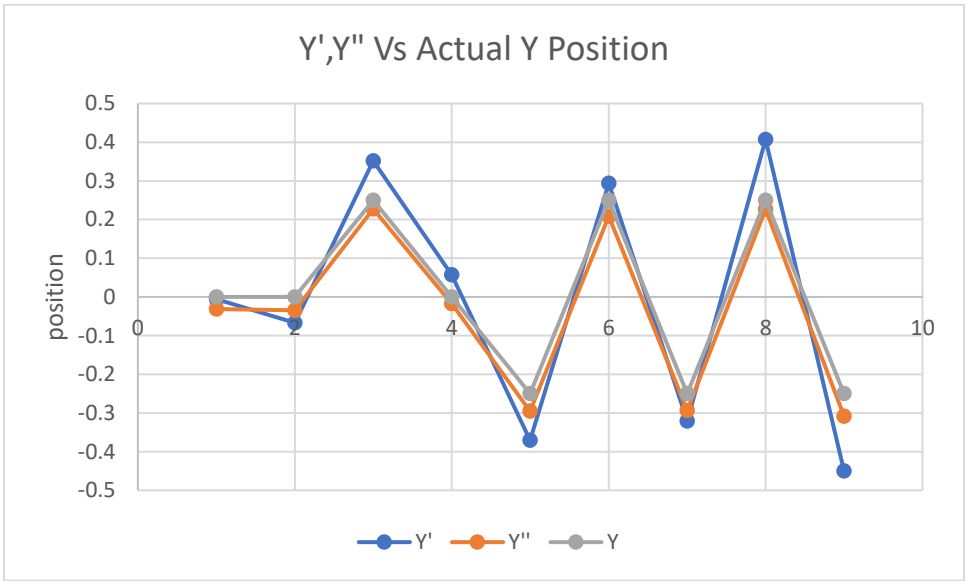

Figure 24: An example of the deviation of the y position from the actual movement of the motors for the Phi-scan method of alignment for motor positions (0,0), (0.25,0), (0,0.25), (-0.25,0), (0,-0.25), (0.25,0.25), (-0.25,-0.25), (-0.25,0.25), (0.25,-0.25).

The Calibrated Phi-scan method uses the relation between the motor position and the 1ϕ components of the Phi-scan. This relation is approximated by a straight line and measured during a calibration step just after loading the sample. The slope value for the 1ϕ component of the X-coil signal versus the x motor position (D' for cosine term and E' for sine term) and the Y-coil signal versus the y motor position (E" for sine term and D"

for cosine term) are measured during the calibration step. These D and E values can be used to find the exact position of the sample from the 1ϕ components. Generally, how this is done is first the needed values, discussed earlier, are inserted into the respective case structure. For the independent method, the values are inserted into a formula node where in the X-coil signal and Y-coil signal position relations are used to find the x and y position based on the 1ϕ and 2ϕ components. The second method merely reads the slope values for the sample and then determines the x and y position with this. As a side note the slope values are found by a systematic process that uses the independent method and known changes in position to find the values needed which are referred to as D and E callibration values. For our samples we typically found values around those seen in Table 1.

Table 1: Here the typical D and E callibration values for our samples are shown.

D'	D''	E'	E''
0.0002872	-0.000127314	-0.00015356	-0.000148211

Other Scan Options

As the project went on it was decided to add more diverse scan options to allow the collection of data not just to align but to check the accuracy of the methods. These Scan methods are also useful outside of this thesis project as they provide new and interesting test oppertunities for others.

Angular Scan

The first of these methods is an angular scan program. This is a combination scan

of Phi scans and a singular X-coil signal and Y-coil signal scan. The reasoning for this is to determine the quality of corrections for the sample shift originating while changing the field angle. One first measures Phi-scans as a function of the field angle. So, the sample is rotated through 360 degrees and multiple phi scans are taken along set field angle increments. Once these scans are complete the interpreter VI is used to find the center at each field angle. A plot of (x_o', y_o') provides an idea about the wobble of the sample when the field angle is changed. Using the measured center positions for each field angle, the X-coil and Y-coil signals are measured as a function of the field angle, but before a measurement is taken at a specific field angle, the position of the sample is corrected for. The remaining angle dependence is a measure for the quality of the automatic sample shift correction system. The results from each of these scans for X-coil signal is then compiled and the percentage deviation is found. This allows one to compare alignments on different samples.

Linear Scan

Linear scans are an automated version of the traditional alignment method. The system will scan the sample position in either the x or y direction to then find the position of the minimum or maximum. The linear scan is done by first moving five large steps in the negative direction and then scanning in the positive direction measuring the X-signal or Y-signal at 10 equidistant points (each separated by a large step size). The results from this are then used to find a parabola and the position of the lowest or highest points is where the sample is close to the ideal alignment position. After the scan, the sample moves to this extreme. This does though present several issues as the size of the steps can

affect how accurate the move will be. Large steps will dilute it and too small steps will miss the edges of the parabola completely. To find the center using this method requires multiple linear scans in the x, y directions resulting in a time consuming process. Though these scans are still accurate enough, the alignment takes more time than a typical Phi-scan; their usage is good to compare to the Phi-scan method.

Contour Scan

The contour program was added to give a better visualization of how the sample's X and Y-coil signals change with the sample's position. A contour plot is first made by choosing the current motor position as the center for a set of points that extends some distance away in both the x and y directions. From there the user can set the resolution and size of the plot made. This allows runs that just create plots of the general region the sample is in or of the entire array enclosed by the coil sets. The precision is to ensure that all changes are caught no matter how minuet they might be. After this is done, the move VI is called, and the sample is moved to the upper left point of the plot area and begins stepping and collecting data. For data collection we pause for at least one second then begin collecting the X and Y-coil signals at each position. This helps reduce noise from rod vibration associated with the acceleration and deceleration of the sample during movement. The X and Y-coil signal values are saved to a 2D array as well as the x and y position of each scan. These values are then used to create an up to date plot that the user can see. The values are also saved to a text file to be accessed later either for further analysis or review.

V. SAMPLE DISCUSSION

Magnetic samples typically measured in the VSM are small pieces of hard or soft magnetic materials. Typically, we measure thin film samples here at Texas State University. These samples are usually cut or punched to a few millimeters in size and attached to the rods with a variety of techniques.. This chapter will focus on the samples and set ups we used for testing with the Alignment program and give an understanding of why they were chosen.

Samples used

The ideal test sample for the software and alignment method would be isotropic (to avoid a sinusoidal angular dependence of the magnetization). However, we found that all samples we used are somewhat anisotropic. Altogether, we have used seven different samples that were considered for testing to validate the program. Below we will discuss what these samples magnetic properties are and how the samples were made.

Copper Floppy - 1

The Copper Floppy – 1 sample was the first sample made and used for testing. It consists (as the name suggests) of copper tape and a piece of a Floppy disc. The copper tape was first adhered to the top and bottom of a 3.5 inch floppy disc. Using a 4mm hole punch a piece of the sample was cut out as close as was possible to the Floppy discs edge. The reason for maintaining close proximity to the floppy disc edge was to ensure that the structure of the disc was as consistent as possible.

Floppy disc material was chosen as the first sample because it should behave as a

soft magnetic material and have low to no anisotropy inherent to the structure. As testing proceeded though it became apparent that the structure of the sample had higher than desired anisotropy for testing with the newer measurement methods that relied on corrective scans. Shown below are a hysteresis curve and torque curve of the sample that summarize the magnetic properties of the sample. The Copper Floppy – 1 sample was easy to cut, was cylindrical symmetric, had a medium magnetic moment, had a medium coercivity, and was not isotropic.

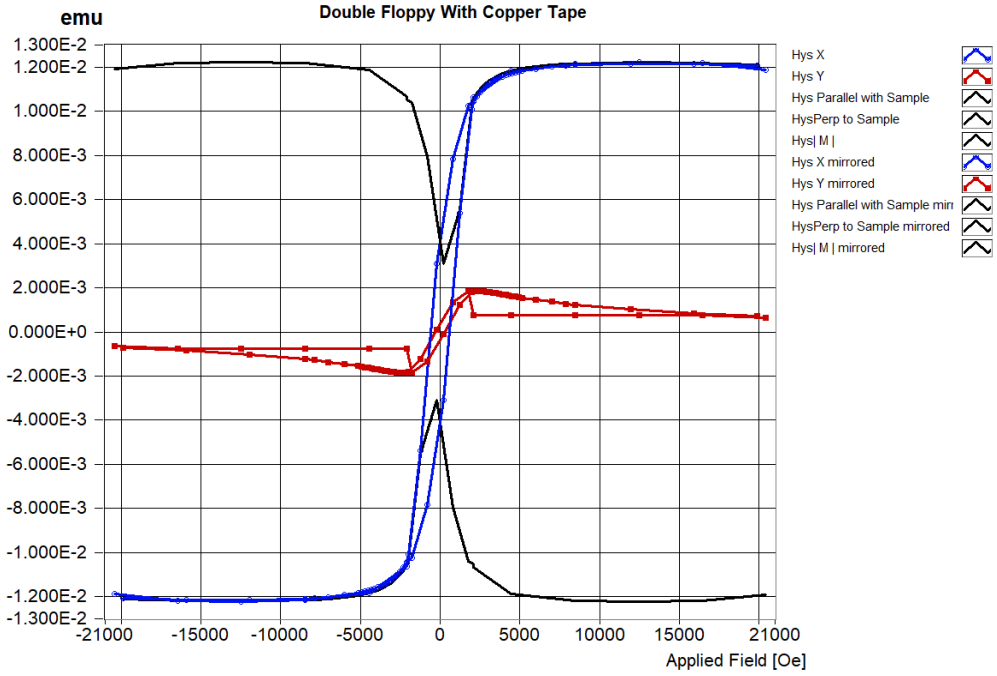

Figure 25: Hysteresis curve of the Copper Floppy - 1 sample.

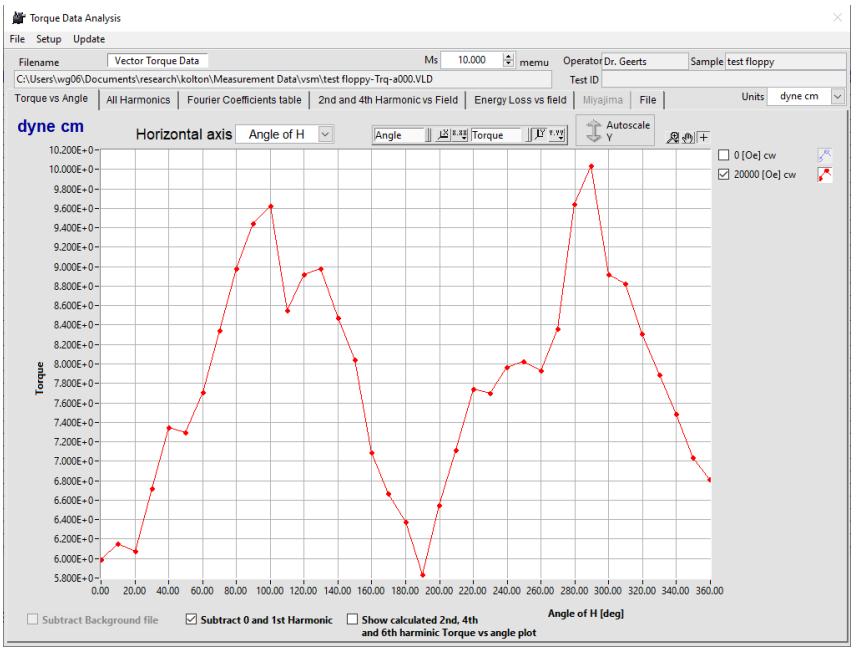

Figure 26: Torque curve of Copper Floppy-1 sample measured by true torque head.

Seen in figure 25 is the Hysteresis of the Copper Floppy – 1 sample. The blue curve tells us what type of material this is which is a soft magnetic material as we expected. The Torque curves in Figure 26 shows though that the sample has a significant and noticeable sinusoidal 2θ torque component which is only present in samples with anisotropy. Also, worth discussing is the M_y hysteresis curve which goes to zero at higher fields. If the sample would be isotropic the M_y hysteresis curve would be zero.

PERM - 1

Since the Floppy Tape sample had a small signal we also wanted to try testing with a sample that had a much higher signal when saturated. A piece of sheet mu-metal was chosen for its high signal and soft magnetic properties. The creation of the sample followed the Copper Floppy – 1 sample now using the metal in place of the Floppy disc. The resulting sample had a large signal because of the larger volume of magnetic material. The sample saturated at a much lower field strength compared to the Floppy's

five thousand Oersted as well. The sample was characterized by the torque head. Below in figures 27, and 28 we see that the sample was a soft magnetic material but not isotropic. The M_y hysteresis curve has non-zero components for small fields which indicates the sample is anisotropic. Also, the torque curve shows a significant 2q torque component.

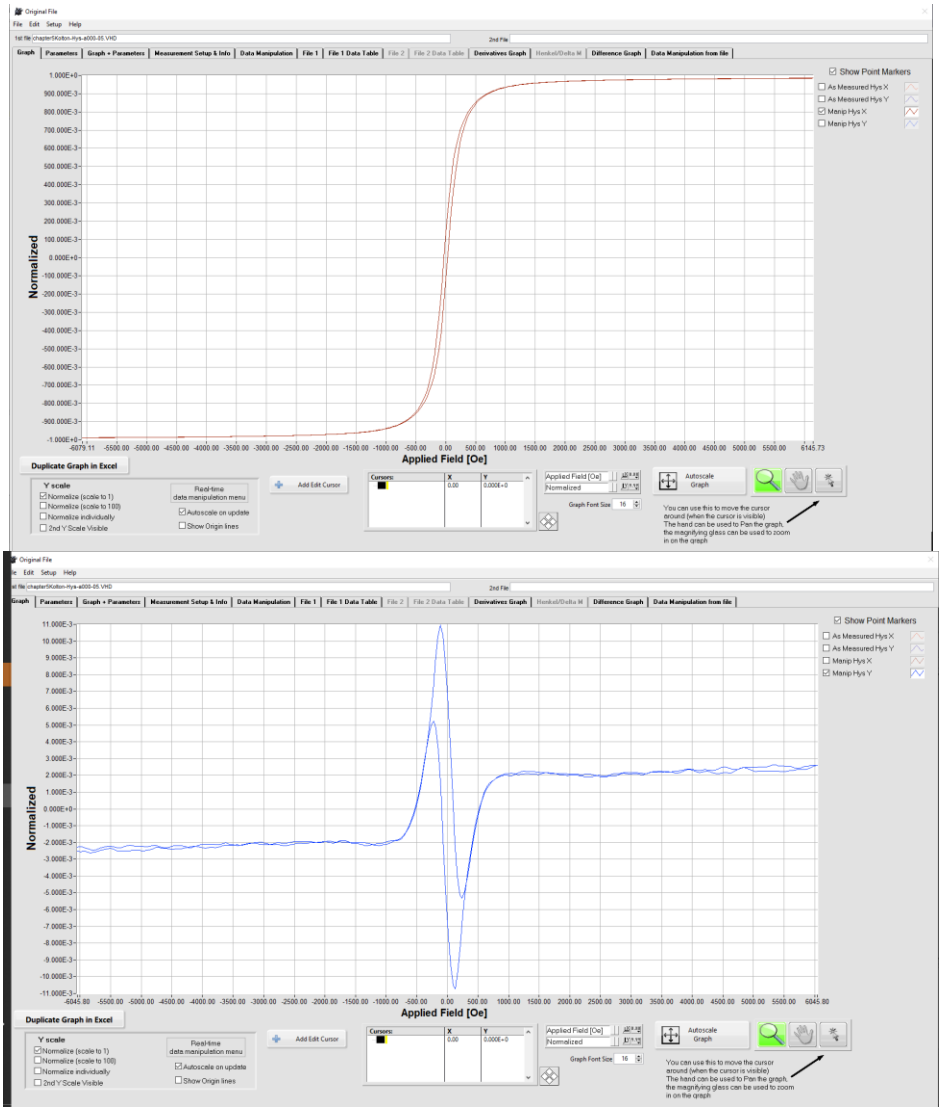

Figure 27: Mx and My Hysteresis curve of the Perm - 1 sample.

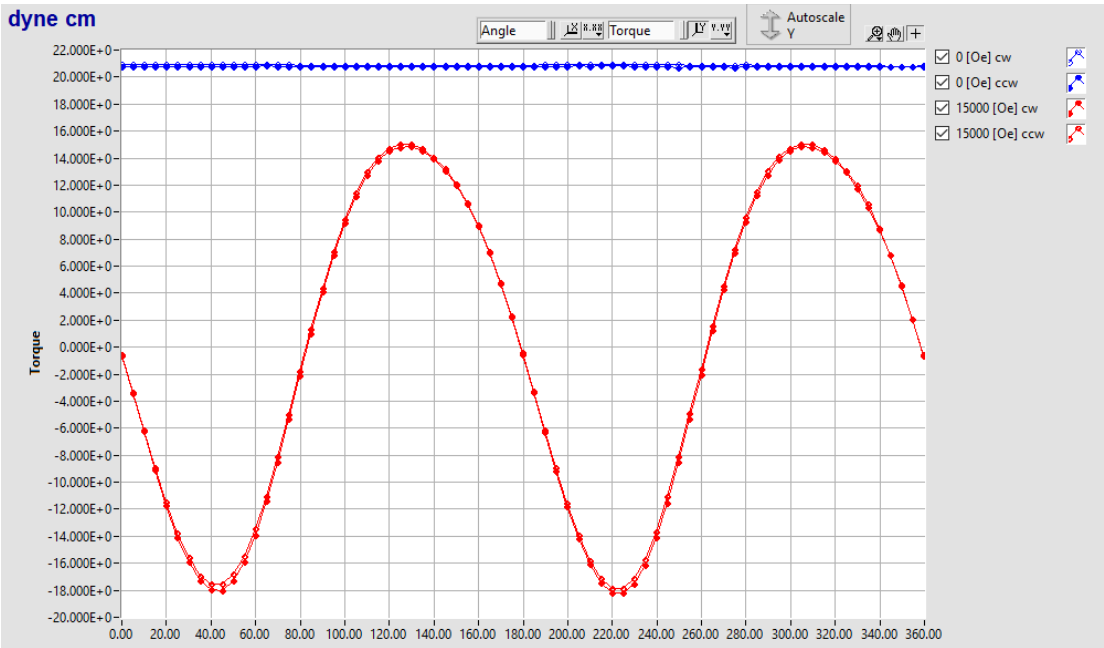

Figure 28: This is the Torque curve of the Perm - 1 sample using the Torque head, it shows a clear 2θ component.

Copper Floppy - 4

Since we still did not have a sample with low enough anisotropy we considered stacking Floppy disk samples at ninety degree angles to of set the anisotropy of the sample. This is where the Copper Floppy – 4 sample comes from. It is a multi-stack variant of the Copper Floppy – 1 sample using 4 floppy disc layers at 0, 90, 0, and 90 degree orientations. The floppy disc layers were stacked using double sided tape and applied with copper-tape. The signal of the sample was four times larger than the original Copper Floppy – 1 sample which was preferable. For this sample we still see a 2θ

component in the torque curve.

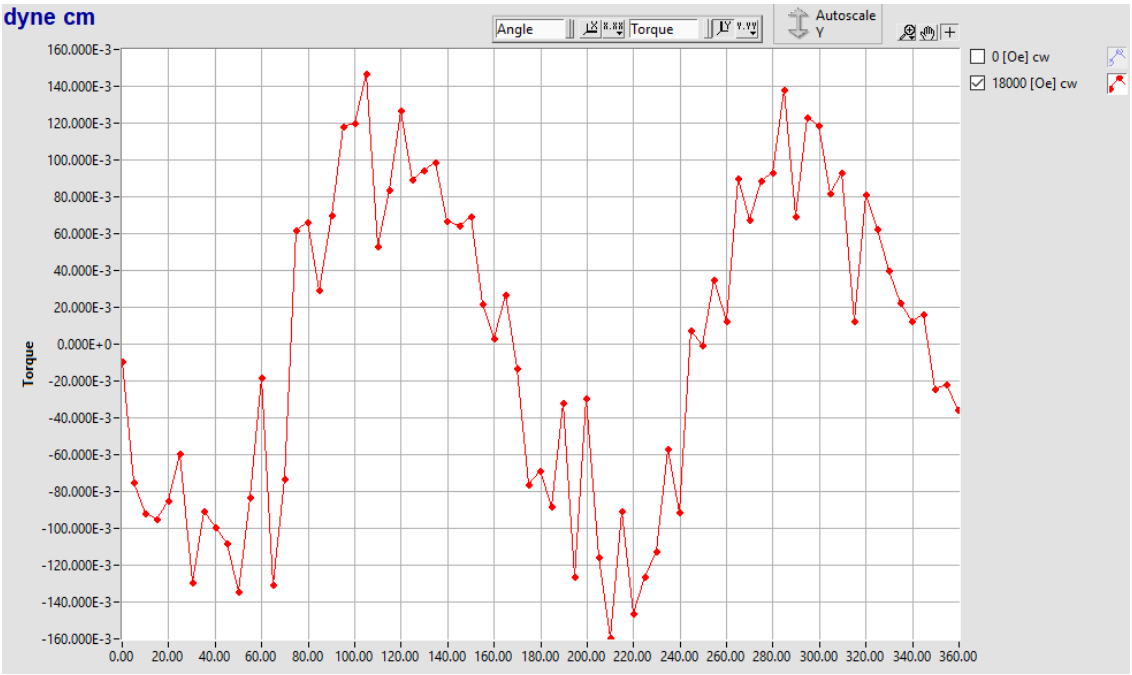

Figure 29: This is a Torque curve of the Copper Floppy - 4 sample using the Torque head, the 2θ component is much smaller than the other samples.

Assorted Samples

Besides the three main samples mentioned before we also had three other samples that were used for testing purposes but in the end were quickly eliminated from being used to gather data. The first being another Copper Floppy sample, called Copper Floppy – 2 (Figure 30.a), this sample had two Floppy discs with random orientation. This led to a larger signal but also a higher anisotropy, removing it from consideration instantly.

The next sample considered was a sample also used by Binod D. C. for his work. It was a large assortment of Floppy Disk punchouts supper glued into a large cylindrical structure (Figure 30.b). At first this seemed like a good choice, the assortment of Floppy Disks in the structure should counter the anisotropy however the shape was not perfect and because of this and other issues it was unable to produce clean and usable results.

The sixth sample considered was a Nickel calibration sample that came with the

MicroSense VSM system (Figure 30.c). The issue was that again it has a noticeable amount of anisotropy making it difficult to use but since it was well defined, we did try using it for measurements that did not require angular changes. This did produce results, however due to its size it was not really worth using compared to the original Copper Floppy samples.

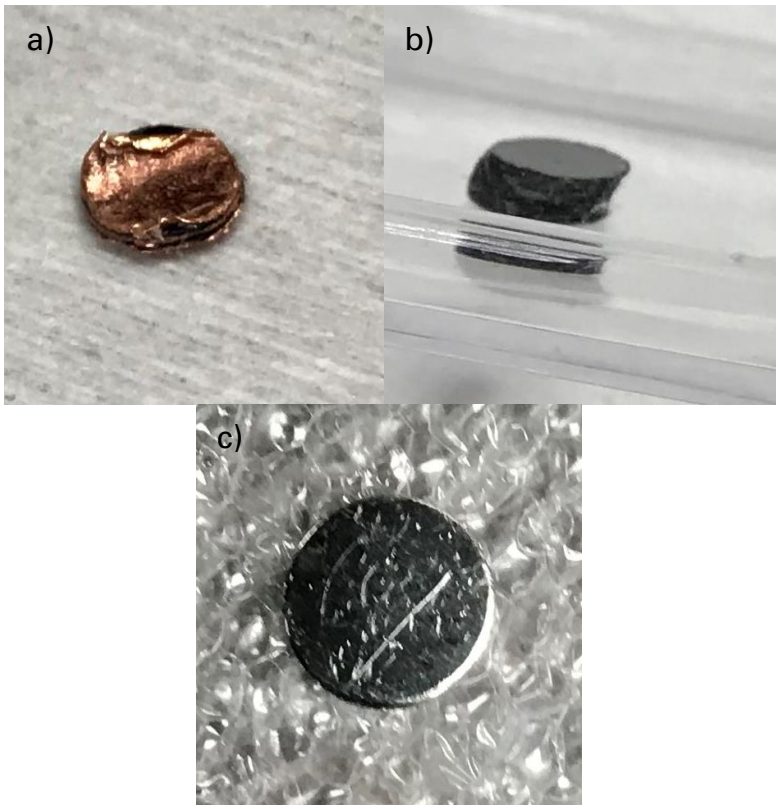

Figure 30: a) shows the Copper Floppy - 2 sample. b) Shows the multi-stack Floppy sample used by Binod D. C. c) Shows the Nickle calibration sample used on the VSM.

The final sample that was added was created for testing the systematic errors on the VSM. This sample was made of a piece of Mu-metal between two pieces of copper tape. This sample differed from PERM-1 that it had a smaller diameter (2 mm). A further discussion of this sample and the tests can be found in Ch. 6.3.

Sample Rod

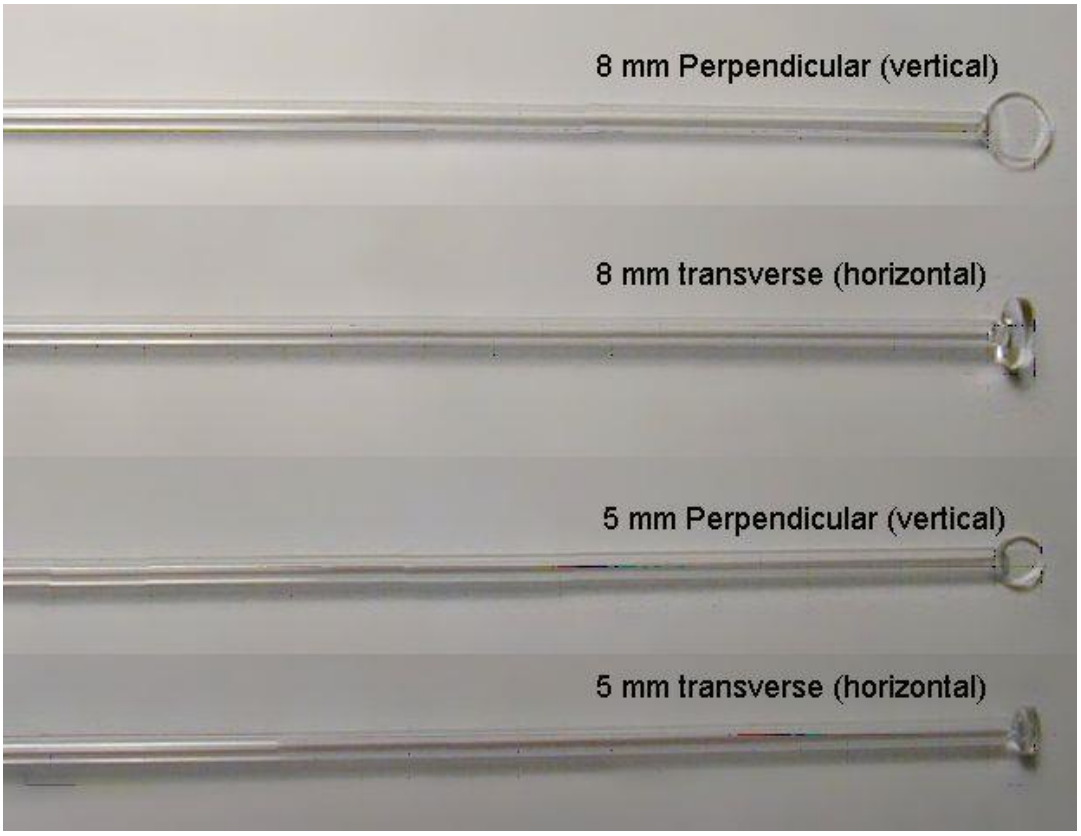

Figure 31: A depiction of the different mounting rods available on the VSM.

VSMs typically have an assortment of rods and their uses depend on the measurements being taken and the properties of the material being measured. Sample rods are typically made of either Pyrex or Quartz these materials have little reaction to larger applied fields present in VSM and are completely isotropic. After material, the next thing to consider is the rods shaft which is for Texas State University is 18cm and either a solid shaft or hollow tube.

The next facet of sample rods to consider is the mounting head this can come in several shapes and sizes (see Fig 31). For this work we used a 5mm Transverse quartz rod. The Transverse refers to the orientation of the circular mounting head in this case it is parallel to the applied field. The other size available to us was the 8mm variant as well

as the perpendicular rods that hold the sample perpendicular to the field which comes in similar size variants. Other types of rods include ones with no mounting head for certain samples and heads designed to accept a cup in which granular material can be inserted into so it can be measured without loss.

There are various methods that may be used to attach a sample to the rod, for example:

1. Double sided sticky tape
2. Vacuum grease (applied to the sample holder, functioning as a temporary adhesive)
3. Super glue
4. Teflon tape (wrapped around the sample and holder)
5. Museum Wax (applied to the sample holder, functioning as a temporary adhesive)
6. Adhesive copper tape

For our testing, the last two methods were used to attach the samples to the rods.

VI. EXPERIMENTAL RESULTS

For the results we collected several sets of data over the development of the program and technique. The first being our initial data collected using the Oriel Controller system and the first working versions of the program. For these tests we primarily focused on the accuracy of the scans as well as making new testing methods. Later on, after the change to the Thorlabs motor controllers and a much more refined set of programs, these tests were then more focused on repeatability and the speed of the system with a real-world use simulated to check against a human attempt. From then on, we made final changes to the programs and added in the unified program to speed testing. Here we were focused again on accuracy and repeatability but also tested other scan versions to ensure we had chosen the best method. The final tests done were for making final changes and checking anomalies in the data, here we have a variety of different tests that we used, some old and some new. This data is gathered here in the following sections first focusing on the accuracy improvements of the system, then the reliability or repeatability of the scans. Finally, we will discuss some of the miscellaneous results like the contour scans and linear scans.

Accurcay Results

For the purposes of this paper, accuracy is determined by calculating the difference between the displacement of the sample determined from the Phi-scan and the displacement calculated from the motor coordinates. So a Phi-scan is performed after the sample has been moved from its central position to a position (x,y) by moving the X-motor x and the Y-motor y units. We are looking for a accuracy of within five microns or

less which will be comparable to the results seen with manual alignments done by others using the VSM. This level of accuracy should be achievable by both of the motor setups that were used for the scans so here we will be comparing the many different set ups we had. To show this we will be discussing the initial test to the program, initially using 0.25mm displacement steps for testing. Later the accuracy for different displacements were explored.

Accuracy with Oriel Encoder setup

At the start of testing, we focused on the accuracy of the sample scans to give us an idea of how the system was working. This helped us make initial assumptions on whether the programs were being executed correctly. This does mean that many of the initial test cannot be directly compared to our later test as either issues that were not discovered till later are affecting results heavily. However, when possible the corrections we made later on will be mentioned to show why an issue is no longer a concern for future uses. For our first testing regime we first centered the sample as close to the central point of the coil set as possible and then ran one more Phi-scan and used that to find the position of the origin. Then the sample was moved to a new position (x1,y1) using the servomotors and a Phi-scan was used to determine the new position relative to the coil sets. After this scan the sample returned to the central position before again moving to another position (x2,y2) and again determine the new position from a Phi-scan at this new position. This method allowed us to gather information on how the alignment function and setup were operating. All scans at this time were conducted with the Oriel Motors using a scan radius of 1mm with 16 sample points per scan and using the Phi-scan

alignment method with no changes. We first tried this with a distance of 0.25mm from the center point, then a distance of 0.5mm and finally a distance of 1mm the results were as follows:

Table 2: Initial 0.25mm movement Results and their Accuracy.

(X,Y)	x' mm	x'' mm	y' mm	y'' mm	Accuracy			
0, 0	0.031	0.051	0.000	0.000	x' mm	x'' mm	y' mm	y'' mm
0.25, 0	0.149	0.282	-0.008	-0.008	-0.133	-0.019	-0.008	-0.008
0, 0.25	0.032	0.072	0.472	0.239	0.000	0.020	0.222	-0.011
-0.25, 0	-0.131	-0.239	0.108	0.022	0.087	-0.040	0.108	0.022
0, -0.25	0.013	0.013	-0.309	-0.255	-0.018	-0.038	-0.059	-0.005
0.25, 0.25	0.167	0.324	0.382	0.241	-0.115	0.022	0.132	-0.009
-0.25, -0.25	-0.138	-0.258	-0.264	-0.243	0.080	-0.059	-0.014	0.007

Table 3: Initial 0.5mm movement Results and their Accuracy.

(X,Y)	x' mm	x'' mm	y' mm	y'' mm	Accuracy			
0, 0	0.004	0.008	0.073	0.000	x' mm	x'' mm	y' mm	y'' mm
0.5, 0	0.305	0.509	-0.059	-0.029	-0.199	0.000	-0.132	-0.029
0, 0.5	0.030	0.090	0.932	0.489	0.027	0.082	0.359	-0.011
-0.5, 0	-0.296	-0.479	0.210	0.027	0.201	0.012	0.137	0.027
0, -0.5	-0.009	-0.046	-0.724	-0.496	-0.013	-0.055	-0.297	0.005
0.5, 0.5	0.358	0.583	0.788	0.460	-0.146	0.074	0.215	-0.040
-0.5, -0.5	-0.321	-0.536	-0.583	-0.467	0.175	-0.045	-0.156	0.034
0, 0 - 2	0.016	0.029	0.068	-0.001	0.013	0.020	-0.005	0.000

Table 4: Initial 1mm movement Results and their Accuracy.

(X,Y)	x' mm	x'' mm	y' mm	y'' mm	Accuracy			
0, 0	0.000	-0.011	-0.053	-0.093	x' mm	x'' mm	y' mm	y'' mm
1, 0	0.580	1.029	-0.301	-0.151	-0.419	0.041	-0.248	-0.058
0, 1	0.046	0.150	1.706	0.864	0.047	0.161	0.760	-0.043
-1, 0	-0.601	-1.033	0.251	-0.024	0.399	-0.022	0.304	0.069
0, -1	-0.055	-0.131	-1.768	-1.047	-0.055	-0.120	-0.715	0.046
1, 1	0.650	1.220	1.494	0.823	-0.349	0.231	0.547	-0.084
-1, -1	-0.670	-1.150	-1.550	-0.948	0.330	-0.138	-0.496	0.145

The above data shows the results after moving to different positions at the chosen distances and then the accuracy of these movements is shown on the right side. The

accuracy was determined by first normalizing the values with the 0,0 scan results then either adding or subtracting from the known distance that the motors moved, depending on the direction moved, giving us an estimate of the accuracy of the different runs. To normalize our data, we simply subtract the x', x", y', and y" values at the scanned center point from all other scanned positions. As can be seen from the data our first attempts at aligning the samples autonomously had many issues as the scans rarely returned truly accurate values. The accuracy makes this even clearer as the going from the values found at 0.25mm to the 1mm there is a clear decrease in the accuracy found. It is worthwhile though to mention that these scans are also done with the original scan method with no modifications or changes. Other issues with these scans will be brought up later as they were determined but here we had determined that the experimental equation found in Binod's work did not fully explain the physics here and that the motors we were using may have issues [Binod].

Accuracy with ThorLabs setup and Program Changes

This leads us to the next set of data taken after we had finished modifying the software and changing over to the Thorlabs Motor controllers. For these scans we only took 0.25mm data. There were two trials run one using the original program with only minor modifications to the software to make the program work. The other was preformed after more extensive changes had been made to the software. Again, all scans were done using a scan radius of 1mm with 16 sample points per scan and using the Phi-scan alignment method, accuracy was also calculated the same, the results are as follows.

Table 5: The 0.25mm movement results and their Accuracy for the Thorlabs motors with little software changes.

(X,Y)	x' mm	x" mm	y' mm	y" mm	Accuracy			
0, 0	0.617	1.112	1.374	0.836	x' mm	x" mm	y' mm	y" mm
0.25, 0	0.774	1.368	1.384	0.781	-0.093	0.006	0.011	-0.055
0, 0.25	0.548	0.995	1.682	0.986	-0.069	-0.117	0.058	-0.100
-0.25, 0	0.383	0.695	1.267	0.755	0.016	-0.167	-0.106	-0.081
0, -0.25	0.534	0.946	0.828	0.514	-0.082	-0.167	-0.296	-0.073
0.25, 0.25	0.706	1.261	1.657	0.953	-0.161	-0.101	0.034	-0.134
-0.25, -0.25	0.381	0.664	0.822	0.503	0.014	-0.198	-0.302	-0.083
0.25, -0.25	0.693	1.210	0.761	0.481	-0.174	-0.152	-0.362	-0.106
-0.25, 0.25	0.387	0.690	1.659	0.963	0.021	-0.172	0.035	-0.124

Table 6: The 0.25mm movement results and their Accuracy for the Thorlabs motors with software corrections added.

(X,Y)	x' mm	x" mm	y' mm	y" mm	Accuracy			
0, 0	-0.064	-0.012	0.142	0.000	x' mm	x" mm	y' mm	y" mm
0.25, 0	0.176	0.242	0.088	-0.002	-0.010	0.005	-0.054	-0.002
0, 0.25	-0.063	0.009	0.527	0.222	0.001	0.022	0.135	-0.028
-0.25, 0	-0.325	-0.260	0.152	-0.018	-0.011	0.003	0.010	-0.018
0, -0.25	-0.082	-0.028	-0.297	-0.262	-0.018	-0.015	-0.189	-0.012
0.25, 0.25	0.182	0.260	0.442	0.201	-0.004	0.023	0.050	-0.048
-0.25, -0.25	-0.335	-0.281	-0.237	-0.258	-0.021	-0.018	-0.130	-0.007
0.25, -0.25	0.164	0.217	-0.348	-0.266	-0.022	-0.020	-0.240	-0.015
-0.25, 0.25	-0.317	-0.247	0.538	0.211	-0.003	0.015	0.146	-0.039

This data has some of the similar issues seen in the earlier scans and this led us to the conclusions that the motors were not a large part of the issues we had encountered. Interestingly though the minor changes we made to software had larger effects on the accuracy and scans as a whole. You can see this as the later scans we made that month showed a large improvement in the accuracy over the original results. Another thing we added to these scans that earlier we did not is more points with actual x and y movements so we could examine better any coupling happening between the two directions. The reasoning for this may be due to the fact we found an issue causing our scans to be more

ellipses rather than circles which is what we need for the symmetry of our equations. Other edits were with proper timing intervals to prevent any influence from vibrations when the sample was moved to new positions. We also began working on the idea that our scan method had a fundamental flaw. At larger distances thanks to the nonlinear component found in the 2ϕ components, errors in the position were introduced as mentioned before in the section Correction Methods. This led to our development of different methods for alignment which leads to our next set of scans.

Accuracy of Corrected Phi-scan method

To improve the accuracy for larger misalignments we explored a method to correct the position dependence for the 2ϕ components by two constants A and B. To test this method scans were done by several jumps to larger and larger distance along the x and y axis of the machine separately. The results then required two passes and thus two zero positions to ensure accuracy across the regime of scans. Altogether three tests were done with the first one being at a distance of 0.75mm and increments of 0.25mm this was done to compare to the regular Phi-scans. The second and third scans were done at a larger distance of 2mm with an increment of .5mm this time. There were two scan regimes done to ensure that the original measurements were accurate. These scans show varying degrees of success and what seemed like little improvements over the Phi-scan method. For these scans we changed to a larger radius of 2mm with the same 16 points per scan. Accuracy was also still calculated the same, the results are as follows.

Table 7: The initial 0.25mm test scan without any Phi-scan corrections.

(X,Y)	x' mm	x'' mm	y' mm	y'' mm	Accuracy			
0, 0	-0.015	-0.006	-0.005	-0.031	x' mm	x'' mm	y' mm	y'' mm
0.25, 0	0.141	0.268	-0.067	-0.035	-0.094	0.024	-0.062	-0.003
0, 0.25	-0.008	0.016	0.352	0.227	0.008	0.021	0.107	0.009
-0.25, 0	-0.176	-0.260	0.057	-0.017	0.089	-0.004	0.062	0.014
0, -0.25	-0.018	-0.028	-0.370	-0.295	-0.003	-0.022	-0.115	-0.014
0.25, 0.25	0.156	0.273	0.294	0.208	-0.078	0.028	0.049	-0.010
-0.25, -0.25	-0.178	-0.295	-0.321	-0.294	0.088	-0.040	-0.065	-0.012
0.25, -0.25	0.143	0.234	-0.450	-0.308	-0.092	-0.010	-0.195	-0.027
-0.25, 0.25	-0.169	-0.231	0.407	0.227	0.097	0.024	0.162	0.008

Table 8: The first Corrected Phi-scan along the x and y directions with a distance of 0.75mm with increments of 0.25mm.

					Accuracy			
(X,Y)	x' mm	x'' mm	y' mm	y'' mm	x' mm	x'' mm	y' mm	y'' mm
0.75, 0.00	0.444	0.739	0.067	-0.022	-0.250	0.013	-0.081	0.111
0.00, 0.75	-0.039	-0.009	0.873	0.564	0.016	0.015	0.271	-0.053
0.50, 0.00	0.291	0.477	0.035	-0.021	-0.153	0.000	-0.113	0.112
0.00, 0.50	-0.045	-0.003	0.535	0.349	0.010	0.021	0.183	-0.018
0.25, 0.00	0.119	0.227	0.005	-0.017	-0.076	0.001	-0.143	0.115
0.00, 0.25	-0.051	-0.022	0.197	0.110	0.005	0.001	0.095	-0.007
0.00, 0.00-X	-0.055	-0.024	0.148	-0.133	0.000	0.000	0.000	0.000
0.00, 0.00-Y	-0.055	-0.024	-0.148	-0.133	0.000	0.000	0.000	0.000
-0.25, 0.00	-0.205	-0.270	-0.052	-0.015	0.100	0.004	-0.200	0.117
0.00, -0.25	-0.061	-0.035	-0.463	-0.348	-0.006	-0.012	-0.066	0.034
-0.50, 0.00	-0.363	-0.519	-0.080	-0.009	0.192	0.005	-0.228	0.124
0.00, -0.50	-0.068	-0.037	-0.830	-0.588	-0.013	-0.013	-0.182	0.045
-0.75, 0.00	-0.520	-0.774	-0.108	-0.005	0.286	0.000	-0.256	0.127
0.00, -0.75	-0.068	-0.043	-1.093	-0.794	-0.012	-0.020	-0.195	0.089

Table 9: The second Corrected Phi-scan along the x and y directions with a distance of 2mm with increments of 0.5mm.

					Accuracy			
(X,Y)	x' mm	x'' mm	y' mm	y'' mm	x' mm	x'' mm	y' mm	y'' mm
2, 0.00	1.149	2.269	0.172	-0.100	-0.829	0.272	0.019	0.066
0.00, 2	0.002	-0.025	2.809	1.489	0.024	-0.021	0.962	-0.345
1.50, 0.00	0.908	1.603	0.149	-0.101	-0.570	0.107	-0.004	0.065
0.00, 1.50	-0.001	-0.014	1.987	1.151	0.021	-0.011	0.639	-0.183
1, 0.00	0.618	1.025	0.111	-0.094	-0.360	0.028	-0.042	0.072
0.00, 1	-0.004	-0.015	1.215	0.727	0.017	-0.011	0.368	-0.107
0.50, 0.00	0.302	0.501	0.065	-0.089	-0.176	0.528	-0.088	0.077
0.00, 0.50	-0.011	-0.008	0.509	0.279	0.011	-0.004	0.162	-0.055
0.00, 0.00-X	-0.022	-0.003	0.153	-0.166	0.000	0.000	0.000	0.000
0.00, 0.00-Y	-0.022	-0.003	-0.153	-0.166	0.000	0.000	0.000	0.000
-0.50, 0.00	-0.347	-0.495	0.001	-0.088	0.175	0.009	-0.152	0.078
0.00, -0.50	-0.030	0.007	-0.887	-0.654	-0.009	0.010	-0.234	0.012
-1, 0.00	-0.656	-1.015	-0.029	-0.097	0.366	-0.011	-0.182	0.069
0.00, -1	-0.037	0.009	-1.591	-1.102	-0.015	0.012	-0.438	0.064
-1.50, 0.00	-0.934	-1.602	-0.049	-0.093	0.588	-0.099	-0.202	0.073
0.00, -1.50	-0.049	0.013	-2.368	-1.501	-0.028	0.016	-0.715	0.165
-2, 0.00	-1.179	-2.306	-0.081	-0.123	0.843	-0.303	-0.234	0.043
0.00, -2	-0.057	0.015	-3.223	-1.844	-0.036	0.018	-1.070	0.322

Table 10: The third Corrected Phi-scan along the x and y directions with a distance of 2mm with increments of 0.5mm.

					Accuracy			
(X,Y)	x' mm	x'' mm	y' mm	y'' mm	x' mm	x'' mm	y' mm	y'' mm
2, 0.00	1.154	2.236	-0.030	-0.056	-0.801	0.260	0.131	-0.049
0.00, 2	-0.036	-0.038	2.998	1.508	0.032	0.022	1.237	-0.224
1.50, 0.00	0.846	1.548	-0.057	-0.038	-0.609	0.072	0.104	-0.031
0.00, 1.50	-0.044	-0.043	2.076	1.118	0.024	0.017	0.815	-0.114
1, 0.00	0.560	0.982	-0.088	-0.016	-0.395	0.006	0.074	-0.008
0.00, 1	-0.049	-0.047	1.261	0.693	0.019	0.014	0.500	-0.039
0.50, 0.00	0.259	0.459	-0.121	-0.010	-0.196	0.506	0.041	-0.003
0.00, 0.50	-0.057	-0.056	0.516	0.218	0.011	0.004	0.254	-0.014
0.00, 0.00-X	-0.045	-0.024	-0.162	-0.007	0.000	0.000	0.000	0.000
0.00, 0.00-Y	-0.068	-0.060	-0.239	-0.268	0.000	0.000	0.000	0.000
-0.50, 0.00	-0.347	-0.505	-0.201	0.009	0.198	0.019	-0.039	0.016
0.00, -0.50	-0.078	-0.068	-0.986	-0.762	-0.010	-0.008	-0.247	0.006
-1, 0.00	-0.647	-1.026	-0.250	0.014	0.398	-0.002	-0.089	0.021
0.00, -	-0.093	-0.078	-1.765	-1.198	-0.025	-0.018	-0.526	0.070
-1.50, 0.00	-0.925	-1.617	-0.296	0.018	0.620	-0.093	-0.135	0.025
0.00, -1.50	-0.106	-0.085	-2.536	-1.579	-0.038	-0.024	-0.798	0.189
-2, 0.00	-1.178	-2.310	-0.345	0.016	0.867	-0.286	-0.184	0.023
0.00, -2	-0.121	-0.093	-3.369	-1.895	-0.053	-0.033	-1.130	0.373

From these results it was plain to see that our overall changes had little effect on the results and in several cases the accuracy was abysmal. This led us to the realization that unless we could solve directly for the nonlinear component we would need to exclude it from our method and use another process to align the samples.

Accuracy for Calibrated Phi-scan method

Other methods were then developed and tested. The one that had the best results was the Calibrated Phi-scan method. This requires the calibration of the system with the sample beforehand so we would know the slope of the 1ϕ components which were known after our earlier testing to be linear. These were also relatively simple to do only a

minimum of two sample points were needed to find the slope, so it was relatively quick. Below are the results from our first test on the Calibrated Phi-scan method wherein we used two different methods to determine the slope:

1. For the first method during the calibration the D and E values were determined from moving the sample to position (x,y), doing a Phi-scan. Then moving the sample to position (-x,-y) and doing another Phi-scan, and then determining the slope of $D'=A_q/x$ and $E'=B_q/y$ or $D''=D_q/y$ and $E''=C_q/x$. Then these calibrated D and E values were used to determine the sample position from the 1ϕ component.
2. For the second method we determined the D and E values separately, this was accomplished by scanning across the different coil axis separately. So we now had four scan points: (x,0) and (-x,0) for the X-coil set, and (0,y) and (0,-y) for the Y-coil set. Using the same formula from step one we then found the D and E values.

The x and y D and E scan had an error when recording the findings and two scan points were lost, however the full scan regime is still comparable. Again, all scans were done using a scan radius of 2mm with 16 points per scan. Accuracy was still calculated the same, the results are summarized in the tables below.

Table 11: Calibrated Phi-scan test where x and then y D and E values were calibrated on seperate runs and the Accuracy checked.

					Accuracy			
(X,Y)	x' mm	x" mm	y' mm	y" mm	x' mm	x" mm	y' mm	y" mm
1, 0.00	1.005	1.077	-0.075	-0.097	0.005	0.047	-0.061	-0.004
0.00, 1	0.024	0.048	1.079	0.860	0.023	0.018	0.093	-0.047
0.50, 0.00	0.502	0.558	-0.041	-0.094	0.002	0.028	-0.027	-0.001
0.00, 0.50	0.014	0.039	1.014	0.373	0.014	0.009	0.528	-0.034
0.25, 0.00	0.248	0.297	-0.028	-0.096	-0.003	0.017	-0.014	-0.003
0.00, 0.25	0.007	0.036	0.262	0.138	0.007	0.005	0.026	-0.019
0.10, 0.00	0.099	0.137	-0.018	-0.093	-0.002	0.167	-0.004	0.000
0.00, 0.10	0.003	0.031	0.095	-0.003	0.003	0.001	0.009	-0.010
0.00, 0.00-X	0.001	0.030	-0.014	-0.093	0.000	0.000	0.000	0.000
0.00, 0.00-Y	0.001	0.030	-0.014	-0.093	0.000	0.000	0.000	0.000
-0.10, 0.00	-0.098	-0.077	-0.009	-0.092	0.002	-0.007	0.005	0.001
0.00, -0.10	-0.001	0.031	-0.121	-0.186	-0.001	0.000	-0.007	0.007
-0.25, 0.00	-0.251	-0.243	0.002	-0.090	-0.001	-0.024	0.016	0.003
0.00, -0.25	-0.006	0.031	-0.277	-0.325	-0.007	0.001	-0.013	0.018
-0.50, 0.00	-0.502	-0.506	0.022	-0.084	-0.003	-0.036	0.036	0.009
0.00, -0.50	-0.014	0.025	-0.538	-0.555	-0.014	-0.005	-0.024	0.038
-1, 0.00	-1.001	-1.031	0.061	-0.076	-0.001	-0.062	0.075	0.017
0.00, -1	-0.031	0.018	-1.028	-1.020	-0.032	-0.012	-0.014	0.073

Table 12: Calibrated Phi-scan test where x and y D and E values were calibrated simultaneously on a singular run and the Accuracy checked.

					Accuracy			
(X,Y)	x' mm	x'' mm	y' mm	y'' mm	x' mm	x'' mm	y' mm	y'' mm
1, 0.00	1.011	0.950	-0.062	-0.106	0.007	-0.073	-0.065	-0.003
0.00, 1	0.034	0.045	1.037	0.976	0.031	0.022	0.034	0.079
0.50, 0.00	0.500	0.490	-0.030	-0.104	-0.003	-0.034	-0.033	0.000
0.00, 0.50	0.020	0.031	0.515		0.017	0.008	0.012	-0.397
0.25, 0.00								
0.00, 0.25								
0.10, 0.00	0.105	0.117	-0.009	-0.104	0.001	-0.123	-0.012	-0.001
0.00, 0.10	0.009	0.022	0.101	0.001	0.005	-0.002	-0.002	0.004
0.00, 0.00-X	0.003	0.023	0.003	-0.103	0.000	0.000	0.000	0.000
0.00, 0.00-Y	0.003	0.023	0.003	-0.103	0.000	0.000	0.000	0.000
-0.10, 0.00	-0.094	-0.072	0.004	-0.104	0.002	0.004	0.001	0.000
0.00, -0.10	0.000	-0.014	-0.100	0.679	-0.003	-0.038	-0.003	0.883
-0.25, 0.00	-0.245	-0.214	0.014	-0.103	0.002	0.012	0.010	0.000
0.00, -0.25	-0.003	0.022	-0.258	-0.365	-0.006	-0.002	-0.011	-0.011
-0.50, 0.00	-0.498	-0.450	0.030	-0.099	-0.001	0.026	0.027	0.005
0.00, -0.50	-0.009	0.018	-0.503	-0.626	-0.013	-0.005	-0.006	-0.022
-1, 0.00	-0.995	-0.908	0.065	-0.095	0.001	0.069	0.062	0.008
0.00, -1	-0.025	0.017	-0.970	-1.157	-0.029	-0.007	0.027	-0.054

From this we found that the accuracy of calibrating x and then y D and E values vs simultaneously calibrating the x and y D and E values gave comparable results. The methods differences were negligible so either method is acceptable for testing. It should though be noted that the simultaneous scan process requires less scans and thus less time to complete. The accuracy compared to our previous alignment processes shows the results were acceptable being very precise at larger distances of 1-2mm while still having good accuracy on the smaller positions. This means that going forward we choose the Calibrated Phi-scan method as they were both faster and had good accuracy for larger distances.

Angular Corrections

One of the main things we wanted to focus on correcting for VSM measurements was Torque scans where the sample is rotated, and the Y-coil signal is measured as a function of the field angle. These scans can contain large errors due to sample misalignment caused by wobble. In particular at large field values, the M_x component is large and therefore the Crosstalk will cause a large systematic error in the Y-coil signal that will not be related to the sample's properties. To have precise positioning samples need to be aligned at each field angle. With our program we hope that these corrections can be automated allowing the users to run these scans with little oversight. To this end we have conducted scans to verify this idea we refer to these from here on as Angular scans. The Angular scans were made at 45 degree increments and the Phi-scan method was used to find the corrected position for each field angle. The First Scan we had that generated accurate results came in March and we repeated this in June and towards the end of the thesis run with several different samples that had varying levels of anisotropy. Below are these corresponding graphs to the results of the X-coil signal and Y-coil signal. What is shown below is the comparison of each X-coil signal and Y-coil signal values at the end of each scan correction. If the correction is successful on isotropic samples the X-coil signal and Y-coil signal should remain constant. For anisotropic samples only the X-coil signal should be independent of the field angle. While the Y-coil signal should reflect the anisotropy.

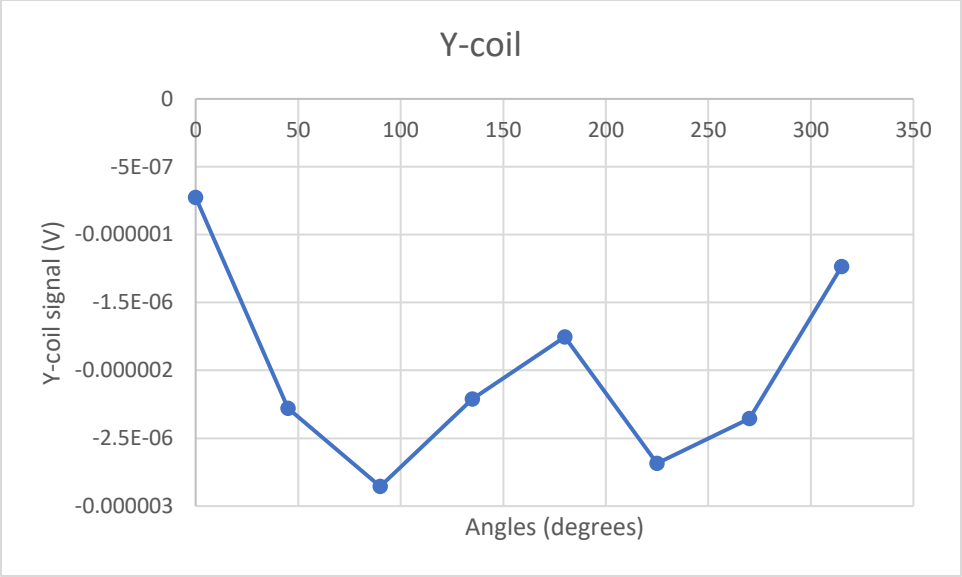

Figure 32: A comparison of the Y-coil signal Vs the angles after correction for the Copper Floppy – 1 Sample.

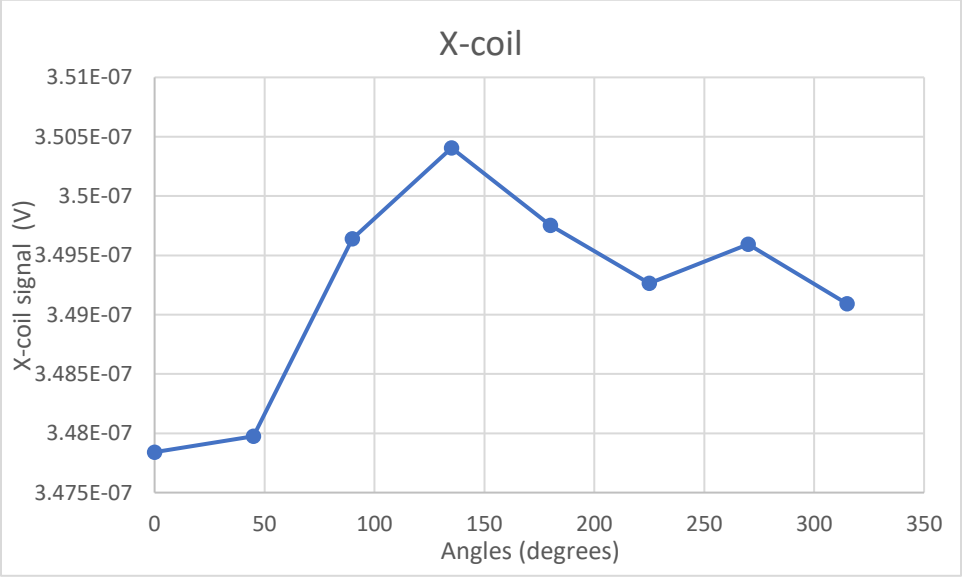

Figure 33: A comparison of the X-coil Vs the Angle correction for the Copper Floppy – 1 Sample.

These initial tests were done on the Copper Floppy – 1 sample which was rotated at 45 degree increments and at each increment scanned and corrected its position. After this it then took a measurement of the resulting X-coil signal and Y-coil signal, if the corrections worked, we should see a relatively similar value for the X-coil signal and Y-coil signal relatively close to zero. Relatively here is used as these signals will see

interference from outside noise and the values used are not accounting for corrections that normally go into the MicroSense software.

Following this we then took this same sample and aligned it by hand using the previously mentioned standard method. These results are listed below and show what is currently the absolute best a human can achieve on their own after several hours of measurement.

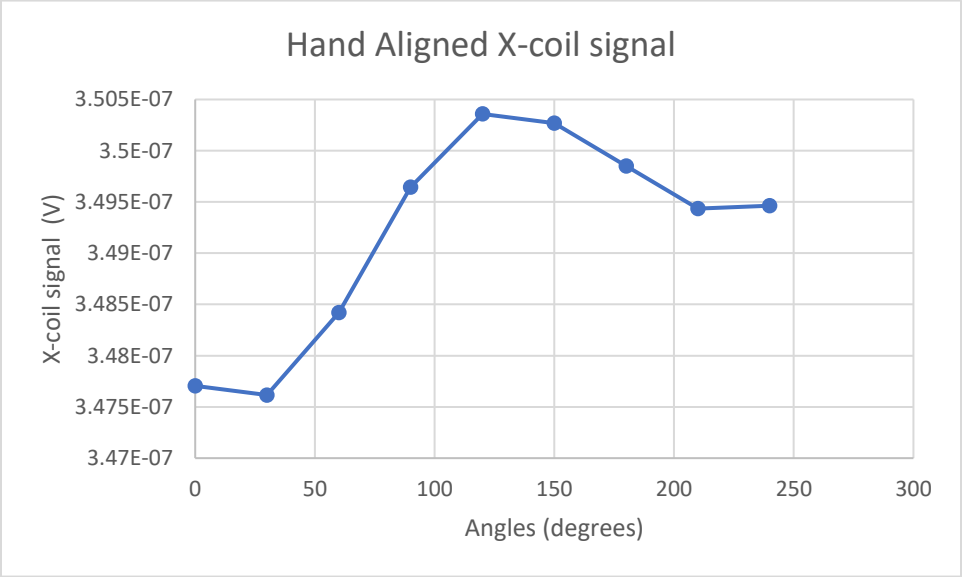

Figure 34: Hand X-coil signal Vs angle corrections for a Copper Floppy – 1 sample.

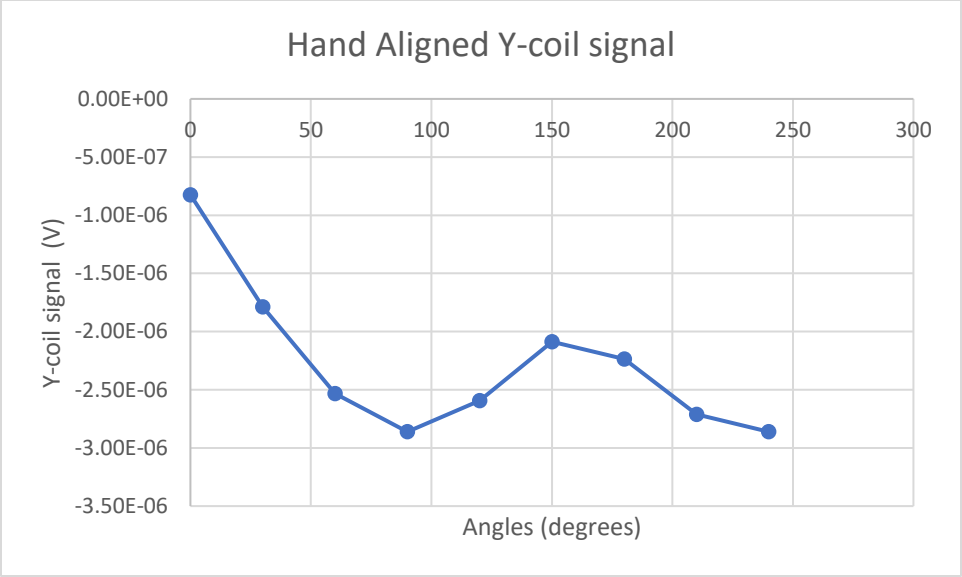

Figure 35: Hand Y-coil signal Vs Angle correction for Copper Floppy – 1 sample.

The easiest comparison of these different scans we can make is to compare the remaining field angle dependence of the X-coil signal. This is the only signal we can compare directly though as the Y-coil signal reflects the anisotropy of the sample. The percent difference is found with the following equation and will be used to compare all the angular scans:

$$Percentage\ difference = \frac{(Max\ value - Min\ value)}{Average\ of\ values}$$

The remaining angular dependence of the Hand X-coil signal is 0.78% and the remaining angular dependence of the auto X-coil signal angular corrected scans was 0.73%. Though the value is not a large improvement over the hand measurement it was done completely independent of human interaction and in under 20 minutes.

We again ran a test using the Copper Floppy – 4 sample with a new set up for the program where this time we achieved a similar result of 0.83%. This while comparable to the other measurements was a real-world use case.

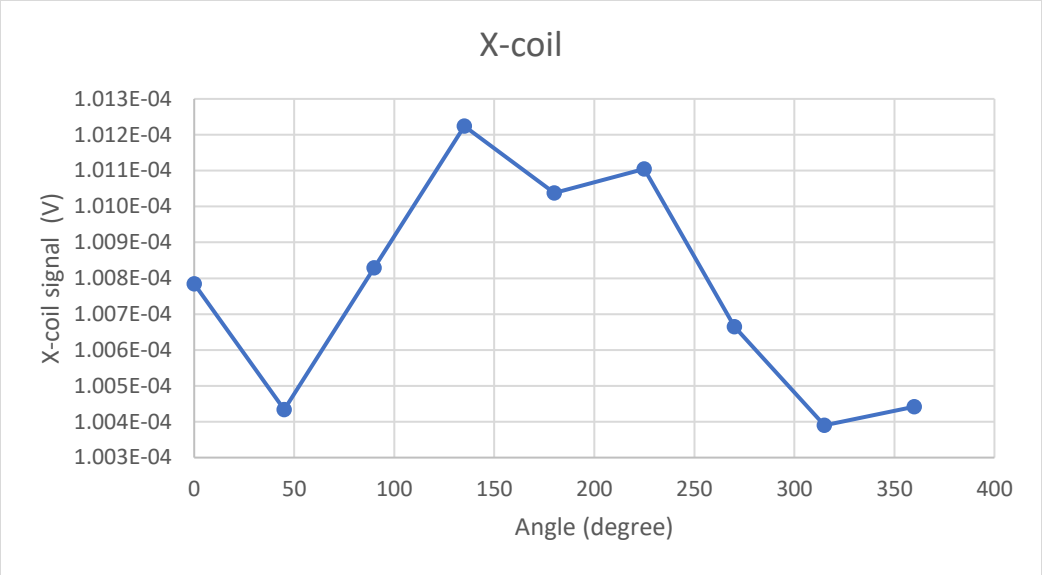

Figure 36: X-coil signal Vs the Angle correction for the Copper Floppy – 4 sample with MicroSense software.

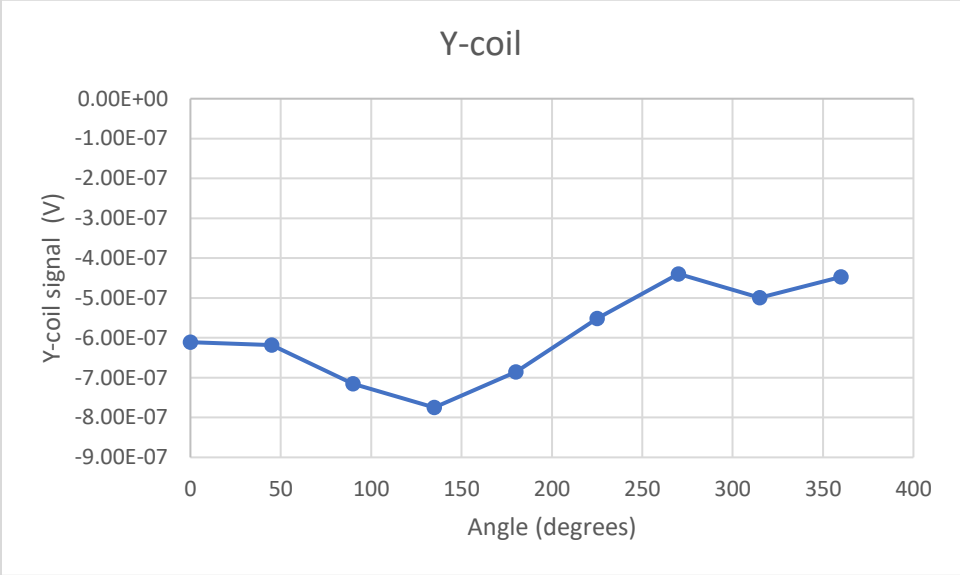

Figure 37: Y-coil signal Vs the Angle for the Copper Floppy – 4 sample with MicroSense software.

Throughout the project we showed an increase in accuracy or when needed kept accuracy constant with the change of our software. This required determining the exact amount of scan points needed for a scan to be of acceptable accuracy while also trying to balance usability by speeding up scans or making the software acceptable to be used with others work. In the end the accuracy of the automatic system was able to match the

alignment of a human. The later measurement would require several times longer.

We also did a final verification scan to ensure these results were usable for research. This was done by taking an isotropic sample and first measuring the torque on the sample. A torque head is unaffected by the samples position so things like wobble will not affect the results. Figure 38 shows the results where a clear two theta component is seen. The amplitude of this component is around 5.25dyne cm.

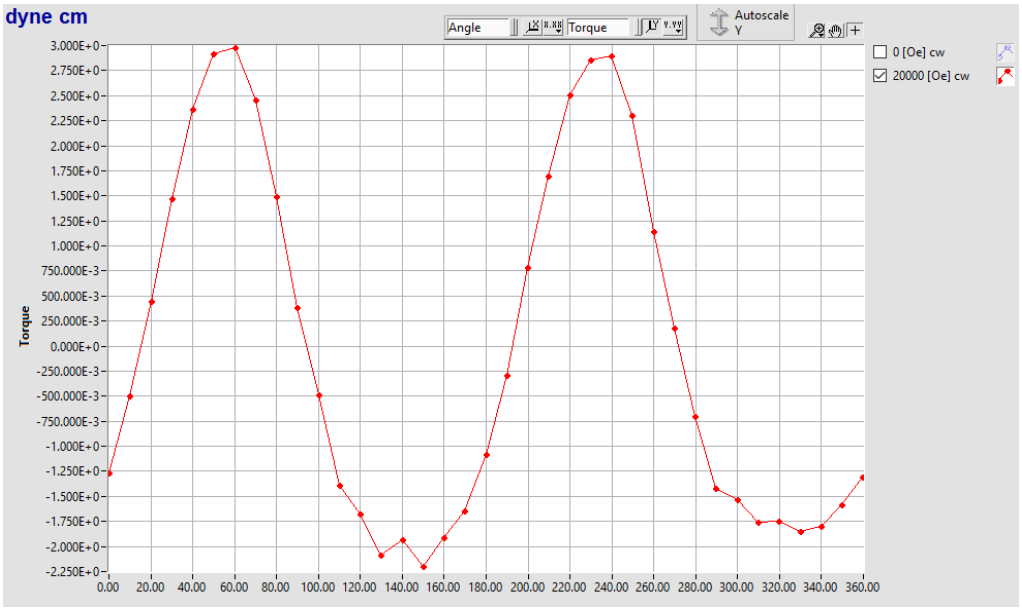

Figure 38: Measurement of the Torque curve on a isotropic sample using a true torque head.

Figure 39: The mounting of the isotropic sample with a purposeful misalignment.

We then ran a torque measurement using the vibrational head on the biaxial VSM. The sample used here was similar in construction to the first but was not the same sample. The sample also had a purposeful misalignment added to it (see Fig 39.) this added a roughly 0.5mm wobble to the measurements. Before the measurement was done the sample position was determined for each field angle using the calibrated Phi-scan method (X-coil signal). The results were then saved to a table and then used to correct the position for the various field angles. Figure 40.a shows the results after the one theta and DC component have been removed. Again, we see a noticeable two theta component with the same general outline as the scan on the torque head. Also important to notice is that the amplitude, around 3.25 dyne cm, is of the same order of magnitude as on the torque head. This shows that we can correct samples torque curves with a high enough accuracy on a biaxial VSM, using the auto-align option, to be compariable to torque curves measured by the torque head. Figure 40.b shows the torque curves measured by biaxial VSM with (green) and without (red) automatic position correction.

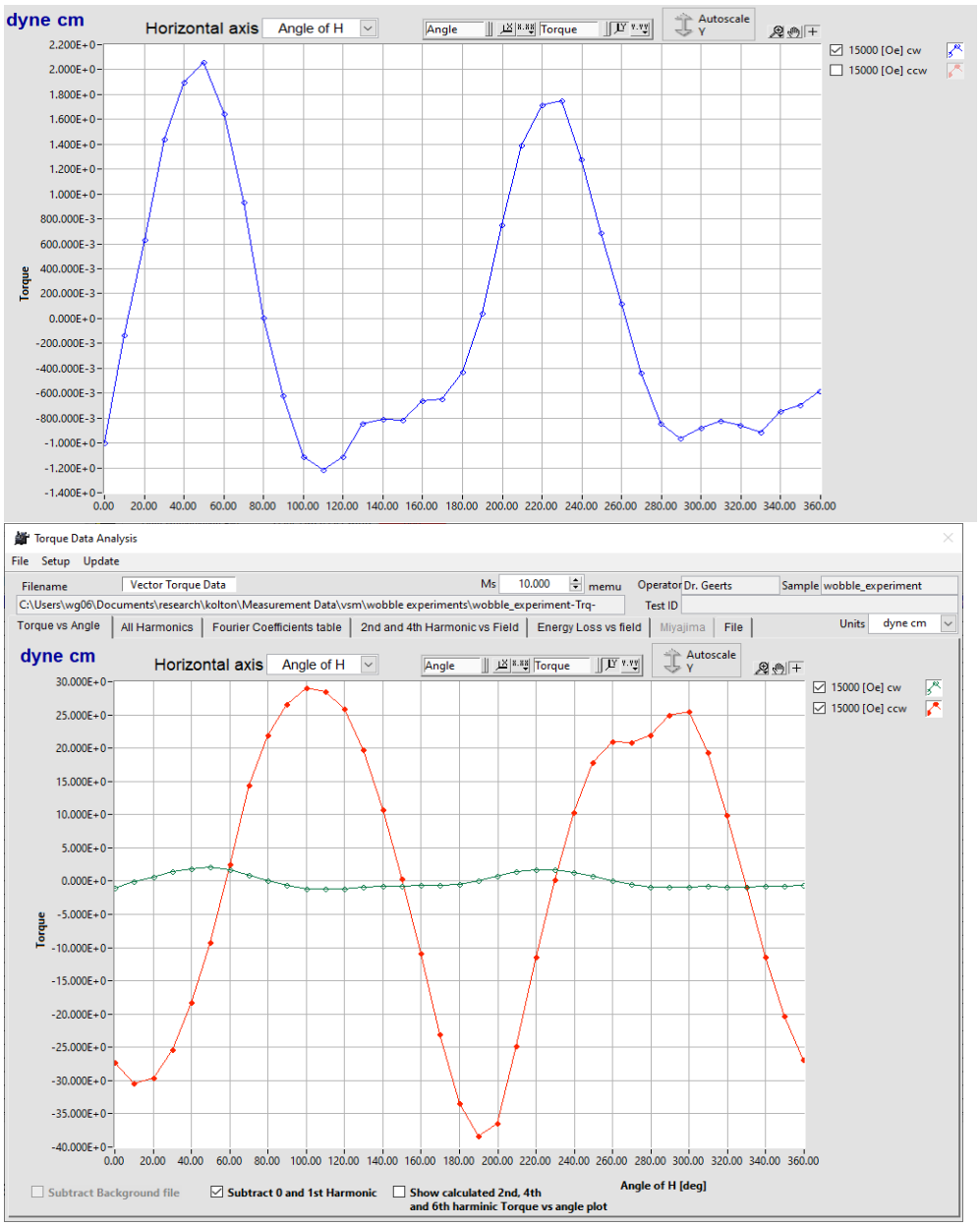

Figure 40: (a) Measurement of the Torque curve on an isotropic sample using the vibrational head; (b) torque curve measured by biaxial VSM with (green) and without (red) automatic position correction.

Repeatability Results

As this system is intended to be used for accuracy alignments that will need to be used with the same sample several times over, the repeatability of the system is incredibly important to determine its usefulness. It also functions as testing for the

programs systems allows us to verify that the program and the motors are correctly working and taking data. Specifically, repeatability we will use the multiple Phi-scans that were done in tandem and then the later designed Double Phi-Scan program results. The Double Phi-scan program was used primarily for testing on the Thorlabs Motors and then later was used in the unified program to ensure that samples were centered. To make a comparison of our different data sets we take the standard deviation between the last scans second run and the new scans first run. The sample is not moved between these runs and should show the same position value.

Repeatability of Different Motor Setups

Below is a listing of the results for the Oriel Encoder Mike set up. For these scans we used a radius of 1mm with 16 points per scan and using the Phi-scan alignment method with no changes.

Table 13: An initial run of test at the same position.

Test#	x' mm	x" mm	y' mm	y" mm
1	-0.090	-0.022	0.062	-0.164
2	-0.092	-0.018	0.065	-0.164
3	-0.091	-0.019	0.064	-0.159
4	-0.091	-0.019	0.063	-0.158
STD	0.001	0.002	0.001	0.003

After this we then moved on to the Thorlabs motors where we used the same initial values as with the older motors set baring the change in speed and acceleration. For these scans though we did not disable realignment, so the standard deviation cannot be taken over all scans. To fix this and allow us to compare to the other earlier runs, the standard deviation was taken from the different runs as we can compare the last scan of

the first run to the first scan of the second run as the position has not changed between these two runs. We then took the standard deviation of all these different comparisons which gave us two good sets of data to pull from. Below is as listing of all the runs and another of the better round of scans. For these scans we again used a radius of 1mm with 16 points per scan using the Phi-scan alignment method with no changes.

Table 14: An averaging of the multiple rounds of double scans.

Scan Runs	x' mm	x" mm	y' mm	y" mm
1	0.005	0.012	0.013	0.007
2	0.002	0.007	0.014	0.002
3	0.004	0.002	0.010	0.008
4	0.005	0.006	0.010	0.005
5	0.006	0.008	0.005	0.006
6	0.006	0.007	0.010	0.002
Avg STD	0.001	0.003	0.003	0.002

Table 15: A averaging of the standard deviation of runs on the second trial.

Scan Runs	x' mm	x" mm	y' mm	y" mm
1	0.005	0.006	0.010	0.005
2	0.006	0.008	0.005	0.006
3	0.006	0.007	0.010	0.002
Avg STD	0.001	0.001	0.003	0.002

What is noticeable is that even at the faster speeds, the Thorlabs Motors resulted in better data than the Oriel Encoder Mikes.

Repeatability of Scan Radius

So, with the added speed we began testing the repeatability by changing different variables of the scan these being the radius of the scans, the number of points scanned, and the number of averages taken at each point in the scan. The first variable tested was

the radius of the scans. Tested were 0.5mm 1mm and 1.5mm Phi-scans. For these tests we did not realign on the first scan, so all scans are at the same point. Seen below are the results showing an increase in repeatability as the scan radius is increased. However the results show that as the radius passes 1mm it no longer experiences a noticeable increase. Results at 1.5mm+ are similar to results obtained at 1mm.

Table 16: The Different Double scans at a radius of 0.5mm, 16 point per scan, and 50 averages per point and their standard deviation.

	x' mm	x'' mm	y' mm	y'' mm
1	-0.022	0.033	0.002	-0.005
1--2	-0.034	0.036	0.027	0.020
2	-0.020	0.023	-0.024	0.005
2--2	-0.042	0.046	-0.005	0.032
3	-0.028	0.034	-0.034	-0.019
3--2	-0.039	0.033	-0.010	0.027
STD	0.009	0.007	0.021	0.020

Table 17: The Different Double scans at a radius of 1mm, 16 point per scan, and 50 averages per point and their standard deviation.

	x' mm	x'' mm	y' mm	y'' mm
1	-0.010	0.006	-0.024	-0.015
1--2	-0.014	0.012	-0.042	-0.023
2	-0.013	0.016	-0.042	-0.028
2--2	-0.016	0.028	-0.017	-0.010
3	-0.012	0.018	-0.032	-0.023
3--2	-0.018	0.012	-0.034	-0.008
STD	0.003	0.007	0.010	0.008

Table 18: The Different Double scans at a radius of 1.5mm, 16 point per scan, and 50 averages per point and their standard deviation.

	x' mm	x" mm	y' mm	y" mm
1	-0.015	-0.001	-0.048	-0.045
1--2	-0.019	0.004	-0.054	-0.031
2	-0.014	0.002	-0.048	-0.047
2--2	-0.015	0.003	-0.060	-0.039
3	-0.015	0	-0.050	-0.049
3--2	-0.016	-0.004	-0.048	-0.042
STD	0.002	0.003	0.005	0.007

Repeatability of Scan Variables

The next parameter we tested was the points scanned. For scans the number of points is calculated by the $n = 2^N$, N here is the resolution value the user choses. So scans grow in binary values of 2, 4, 8, 16, 32. Here we chose 16 and 32 points to test as 8 is the minimum number of points needed to produce usable data. However, 8 points does not fully cover all possible information and any 2ϕ jumps may not be fully caught. For these scans we used a radius of 2mm. Though improvements are low past 1.5mm this gives us an assured accuracy for the scans. Below are the results showing what improvements were seen.

Table 19: The Different scans for a 16 point scan process and their standard deviation.

	x' mm	x" mm	y' mm	y" mm
1	-0.011	0.006	-0.015	-0.030
1--2	-0.012	0.002	-0.008	-0.024
2	-0.010	0.003	-0.017	-0.028
2--2	-0.011	0.004	-0.022	-0.019
3	-0.008	0.003	-0.021	-0.033
3--2	-0.010	0.003	-0.014	-0.029
STD	0.001	0.001	0.005	0.005

Table 20: The Different scans for a 32 point scan process and their standard deviation.

	x' mm	x" mm	y' mm	y" mm
1	-0.006	-0.001	-0.007	-0.029
1--2	-0.008	0.003	-0.013	-0.027
2	-0.008	0.000	-0.015	-0.034
2--2	-0.010	0.000	-0.014	-0.026
3	-0.009	-0.003	-0.018	-0.037
3--2	-0.009	-0.006	-0.022	-0.030
STD	0.001	0.003	0.005	0.004

Finally, we tested the number of averages taken at each sample point (the number of averages used to produce the recorded values for the X-coil signal and Y-coil signal). The more values taken the less effect noise has, more averages means that it requires more time to complete the Phi-scan. Until this point all scans used fifty averages for their Phi-scans. So if the repeatability is not significantly lower than previous, the decrease in time is worth the change. For these scans again the radius was set to 2mm, 16 points per scan, and the Calibrated Phi-scan method was used for alignment. Below's table shows the result:

Table 21: The Different scans for a 10 averages per point scan process and their standard deviation.

	x' mm	x" mm	y' mm	y" mm
1	-0.012	-0.005	0.042	-0.050
1--2	-0.012	-0.002	-0.036	-0.045
2	-0.011	-0.006	-0.044	-0.054
2--2	-0.013	-0.003	-0.035	-0.041
3	-0.012	-0.008	-0.042	-0.053
3--2	-0.012	-0.004	-0.051	-0.045
STD	0.001	0.002	0.034	0.005

The Final decision after these tests was that scans could be done acceptably at a radius of 1mm with 16 sample points and 10 averages per point. This allows for fast 1

minute Phi-scans that retain a reliable central point and can be done with other VSM implements like with the furnace raised or with a small pole piece gap that would allow measurements at higher fields. For testing though scans were done at 2mm to ensure any issues were noticed. Also higher averages were used when necessary. These values are all configurable in the Phi Scan program meaning that when necessary users can change the values for their own scans.

VSM Systematic Error testing

Earlier when introducing the VSM some of the systematic errors that can be encountered were discussed. These are things like bending of the rod from high fields on samples with a high magnetic moment and wobble caused by a misalignment of the sample with the center of the mounting rod. Here in this section, we will discuss the magnitude of these systematic errors using the alignment program. For each of these tests we used the same sample, i.e. a Copper mu-metal punch out of about 2mm diameter. The sample had very low anisotropy and a magnetic moment of around 0.1538 emu.

We first explored whether the D and E values used for the Calibrated Phi-scan method would be constant across different field values. The table below shows the field dependence of the D and E values between -5000Oe and -15000Oe.

Table 22: The D and E values calculated at different field strengths.

Field	D'	D"	E'	E"
-15000	-6.3253E-04	-2.9234E-04	3.0718E-04	-2.6458E-04
-10000	-6.3155E-04	-2.9133E-04	3.0486E-04	-2.6264E-04
-5000	-6.2677E-04	-2.9095E-04	3.0518E-04	-2.6342E-04
STD	3.0804E-06	7.2157E-07	1.259E-06	9.7242E-07

For theses scans the samples D and E component showed little change with field

values. The slight changes that are seen are mostly caused by the small field dependent changes of the sample's magnetic moment and or slight bending of the rod.

Also, measurements were done of the sample's position across a changing field strength. These had the field starting at 20000Oe and then dropped by 5000Oe until we reached 5000Oe. The results are shown below in table 23. As the field decreased the position of the sample saw little change. The x direction had the smallest change with a standard deviation of 6.6E-3. The y direction on the other hand has a much higher deviation of 1.5E-2. This is still a small value though.

Table 23: The found positions at different high field values.

Field (Oe)	x mm	y mm
20000	2.466E+00	1.562E+01
15000	2.468E+00	1.564E+01
10000	2.459E+00	1.561E+01
5000	2.454E+00	1.561E+01
STD	6.626E-03	1.492E-02

In the end it seems that samples that have a magnetic moment of 0.1emu do not cause significant bending of the rod. This is consistent with the fact that for the same samples the D and E values are unaffected by the field strength.

To test the wobble, we purposefully misaligned the sample by roughly 0.5mm. An angular scan at 10 degree increments was then done. The position at each angle was recorded and plotted as a function of the x and y position Figure 41 shows the results. A clear wobble of 1.75mm is seen in the scan that roughly matches the offset that the sample was given.

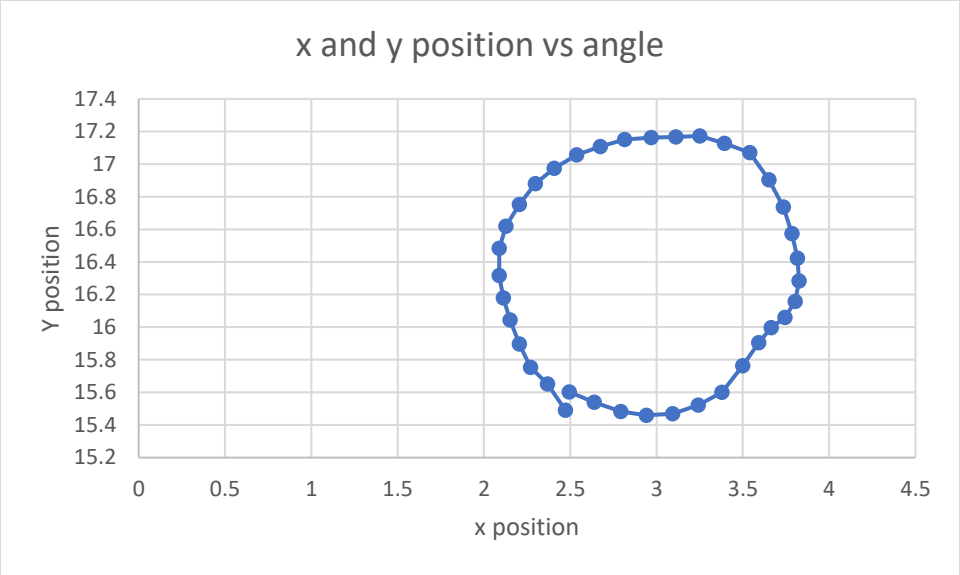

Figure 41: A plot of the position at angular increments of 10 degrees.

While preforming these scans the coil signals at the corrected positions was recorded. (see Fig 11.) Similarly, to the Angular scans we did before we also found the percent difference. In this case we managed a lower percent difference than any of the other scans done of 0.56%.

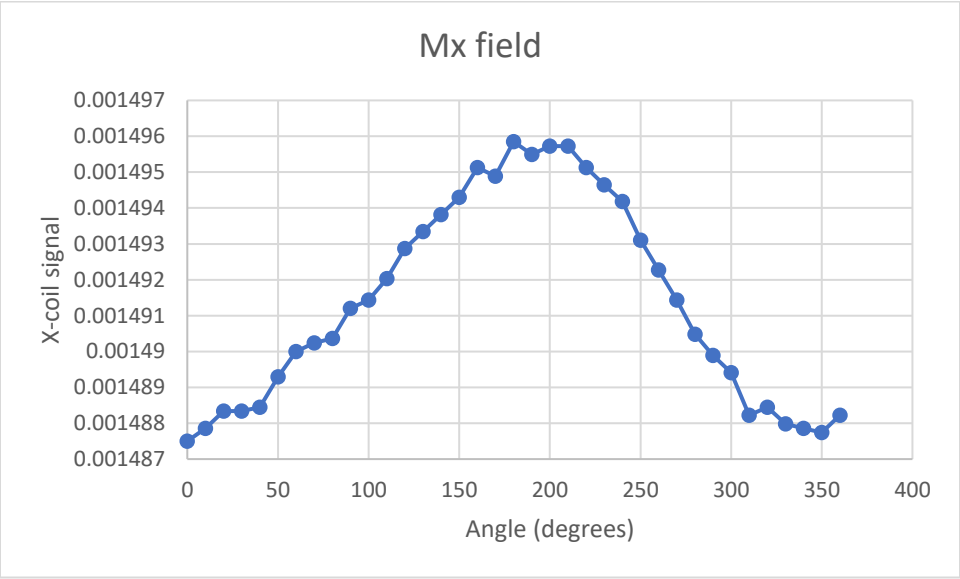

Figure 42: The X-coil signal as a function of the field angle for the mu-metal sample.

Other Test

To further understand how the 1ϕ and 2ϕ components depend on the center of the Phi-scan, contour scans were collected for the 1ϕ and 2ϕ components as a function of (x_o,y_o). For the contour scan, the results clearly shows that the non-linear components at larger distances that we discussed in chapter 3 caused issues when using the Phi-scan method for largely misaligned samples.

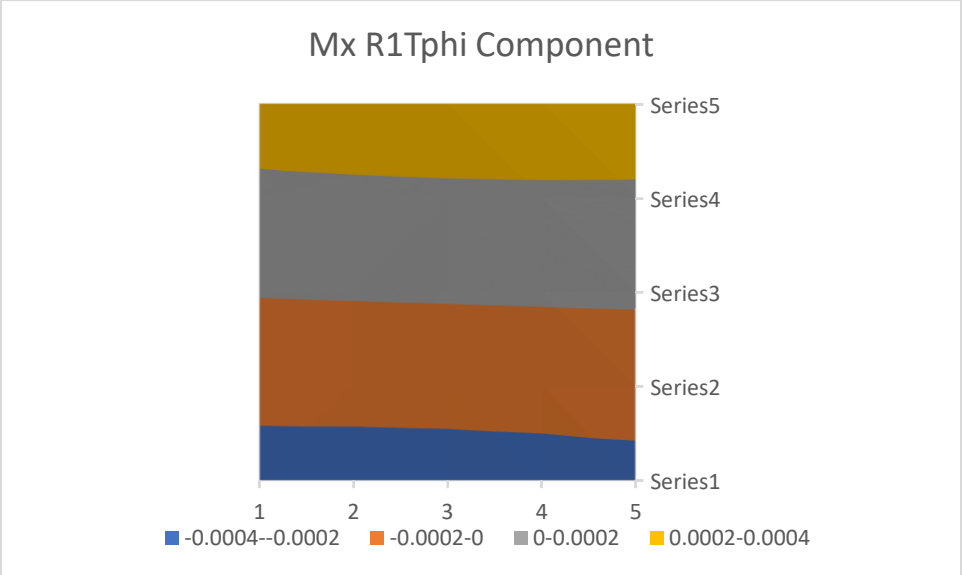

Figure 43: A Contour plot of the different scan points showing the Linear Slope of the Mx real 1ϕ component.

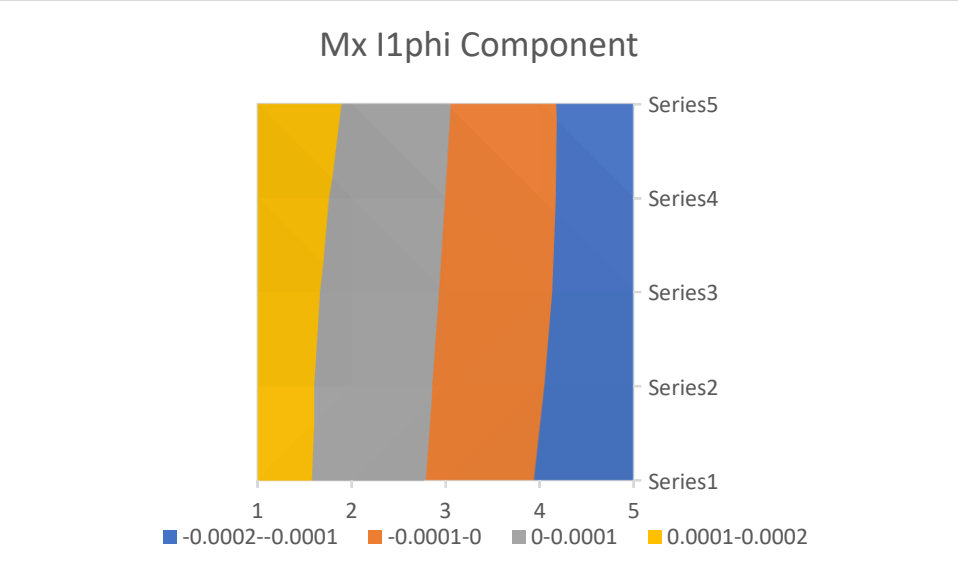

Figure 44: A Contour plot of the different scan points showing the Linear Slope of the Mx Imaginary 1ϕ component.

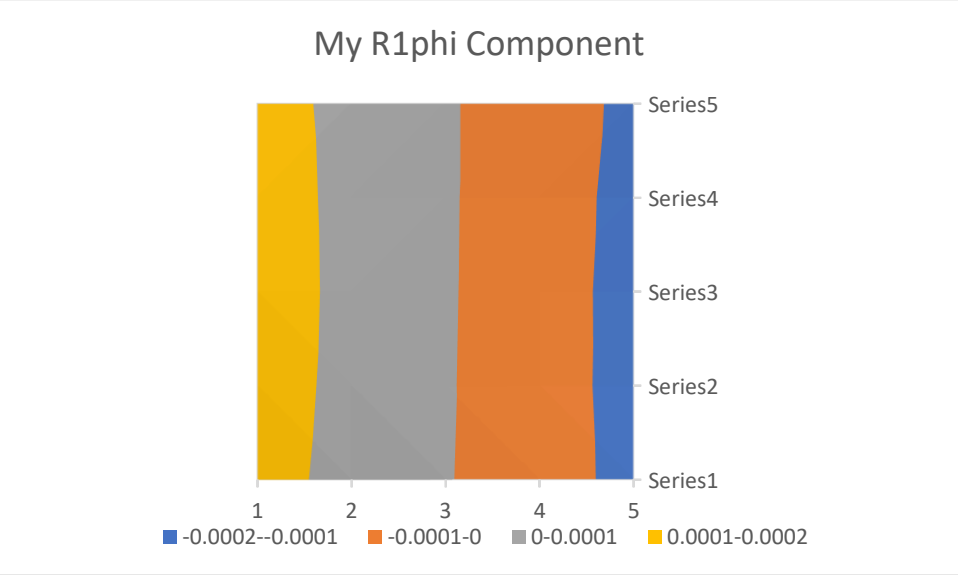

Figure 45: A Contour plot of the different scan points showing the Linear Slope of the My Real 1ϕ component.

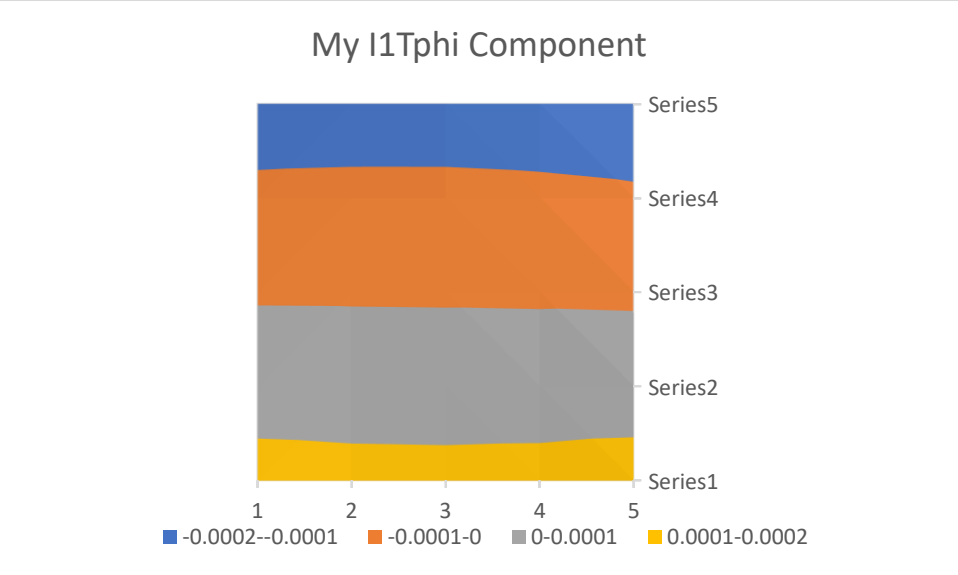

Figure 46: A Contour plot of the different scan points showing the Linear Slope of the My Imaginary 1ϕ component.

As can be seen even at a distance of 1mm in the positive and negative directions the 1ϕ components are still linear. Now we move on to the 2ϕ components contour representation:

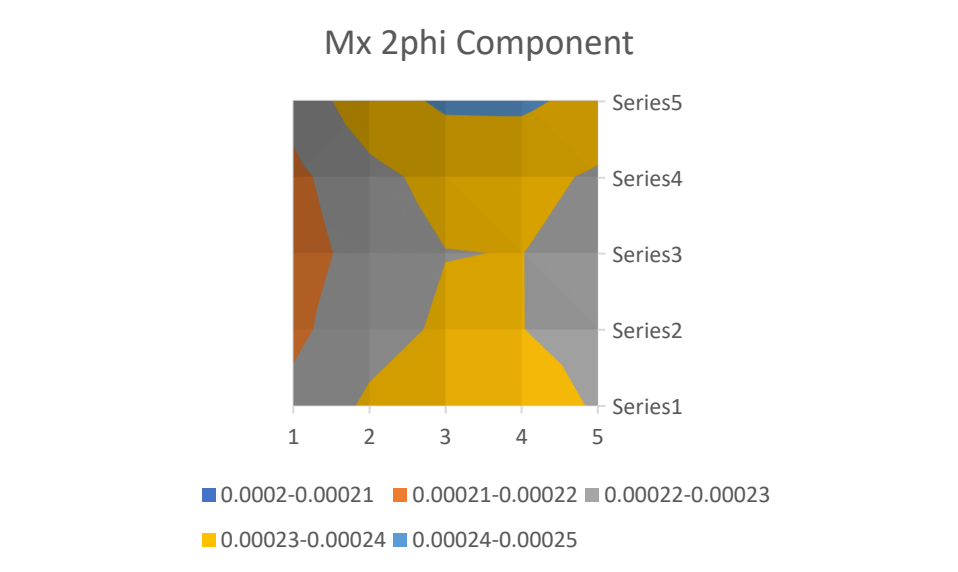

Figure 47: The Mx Real 2ϕ component contour representation.

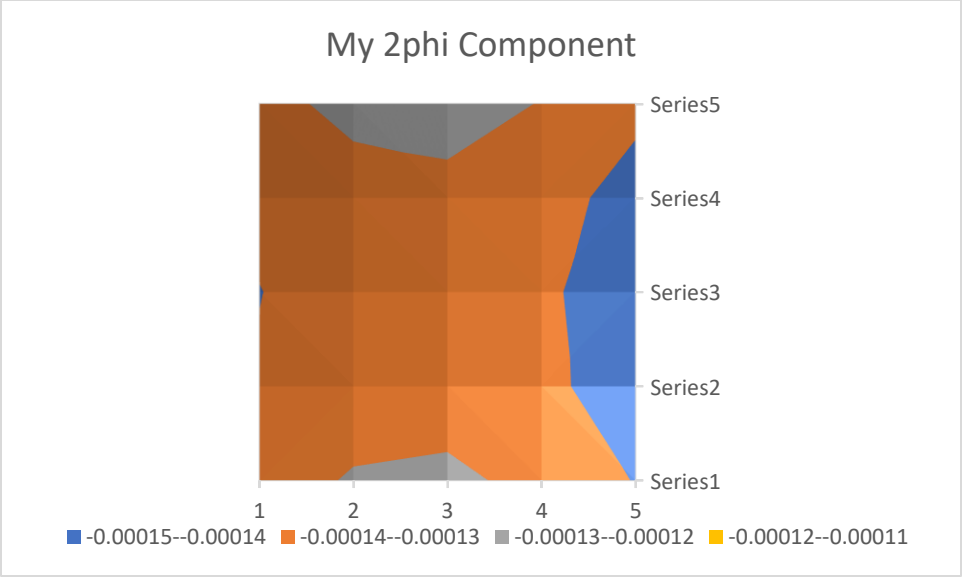

Figure 48: The My Imaginary 2ϕ component contour representation.

The 2ϕ components should follow the original equation be constant across all positions, but as we have stated they have an non-linear component that becomes large at bigger distances.

Below are several contour plots made for the PERM -1 and Copper Floppy – 1 Samples:

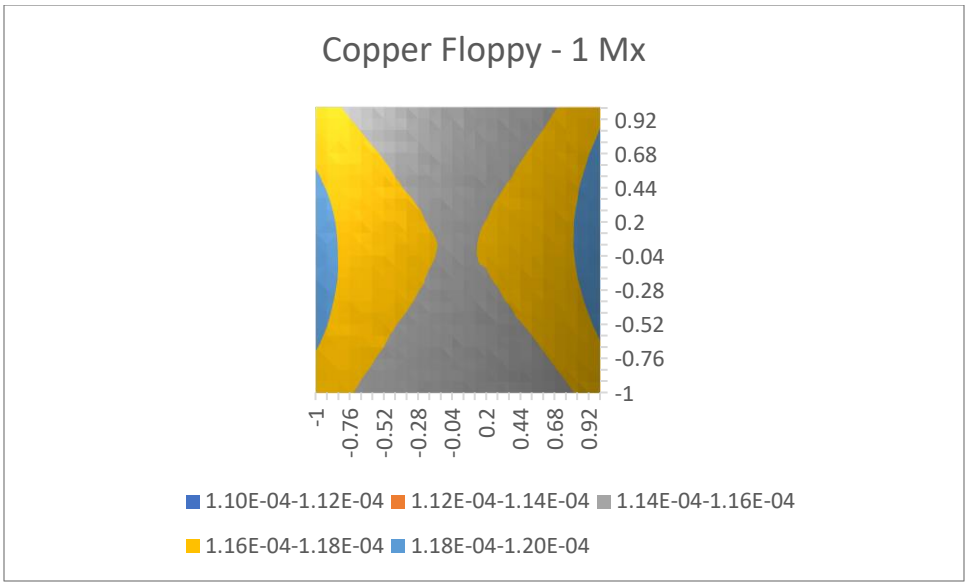

Figure 49: Mx contour plot of the Copper Floppy - 1 sample.

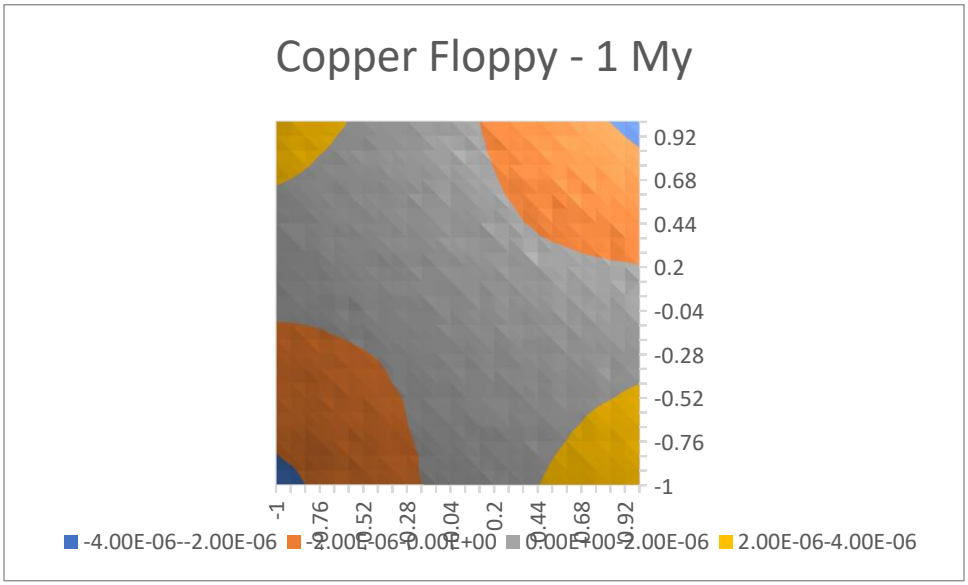

Figure 50: My contour plot of the Copper Floppy - 1 sample.

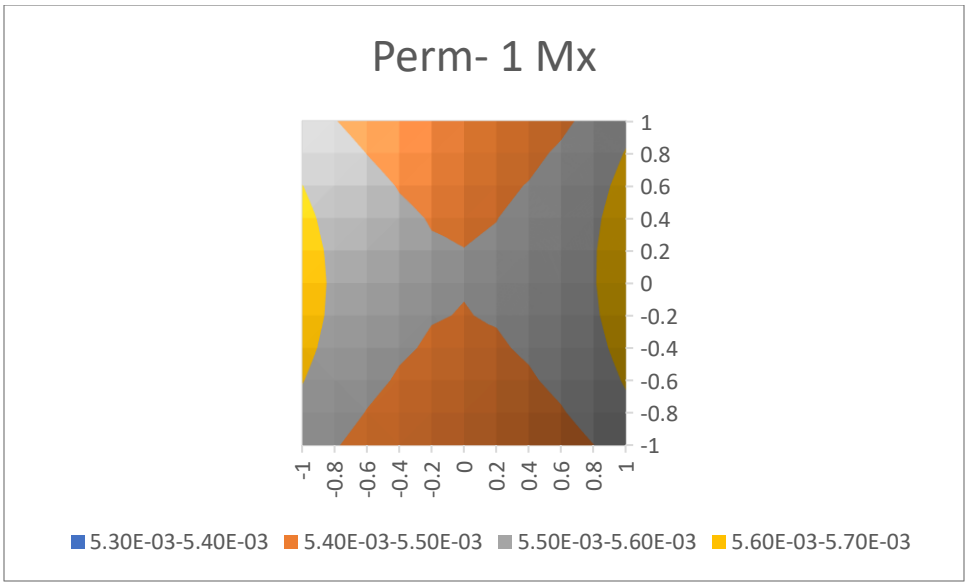

Figure 51: Mx contour plot of the Perm - 1 sample.

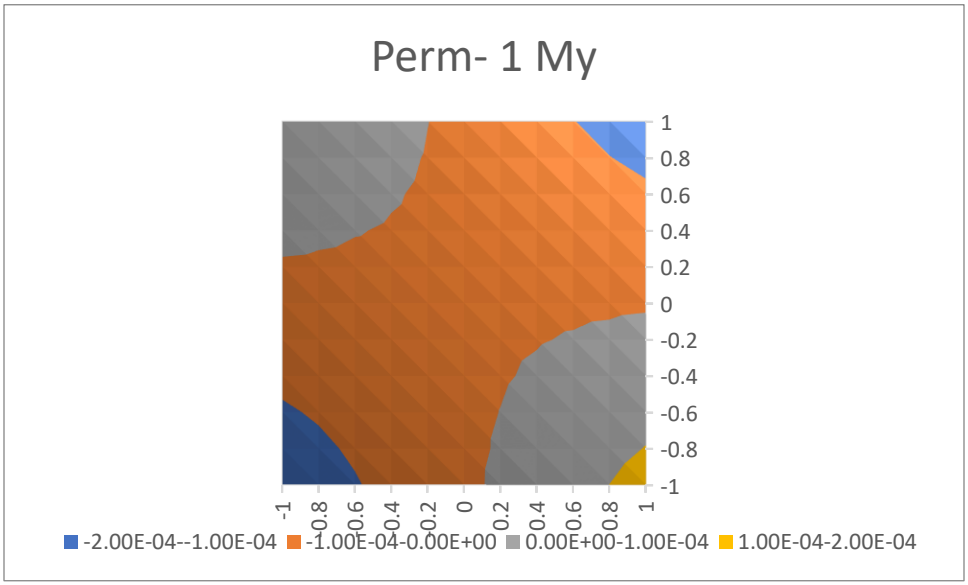

Figure 52: My contour plot of the Perm - 1 sample.

Another test regime that was attempted was linear scans using the original scan method Simon Foner discussed in his work. These Scans were done along either the x or y axis. We first scanned in one direction and then in reverse at increments of 0.05mm collecting the M_x and M_y data at each point. This gives us a clearer image of why

maximizing the X-signal in the y and z directions and minimizing the X-signal in the x direction is done.

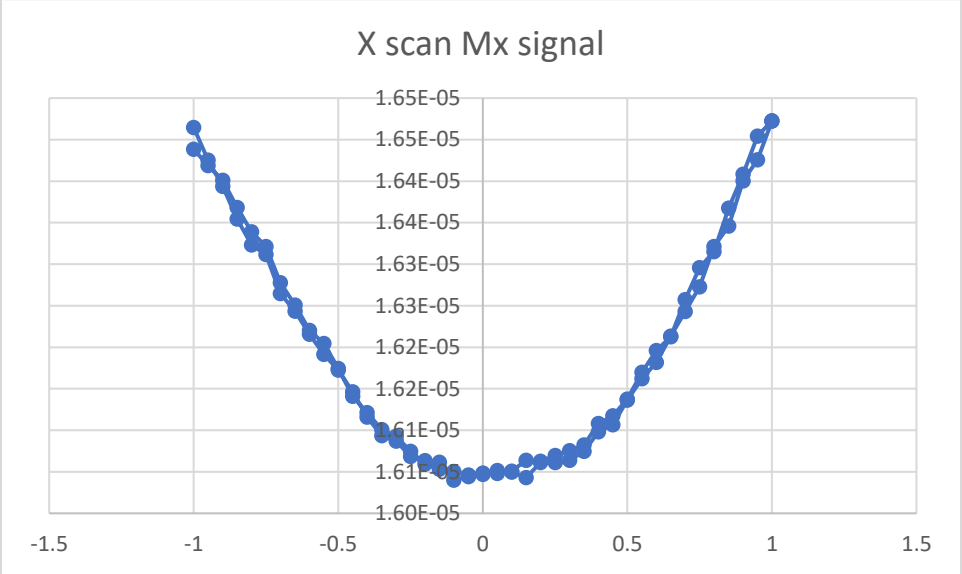

Figure 53: A linear scan in two directions, from -1mm too 1mm and back, for the Mx signal of the Copper Floppy - 1 sample.

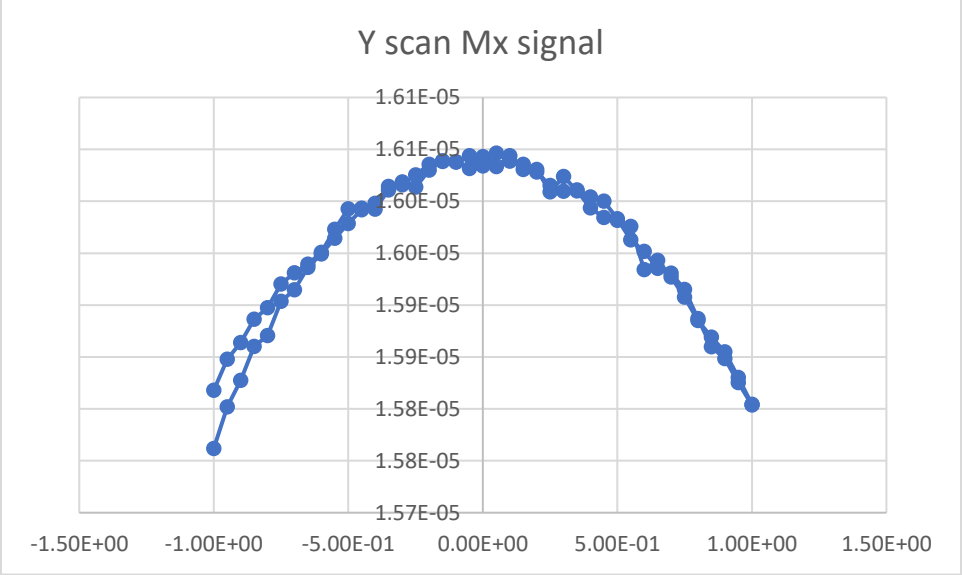

Figure 54: A linear scan in two directions, from -1mm too 1mm and back, for the My signal of the Copper Floppy - 1 sample.

As can be seen here we had the sample well centered. Both of these scans show a

center point on zero. What is also shown is that the values do not change greatly when the direction of the scans changes. The center when scanned from the left or the right is at the same location as the center when scanned from right to left. Other linear scans were done earlier that did not exactly show this and this was fixed by adding an approach from the same direction control in the software. This ensures that the motors final movement when going to a new position is always going in the same direction.

VII. CONCLUSION

This thesis has laid out a process in which a VSM with a modified Mallinson coil set can have its sample alignment process automated. The work builds upon the model developed by Binod D.C. that describes the effect of wobble on the sensitivity and cross talk. The sample is moved in a circular trajectory in the xy-plane while the X and Y coil signals are measured. The position of the sample can be determined from the 1ϕ components of these Phi-scans. We implemented this method on a MicroSense VSM and used it to develop a system that allows one to automatically correct for sample-shifts during measurements. These corrections reduce the systematic error caused by sample shifts caused by field angle changes, field changes, or temperature changes. The realized system improves measurement speed, reproducibility, and accuracy compared to a system without automatic position correction. In the results section we detailed several results illustrating the accuracy, and repetability of the system. Our fully automatic angular scan results compared to the best results of a detailed manual alignment. In both accuracy and repeatability, we were able to hit or exceed the mark we set of five microns to determine the position of the sample. While the Phi-scan method is imprecise at large distances, it will still align the sample and better center can be obtained by performing two Phi-scan based alignments after each other. The Calibrated Phi-scan method though, has high accuracy being suitable to align samples for both large and short distances. The repeatability for both methods has been shown to be very good, with the typical standard deviation being below 0.01. For this work we have presented a new method for autonomously aligning magnetically low-anisotropic samples and laid the ground work for future studies to examine ways to align other sample types and using different sample

rods.

Through the course of the thesis work we encountered several issues, these ranged from issues with programing errors to measurement error. The main issue we encountered was sample position determined from the 1ϕ components over the 2ϕ components (the Phi-scan method) contain an error for large sample misalignments. This was demonstrated experimentally but also by a discussion of the physics behind how the sample in a VSM interacts with the coil-set. This error was corrected for by the development of the Calibrated Phi-scan method which relied only on the 1ϕ component (removing the nonlinear 2ϕ component from the method). Preliminary results suggest that the Calibrated Phi-scan method might be less accurate for samples with a large anisotropy. This is because the D and E calibration values are taken at one angle and differ with field angle for large anisotropy samples that can no longer be saturated along the field.

There are several future studies that may come from this work:

1. A further study into different sample scan methods for other measurement procedures such as a more thorough examination of how the sample's position is affected by the field strength and/or the temperature. The modified Phi-scan method might be able to correct these types of sample shifts. A closer study of this may lead to a better method to align or to further understanding of the issue.
2. Use of the auto alignment method with other coil sets, including the Benito coil set discussed in Ch 2 would present an interesting study opportunity. This coil set may have a higher signal to noise ratio for larger horizontal coils spacing compared to the modified Mallinson coil-set. Its design also would benefit from

auto alignment since the coils in the system do not lead to an easy to access system like the Modified Mallinson coil set.

3. The model developed in Mathematica can be used to characterize the effect of sample size on the VSM signal generated by 3D printed magnetic samples. The work that may take advantage of this is already in development at Texas State University and has exciting prospects.

APPENDIX SECTION

APPENDIX A: Mathematica code

Below is one of the Mathematica code sets that were used to model the VSMs coil signals. This is specificically the code for the X-coil sets signal.

```
Xc=10.25;
Yc=0;
Zc=8;
Cb=2;
Cd=15;
Cl=1;


B1:=(Cb/2)^4(Cl/Cb)*(1/6)((Cd/Cb)^3-1)*1
B3:=-(Cb/2)^6(Cl/Cb)*(1/120)(9((Cd/Cb)^5-1)-20(Cl/Cb)^2((Cd/Cb)^3-1))*1
B5:=(Cb/2)^8(Cl/Cb)*(1/336)(15((Cd/Cb)^7-1)-84(Cl/Cb)^2((Cd/Cb)^5-
1)+56(Cl/Cb)^4((Cd/Cb)^3-1))*1

Vx1[x_,y_,z_]:=
   B1(1/Sqrt[(Xc-x)^2+(Yc-y)^2+(Zc-z)^2]^2)LegendreP[1,(Xc-x)/Sqrt[(Xc-
x)^2+(Yc-y)^2+(Zc-z)^2]]+
  B3(1/Sqrt[(Xc-x)^2+(Yc-y)^2+(Zc-z)^2]^4)LegendreP[3,(Xc-x)/Sqrt[(Xc-
x)^2+(Yc-y)^2+(Zc-z)^2]]+
  B5(1/Sqrt[(Xc-x)^2+(Yc-y)^2+(Zc-z)^2]^6)LegendreP[5,(Xc-x)/Sqrt[(Xc-
x)^2+(Yc-y)^2+(Zc-z)^2]]

Vx2[x_,y_,z_]:=
    B1(1/Sqrt[(-Xc-x)^2+(Yc-y)^2+(Zc-z)^2]^2)LegendreP[1,(-Xc-x)/Sqrt[(-Xc-
x)^2+(Yc-y)^2+(Zc-z)^2]] +
   B3(1/Sqrt[(-Xc-x)^2+(Yc-y)^2+(Zc-z)^2]^4)LegendreP[3,(-Xc-x)/Sqrt[(-Xc-
x)^2+(Yc-y)^2+(Zc-z)^2]] +
   B5(1/Sqrt[(-Xc-x)^2+(Yc-y)^2+(Zc-z)^2]^6)LegendreP[5,(-Xc-x)/Sqrt[(-Xc-
x)^2+(Yc-y)^2+(Zc-z)^2]]

Vx3[x_,y_,z_]:=
   B1(1/Sqrt[(-Xc-x)^2+(Yc-y)^2+(-Zc-z)^2]^2)LegendreP[1,(-Xc-x)/Sqrt[(-Xc-
x)^2+(Yc-y)^2+(-Zc-z)^2]]+
  B3(1/Sqrt[(-Xc-x)^2+(Yc-y)^2+(-Zc-z)^2]^4)LegendreP[3,(-Xc-x)/Sqrt[(-Xc-
x)^2+(Yc-y)^2+(-Zc-z)^2]]+
```

```
  B5(1/Sqrt[(-Xc-x)^2+(Yc-y)^2+(-Zc-z)^2]^6)LegendreP[5,(-Xc-x)/Sqrt[(-Xc-
x)^2+(Yc-y)^2+(-Zc-z)^2]]

Vx4[x_,y_,z_]:=
   B1(1/Sqrt[(Xc-x)^2+(Yc-y)^2+(-Zc-z)^2]^2)LegendreP[1,(Xc-x)/Sqrt[(Xc-
x)^2+(Yc-y)^2+(-Zc-z)^2]]+
  B3(1/Sqrt[(Xc-x)^2+(Yc-y)^2+(-Zc-z)^2]^4)LegendreP[3,(Xc-x)/Sqrt[(Xc-
x)^2+(Yc-y)^2+(-Zc-z)^2]]+
  B5(1/Sqrt[(Xc-x)^2+(Yc-y)^2+(-Zc-z)^2]^6)LegendreP[5,(Xc-x)/Sqrt[(Xc-
x)^2+(Yc-y)^2+(-Zc-z)^2]]


Sxx[x_,y_,z_]=(D[(D[Vx1[k,y,j]+Vx2[k,y,j]-Vx3[k,y,j]-Vx4[k,y,j],k]/.k->x),j]/.j-
>z);

Sxx[x_,y_,p_,θ_] = Sxx[(x+p*Cos[θ]),(y+p*Sin[θ]),0];

x = 2;
y = -2;
p = 1.5;


T := {}

For[i=0,i<2*π,i =i+(π/8), AppendTo[T,Sxx[x,y,p,i]]];

ListPlot[T]

Z = Fourier[T];
S =Im[Z];
J = Re[Z];

Export["DataTable.xlsx",{S,J}]

Quit[]
```

APPENDIX B: Write up for Oriel Encoder control setup

Connections

For a modern connection for the system a cable that converts from the DB25 connector to DB9 connnection is required. The connection only requires three wires between the two ports. Listed below are the numbered figures of the two connection ports also shown are the needed connections that will be needed for proper communication.

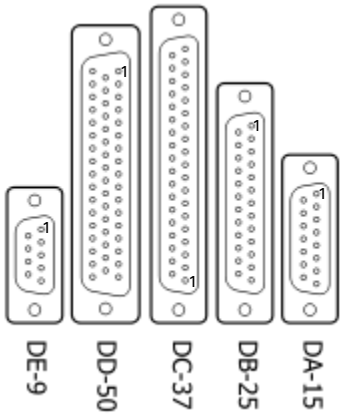

DB9		DB25	Connection type
2	to	2	TXD
3	to	3	RXD
5	to	7	GND
|	jumped		
6			CTS
|	jumped		
4			RTS

From the DB9 connector a serisal to USb converter can be used to allow communication with modern computers.

LabVIEW communication

For LabVIEW to interact with connected serial devices a separate set of software will be required. The user will need to download and set up (if not already installed) NI-MAX. This is a hardware integration system that is par tof the DAQ software packadge. Users will also need to download and set up (again if not already installed) NI-VISTA. This is the software that will actually handle the communication to the serial ports. Included in it is LabVIEW VIs for serial communication and a manual testing program.

When setting up the Oriel Encoder communication in NI-MAX you will need to configure the baud rate and other settings based on what the controller is set to. The baud

rate can be changed manually on the controller (instructions for this can be found in the Oriels instruction manual).

Oriel Encoder commands

The Oriel Encoder controller has three main types of commands:

1. Single commands which require no reed after, and are all one character.
2. Multi-character commands, these require first a character and then a string depending on the command. Aftrer the command is sent and the motor completes its operation a confirmation will need to be read from the controller.
3. Inquires, these are single character commands that requrest different states of the motor and controller. All Inquires are required to be read out after the commands are sent.

Below are the list of the different commands that are included with the Oriel Encoder system.

Single Commands

- L\n = Switches system to local control, returns “off line”.
- R\n = Switches system to remote control, returns “on line”.
- <\n = Begins running the current motor down, will not stop unless commanded.
- >\n = Begins running the current motor up, will not stop unless commanded.
- S\n = Stops current motors movements, will stop < and > commands.

Multi-commands

- CX\r\n (X= A,R) = Clears either the A(Absolute) register, or the R(Relative) register.

- GX\r\n (X=+/-999999) = Moves the current motors actuator to the absolute position (um) selected.
- MX\r\n (X=1,2,3) = Selects which motor the controller will operate, will not work when motors are in motion.
- TX\r\n (X=+/-999999) = Moves motor chosen amount (um).
- VX\r\n (X=0.5-200) = Sets the speed of the motor.

Inquire commands

- A\n = Repors the current absolute position of the selected motor.
- P\n = Repors the current relative position of the selected motor.
- I\n = Returns a detailed reports of current motors information. (velocity, positon, etc).
- Z\n = Returns a caracter (a-e) depending on the motors status:
    a) Motor stopped – Normal
    b) Running down – running in reverse
    c) Running up – running forward
    d) Overload down – has reached reverse limit
    e) Overload up – has reached forward limit

REFERENCES

Arfken, G. B., Weber, H. J., & Harris, F. E. (2013). *Mathematical Methods for Physicists, Seventh Edition.* Academic Press.

Bernards, J. (1993). Design of a detection coil system for a biaxial vibrating sample magnetometer and some applications. *Review of Scientific Instruments 64*, 1918-1930. Retrieved from https://doi.org/10.1063/1.1143977

Bernards, J., Van Engelen, G., & Cramer, H. (1993). An Improved Detection Coil System for a Biaxial Vibrating Sample Magnetometer. *Journal of Magnetism and Magnetic Materials 123*, 141-146.

D.C., B. (2019). *The magnetic Characterization of Permalloy and Permalloy Oxide Grown by RF Magnetron Sputtering.*

Dwight, K., Menyuk, N., & Smith, D. (1958). Further Development of the Vibrating-Coil Magnetometer. *Journal of Applied Physics 29*, 491-492.

Foner, S. (1956). Vibrating Sample Magnetometer. *Review of Scientific Instruments 27*, 548.

Foner, S. (1959). Versatile and Sensitive Vibrating-Sample Magnetometer. *Review of Scientific Instruments 30*, 548-557. Retrieved from https://doi.org/10.1063/1.1716679

Foner, S. (1970). *United States of America Patent No. 3,496,459.*

Geerts, W. J., & D. C., B. (2019). *Automated Sample Positioning System for a Vibrating Sample Magnetometer Employing a Modified Mallinson Coil Set.* San Marcos .

Griffiths, D. J. (2013). *Introduction to Electrodynamics, Fourth Edition.* Pearson.

Hoon, S. R. (1983, April 1). An Inexpensive. Sensitive Vibrating Sample Magnetometer. *European Journal of Physics*, pp. 61-67.

Hummel, R. E. (2011). *electronic Properties of Materials, Fourth Edition.* Springer.

Jackson, J. D. (1999). *Classical Electrodynamics.* John Wiley And Sons, Inc.

Lubell, M. S., & Venturino, A. S. (1960). Vibrating Sample Magnetometer. *Review of Scientific Instruments*, 207-208.

Mallinson, J. (1965). Magnetometer Coils and Reciprocity. *Journal of Applied Physics*, 2514-2515.

Mia, M. D. (2020). *Growth and characterization of Ga2O3, (Ga1-xGdx)2O3 & (Ga1-xFex)2O3 thin films by pulsed laser deposition.* San Marcos: Texas State University.

Richter, H. (1992). On the Construction of Detection Coils for a Vectorial Vibrating Sample Magnetometer. *Journal of Magnetism and Magnetic Material 11*, 201-213.

Samwel, E. O., Bolhuis, T., & Lodder, J. C. (1998). An Alternative Approach to Vector Vibrating Sample MAgnetometer Detection Coil Setup. *Review of Scientific Instruments*, 3204-3209.

Smith, D. O. (1956). Development of a Vibrating-Coil Magnetometer. *Review of Scientific Instruments 27*, 261-268.

SWT Physics Department. (2006, 5 22). *Vibrating Sample Magnetometer*. Retrieved from txstate: https://gato-docs.its.txstate.edu/jcr:7543b8ec-f619-49c3-888f-01c3ad13c7da/vsm.pdf

Van Oosterhout, G. W. (1957). A Rapid Method For Mesuring Coercive Force and Other Ferromagnetic Properties of Very Small Samples. *Applied Science Reserch,* 101-104.

Zijlstra, H. (1967). *Selected Topics in Solid State Physics.* New York: American Elsevier Publishing Company, Inc.